

Aus dem Bereich Molekulare Zellbiologie  
Theoretische Medizin und Biowissenschaften  
der Medizinischen Fakultät  
der Universität des Saarlandes, Homburg/Saar

# **High Resolution 3D-Imaging of the Physiology and Morphology of Isolated Adult Cardiac Myocytes from Rat and Mice.**

*Dissertation zur Erlangung des Grades eines Doktors der  
Naturwissenschaften*

**der Medizinischen Fakultät**

der UNIVERSITÄT DES SAARLANDES

2009

vorgelegt von: Karin Hammer

geb. am: 29.05.1977 in Zweibrücken

---

*,... It must therefore be concluded that the blood in the animal body moves around in a circle continuously, and that the action or function of the heart is to accomplish this by pumping. This is the only reason for the motion and beat of the heart.'*

**William Harvey**

Exercitatio Anatomica De Moto Cordis et Sanguinis in Animalibus, 1628.

# Index

I.	Zusammenfassung.....	1
II.	Summary .....	4
III.	Introduction .....	7
A.	The Heart.....	8
1.	Morphology of the Heart .....	8
2.	Physiology of the Heart .....	10
3.	Pathophysiology of the Heart.....	12
B.	Cardiac Myocytes .....	14
1.	Morphology of Cardiac Myocytes.....	14
2.	Physiology of Cardiac Myocytes .....	15
C.	Cell Culture.....	21
D.	Objectives .....	22
IV.	Material and Methods.....	25
A.	Adult Rat Cardiac Myocytes .....	25
B.	Adult Mouse Cardiac Myocytes .....	26
C.	Adenovirus Constructs and Transfection .....	28
D.	Fluorescent small molecule dyes .....	33
E.	Confocal Microscopy .....	38
F.	Data Analysis .....	47
G.	Calcium-Spark Analysis .....	48
V.	Results .....	50

A.	The Morphology of Adult Cardiac Myocytes in Long Term Culture .....	50
1.	Plasmamembrane and Transverse Tubular System .....	50
2.	Mitochondria.....	54
3.	Endoplasmic/Sarcoplasmic Reticulum .....	59
4.	Golgi Apparatus .....	61
5.	Actin filaments.....	63
B.	The Physiology of Adult Mouse Myocytes – Ca <sup>2+</sup> Sparks.....	64
1.	Evaluation of the MatLab Algorithm.....	64
2.	Characterization of Ca <sup>2+</sup> Sparks in the Major Compartments of the Heart .....	68
3.	The Impact of TRPC1/C4 Double Knock-Out Mutant With and Without Chronical β-Stimulation on Ca <sup>2+</sup> Sparks.....	70
4.	The Impact of Over Expression of Rac1 in Mouse Hearts on Ca <sup>2+</sup> Sparks.....	73
VI.	Discussion .....	76
A.	The Morphology of Adult Cardiac Myocytes in Long Term Culture .....	76
1.	Plasmamembrane .....	77
2.	Mitochondria.....	81
3.	Endoplasmic/Sarcoplasmic Reticulum .....	84
4.	Golgi Apparatus .....	85
5.	Actin Filaments.....	86
B.	The Physiology of Cardiac Myocytes .....	87
1.	MatLab Spark Algorithm.....	87
2.	Characterization of Ca <sup>2+</sup> Sparks in the Major Compartments of the Heart .....	89
3.	The Impact of TRPC1/C4 double Knock-Out in the Heart on Ca <sup>2+</sup> Sparks with and without chronic β-stimulation .....	92

4.	The Impact of Overexpression of Rac1 in Mouse Hearts on Ca <sup>2+</sup> Sparks.....	95
C.	Conclusion.....	98
VII.	Literature.....	100
VIII.	Publications.....	108
IX.	Abbreviations.....	109
X.	Acknowledgments.....	111
XI.	Curriculum Vitae.....	112

## **I. Zusammenfassung**

### **Hochauflösendes 3D-Imaging der Physiologie und Morphologie von isolierten, adulten Kardiomyozyten aus Ratte und Maus**

Die Kultivierung adulter Kardiomyozyten stellt ein sinnvolles Werkzeug dar, um die Physiologie und die Pathophysiologie von Kardiomyozyten auf Einzelzellebene zu untersuchen und dabei experimentelle Methoden anzuwenden, die eine längere Kultivierung erfordern, wie z.B. die Expression von genetisch kodierten Biosensoren oder fluoreszierenden Fusionsproteinen. Die in unserer Arbeitsgruppe angewandte Kultivierungsmethode ist ein guter Ansatz, um die Struktur und die Physiologie bezüglich des globalen  $\text{Ca}^{2+}$  Haushalts und der Kontraktilität der kultivierten Zellen während einer Woche in Kultur aufrechtzuerhalten.

Ich habe subzelluläre Strukturen während einer Kultivierungsdauer von 1 Woche beobachtet, um die Konservierung oder aber auch mögliche Veränderungen von verschiedenen Zellorganellen aufzuzeichnen. Dazu habe ich die Plasmamembran, die Mitochondrien, das Sarkoplasmatische Retikulum, den Golgi Apparat und Aktinfilamente mit fluoreszierenden Fusionsproteinen markiert und wo dies möglich war zusätzlich mit einem spezifischen Farbstoff gefärbt. Danach wurden die Organellen mit einem hochauflösenden Konfokalmikroskop aufgenommen. Die Färbung der Plasmamembran zeigte die typischen Einschnürungen, die sog. T-Tubuli an Tag 0 sehr deutlich, wobei diese bis zum Tag 6 komplett verloren gingen. Diese Beobachtung wurde mit beiden Markierungsmethoden gemacht, wobei das Fusionsprotein mehr Strukturen anfärbte, besonders an Tag 1 und Tag 3 in Kultur. Die Mitochondrien lagen in frisch isolierten Zellen als sehr geordnete Strukturen vor, die in Form von einzelnen Päckchen durch Lücken getrennt waren, deren Abstand sich im Laufe der Kultivierungswoche vergrößerte. Die Ergebnisse aus beiden Markierungsmethoden stimmten überein. Mit FRAP Messungen (fluorescence recovery after photobleach = Wiederkehren der Fluoreszenz nach Photobleichen) konnte gezeigt werden, dass die Mitochondrien bereits an Tag 0 funktionelle Verbindungen hatten, die an Tag 6 stärker ausgeprägt waren, d.h. einen besseren Austausch aufwiesen. Das Sarkoplasmatische Retikulum (SR) konnte nur mit dem Fusionsprotein markiert werden, da es keinen ausreichend guten Farbstoff für dieses Organell gab. Das SR war als sehr feine, netzartige Struktur in der ganzen Zelle sichtbar

und hatte eine klare Strukturierung, die im Laufe der Kulturwoche etwas weniger gut organisiert war. Das SR war auch nach einer Woche immer noch in der Zelle verteilt und schien seine Aufgaben kaum verändert zu erfüllen (wie frühere Daten aus unserer Arbeitsgruppe bereits zeigten). Auch der Golgi Apparat konnte aus den oben genannten Gründen nur mit dem Fusionsprotein markiert werden. Der Golgi Apparat war als vesikuläre Struktur sichtbar, die gleichmäßig in der ganzen Zelle verteilt war. Allerdings kam es hier während einer Woche Kultur zu einer Umorganisation, sodass dieses Organell nur noch im Bereich um die Kerne zu finden war. Die Aktinfilamente wurden ebenfalls nur mit einem Fusionsprotein markiert und ihre Anordnung spiegelte die der Myofilamente wieder und wurde während der Kultur nicht verändert. Zur Stabilisierung der Zellstruktur wurde dem Medium CytochalasinD zugesetzt. Dies führte in der Tat zu einer Minimierung der beobachteten Veränderungen, auch wenn diese nicht gänzlich verhindert werden konnten. Die hier beschriebenen Veränderungen sind leicht reproduzierbar, wodurch diese Kultivierungsmethode als sehr nützlich für Langzeitexperimente angesehen werden kann und die hier beschriebenen Veränderungen als eine Grundlage für weitere Experimente dienen können.

Im zweiten Teil meiner Arbeit habe ich die Physiologie der Kardiomyozyten näher untersucht, indem ich  $\text{Ca}^{2+}$  Sparks analysiert habe, die als die grundlegenden Signale bei der Erregungs-Kontraktions-Kopplung angesehen werden. Für diese Messungen wurde ein Konfokalmikroskop verwendet, das mit hoher Geschwindigkeit (100 Hz) zweidimensionale Zeitserien aufnehmen konnte. Um alle Informationen aus diesen Daten verarbeiten zu können, wurde von Frau Aline Flockerzi ein MatLab basierter Algorithmus entwickelt, der  $\text{Ca}^{2+}$  Sparks in zweidimensionalen Zeitserien detektiert und analysiert. Zunächst habe ich den Algorithmus mit Modellzellen, die Modellsparks enthielten, getestet, danach habe ich Sparks analysiert, die in den Zellen aus den drei Hauptkompartimenten des Herzens) den beiden Vorhöfen und den Ventrikeln) gemessen wurden. Die Amplituden der Sparks aus den linken Vorhöfen waren signifikant höher als die der rechten Vorhöfe und beide waren größer als die der ventrikulären Sparks. In den beiden Vorhöfen war die Abklingzeit der Sparks gleich, aber geringer als die in den Ventrikelzellen, diese hatten auch eine größere räumliche Ausdehnung als die Vorhofzellen. Diese Daten zeigten Unterschiede in der  $\text{Ca}^{2+}$  Homöostase ( $\text{Ca}^{2+}$  Erhöhung und Beseitigung) zwischen den einzelnen Kompartimenten auf und können als Grundcharakterisierung dienen.

TRPC1/C4 Doppel-Knock-Out Mäuse wurden analysiert, da eine Beteiligung von TRPC Kanälen an der Entstehung von kardialen Hypertrophien vermutet wurde. Zunächst wurde der Effekt des Doppel-Knock-Out in den drei Hauptkompartimenten des Herzens analysiert, wobei sich herausstellte, dass die meisten Parameter unbeeinflusst blieben. Lediglich die Sparkamplituden in den linken Vorhöfen und den Ventrikeln waren verändert. Als Nächstes wurde der Einfluss von chronischer Infusion von Isoproterenol, einem  $\beta$ -adrenergen Agonisten, der Hypertrophien auslöst, auf Wildtypmäuse und auf Doppel-Knock-Out Mäuse untersucht. Die chronische Infusion führte zu einer Verringerung der Sparkamplituden in Wildtypmäusen, aber nicht in Doppel-Knock-Out Mäusen, wobei in den Doppel-Knock-Out Mäusen die Abklingzeit signifikant verringert war. Die räumliche Ausbreitung war in keiner Gruppe verändert. Diese Daten zeigten eine Beteiligung dieser TRP Kanäle an der  $\text{Ca}^{2+}$  Homöostase in gesunden und hypertrophen Tieren.

Ein weiterer potentieller Kandidat für die Beteiligung an der Entstehung von kardialen Hypertrophien war die Rac1 GTPase, deren Einfluss in Rac1 überexprimierenden Mäusen untersucht wurde. Hier wurden wieder alle drei Hauptkompartimente des Herzens analysiert. Die auffälligsten Veränderungen wurden in den Sparkamplituden festgestellt, die in allen Kompartimenten der Rac1 überexprimierenden Mäuse signifikant erhöht waren. Die Abklingzeit blieb in allen Kompartimenten unverändert, aber die räumliche Ausbreitung war in allen Kompartimenten nach Rac1 Überexprimierung reduziert. Diese Daten zeigten, dass die Überexprimierung von Rac1 in Kardiomyozyten zu Veränderungen der  $\text{Ca}^{2+}$  Homöostase führen kann. Diese Veränderungen unterschieden sich in den einzelnen Kompartimenten des Herzens, was auch auf die unterschiedliche Morphologie der Zellen zurückzuführen war. Diese waren aber auch vergleichbar mit Veränderungen wie sie bei Vorhofflimmern beobachtet wurden.

Die hier vorgestellten Daten zeigten, dass der MatLab Algorithmus geeignet ist, um  $\text{Ca}^{2+}$  Sparks in Kardiomyozyten zu detektieren und zu analysieren und somit ein wichtiger Bestandteil von zukünftigen Studien verschiedener Krankheitsmodelle sein wird.



## II. Summary

Culturing adult cardiac myocytes denotes a useful tool to study the physiology and pathophysiology of cardiac myocytes on a single cell level. That allows to apply experimental settings that require the culturing of cells such as the expression of genetically encoded biosensors or fusion proteins. The previously introduced cell culture method in our lab provided a good approach to maintain the structure and physiology in terms of global  $\text{Ca}^{2+}$  signaling and contractility of the cultured myocytes during one week.

I observed subcellular structures over a culture period of one week to assess possible alterations or the preservation of various cell organelles. I labeled the plasmamembrane, the mitochondria, the sarcoplasmic reticulum, the Golgi apparatus and the actin filaments with fluorescent fusion proteins and (where possible) with small molecule dyes and subsequently imaged the organelles with a confocal microscope. With both labeling methods the plasmamembrane displayed the typical transverse tubules (t-tubules) at day *in vitro* (DIV) 0 which were reduced until DIV6, when no t-tubules were detectable, whereas more labeling was observed with the fluorescent fusion protein especially at day 1 and day 3 in culture. The mitochondria displayed a highly organized pattern in the cells displaying a cross striation pattern which adapted in such a way that the distance between two gaps (between two single mitochondria) increased during the time in culture. These observations were made with both labeling methods. FRAP experiments (fluorescence recovery after photobleach) revealed that mitochondria had connections already at DIV0 to some extent, which were more pronounced at DIV6, indicating a better exchange rate. The sarcoplasmic reticulum (SR) could only be observed with a fusion protein since no adequate small molecule dye was available. The SR was visible as fine network which was highly organized at DIV1. During culture this organization was lost to some degree, whereas the SR was still distributed and, based on earlier findings in our group, still functioning. The Golgi apparatus was also solely labeled with a fluorescent fusion protein for the same reasons as for the SR. This organelle was initially visible as a vesicular structure evenly spread throughout the cell which was rearranged after one week in culture, where the organelle accumulated around the nuclei. The actin filaments could be labeled with a fluorescent fusion protein facilitating live cell imaging. The actin filaments reflected the organization of the myofilaments and the arrangement was not altered during the week in culture. The supplementation of the culture medium with CytochalasinD which was believed to increase the cellular maintenance, did lead to a reduction of the above

described alterations, but could not inhibit them completely. The alterations observed were very reproducible and thus this culture method is a useful tool for longterm experiments, high content screening experiments or experiments using genetically encoded biosensors.

The second part of my thesis focused on the physiology of cardiac myocytes in particular with  $\text{Ca}^{2+}$  sparks that represent the fundamental  $\text{Ca}^{2+}$  signals of excitation contraction coupling (ECC). The confocal microscope used for the imaging of  $\text{Ca}^{2+}$  sparks comprises a high acquisition rate and sufficient spatial resolution allowing us to record two-dimensional time series with an acquisition speed of about 100 Hz. First a MatLab based analysis algorithm was introduced by Aline Flockerzi which allowed the detection and analysis of  $\text{Ca}^{2+}$  sparks in these two-dimensional time series. I first tested the algorithm with model cells and sparks to subsequently analyze real sparks from mouse myocytes isolated from the three major compartments of the heart, the left and the right atrium and the ventricles. The amplitudes of the left atria were significantly higher than those found in the right atria and both were higher than the amplitudes from ventricular sparks. Decay time constant was the same for both atria whereas the ventricles had a significantly longer decay time. Ventricular sparks also had a larger spatial spread than atrial sparks. These data indicated differences in  $\text{Ca}^{2+}$  handling (increase and removal mechanisms) due to different morphologies and functions of the different compartments of the heart and can be used as a baseline for further analysis of diseased cells.

TRPC1/C4 double-KO (knock-out) mice were analyzed because TRPC channels were thought to be involved in the development of cardiac hypertrophy. First the double-KO were analyzed in comparison to wild-type mice (WT), which revealed that most parameter remained unaltered but the amplitudes in left atria and ventricles were altered due to the KO. Next, the impact of the chronic infusion with isoproterenol, a  $\beta$ -adrenergic agonist which is believed to induce hypertrophy in the heart, was tested in ventricles from WT and KO mice. The treatment induced a reduction of amplitudes in WT but not in KO and a reduction of decay time in KO but not in WT. The spatial spread was increased in WT due to chronic infusion with Isoproterenol. Thus these data showed the involvement of these TRP channels in  $\text{Ca}^{2+}$  handling in mice with and without induced hypertrophy.

Another potential candidate to be involved in the development of cardiac hypertrophy is the Rac1 GTPase, which was analyzed in Rac1 overexpressing mice. Here, again all three major compartments of the heart were analyzed. The most dramatic alterations were

observed within the amplitudes of the sparks from all three heart compartments, which were significantly increased. Decay time was not altered but the spatial spread was reduced in all compartments of the heart due to the Rac1 overexpression. These data demonstrated that the overexpression of Rac1 in myocytes caused alterations of the  $\text{Ca}^{2+}$  handling which were different in the different heart compartments but reflected alterations known from atrial fibrillation (AF).

These data show that the MatLab algorithm is a very useful tool to detect and analyze  $\text{Ca}^{2+}$  sparks in a large number and thus is a useful tool for future studies of different disease models.

### **III. Introduction**

The revolutionary perception of William Harvey in the 17<sup>th</sup> century set the fundamentals for many scientists to study the function of the heart in the following centuries by giving a whole new view on the function of the heart. Although tremendous effort has been put into understanding the physiology and the pathophysiology associated with the circulation and the heart as a pump, many questions remain unanswered.

The fundamental metabolism of each animal, independent of size and organization level, requires nutrition from the outside and consequently needs to dispose the debris. While cells in organs have no or limited access to the environment, they are in need of supply systems like the circulatory system found in animal bodies. This system supplies all cells of the body with metabolic substrates like oxygen, amino acids or glucose and in turn it removes the unwanted residues of the metabolism like carbon dioxide or lactic acid. The blood being pumped throughout the body serves as transport medium for gases, fluids, electrolytes and also heat between the cells comprising organs and the outside.

A major part of this system is the heart which pumps the blood through the body and thus serves as the motor driving the circulation.

## **A. *The Heart***

### **1. Morphology of the Heart**

The heart is the center of the circuit by which the blood is transported through the body. It is located in the chest between the two lungs and is surrounded by the Pericardium, a membrane sac which consists of collagen and elastic tissue. Between the Pericardium and the heart is a serous liquid which ensures proper and inviscid movement of the heart. The circuit it is supplying can be separated into two parts, the first one is the pulmonary circuit and the second is the systemic circuit. The pulmonary circuit, also referred to as the small circuit pumps low oxygenated blood into the lungs where it will be saturated with oxygen and then is transported back into the heart where it will be pushed into the main body arteries with high pressure entering the systemic circuit. These arteries will be split up until only very small vessels are left that can enter the organs that need to be supplied.

The heart itself is a muscular pump which consists of 4 compartments, from which 2 receive the blood from the circuit, the so called atria and two expel the blood with high pressure back into the circuits, the ventricles. The right atrium receives blood from the systemic part of the circulation with low oxygen amount and pumps it into the right ventricle, which then pumps it into the small lung circuit, where the blood will be oxygenated. Coming from the lungs, the blood is received by the left atrium which pumps it into the left ventricle, which has the thickest wall, because the left ventricle pumps the blood back into the body circuit and thus needs to apply high pressure (see also Fig. 1). To assure that the blood cannot flow backwards in the system, special valves are located at each entry and exit of a ventricle. Between the right atrium and the right ventricle the Tricuspid Valve is located at the entry of the right ventricle and consists of three leaflets and three papillary muscles which anchor in the ventricle. The entry to the Pulmonary Artery is guarded by the Pulmonary Valve which has three cusps and is in open state during systole. At the entry of the left ventricle the Mitral Valve is located and consists of two leaflets that are connected to the papillary muscles that anchor in the ventricle, similar to the Tricuspid Valve of the right heart. The entry of the Aorta is guarded by the Aortic Valve that comprises three cusps that open during systole. All valves are located at the cardiac skeleton which provides stability and some electrical isolation for the heart and is situated between the atria and the ventricles.

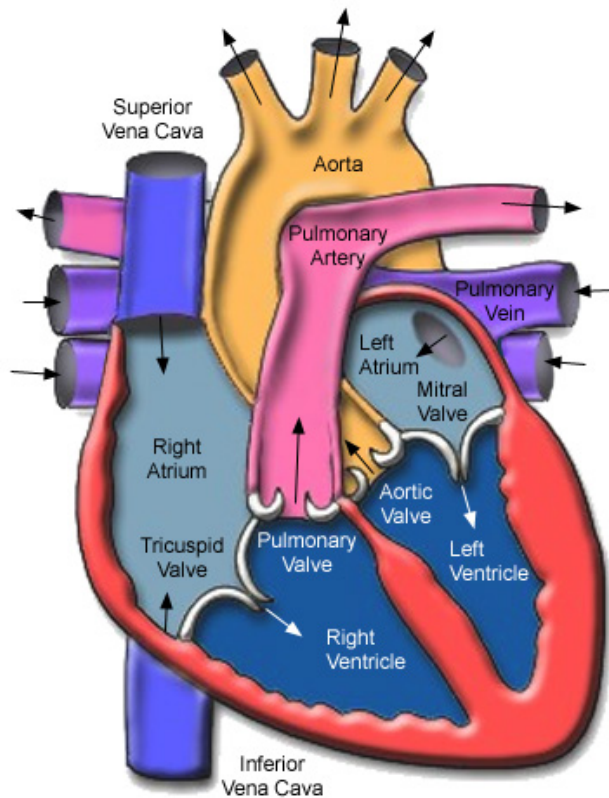


**Figure 1: Graphical illustration of the anatomy of the heart.** A sagittal cross section of the heart depicts the four chambers found in the heart. The right atrium receives blood from the body via superior Vena Cava and pumps it into the right ventricles. Via the pulmonary valve the blood is then pumped with high pressure into the lungs via the Pulmonary Artery. The left atrium receives the oxygenated blood from the lungs via the Pulmonary Vein and then pumps it into the left ventricle, which pumps the blood with high pressure back into the body circuit via the Aorta. Image taken from [www.texasheart.org](http://www.texasheart.org).

The wall of the heart consists of several layers, whereas underneath the Pericardium lies the Epicardium which is a sac of flat mesothelial cells which build the outer shell of the heart. The actual muscle is the Myocardium which consists of the cardiac myocytes. These heart muscle cells are connected via gap junctions at their short ends, allowing them to communicate and propagate signals. These cells are not innervated by motoneurons but are autonomously active. There are different types of myocytes, working myocytes that have a different morphology depending on where they are derived from (atrial cells and ventricular cells) and myocytes attributed to the heart conduction system. Cardiac myocytes are end- differentiated cells so proliferation is no longer possible after the postnatal stage. The innermost layer of the heart wall is the Endocardium which is a smooth inner layer consisting of endothelial cells.

Furthermore there are vessels found in the heart, the largest ones are the main vessels transporting the blood from and towards the chambers, namely the Aorta and the Pulmonary Artery as the arteries and the Pulmonary Veins and the Vena Cava Superior as the veins. The adequate supply of the Myocardium is achieved by the coronary artery system.

Fibroblasts are found within the heart as well, they provide the main source for the formation of the extracellular matrix (ECM) which surrounds the cells. The ECM serves as support for the myocytes and is involved in physiological and pathophysiological processes in the heart. It is composed of a variety of proteins with different functions. There are structural proteins such as collagen and elastin; adhesion molecules such as laminin, fibronectin and certain types of collagen. ECM proteins are also ligands for integrins that are expressed on cell surfaces, by which binding to ECM is managed. There is also an autonomic nervous system in the heart which consists of nerve fibers that are separated from the myocytes by fibroblasts and collagen. Innervation of the heart is achieved by parasympathetic and sympathetic fibers regulating the heartbeat.

## **2. Physiology of the Heart**

The main duty of the heart is to pump blood through the body to ensure the supply of every single cell in the body including the cardiac myocytes themselves. The rhythmic contractions of the heart achieving this duty are referred to as the cardiac cycle. The frequency of these cycles is the heart rate. It can be divided into two phases, the diastolic and the systolic phase. Systole occurs when the ventricles contract and the pressure of the blood system reaches its maximum accordingly diastole represents the phase when the ventricles are fully relaxed and the blood pressure is low.

At the onset of a cardiac cycle the atria are filled with blood, the right atrium receives deoxygenated blood from the systemic part of the circulation via the Vena Cava Superior and at the same time the left atrium receives oxygenated blood from the pulmonary circuit via the pulmonary veins. At this time the ventricles are relaxed and their pressure is lower than the atrial pressure. The atrio-ventricular valves (Tricuspid Valve and Mitral Valve) are open at this time allowing the filling of the ventricles with the blood from the corresponding atria. The flow through these valves is unidirectional, preventing backflow of the blood into the atria. They are closed as soon as the blood pressure in the ventricles

exceeds the pressure in the atria. The pressure in the ventricles and thus the closing of the valves is also volume dependent.

Specialized myocytes responsible for the onset and propagation of an electrical signal will contract at the advent of the systole, leading to a contraction of the atria, which subsequently will press the final blood volume left into the ventricles. This signal which had its beginning at the Sinus Node located in the right atrium is spread throughout both atria and is delayed at the atrio-ventricular Node (AV Node) which is located at the border of the left atrium and ventricle. This ensures a complete contraction of the atria and their depletion. The excitation is then propagated via the Bundle of His and the left and right bundle branches towards the Purkinje Fibers as depicted in Fig. 2. By that both ventricles contract and force the blood with high pressure into the arteries. Shortly after the onset of the ventricular contraction the Pulmonary and the Aortic Valve opens to give way for the blood, allowing a rapid ventricular ejection. Between the closing of the atrio-ventricular valves and the opening of the Pulmonary and Aortic Valves the ventricles are in a short state of isometric contraction (contraction with constant volume).

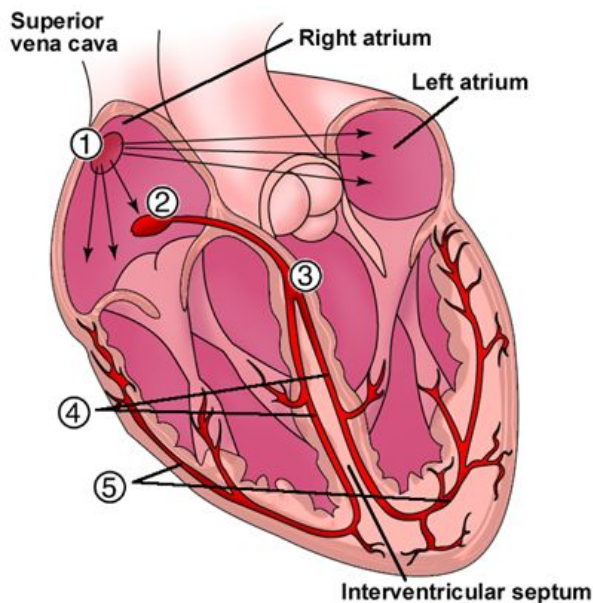


**Figure 2: Schematic drawing of the heart conduction system.** Within the right atrium the Sinus Node is located (1) and its excitation will be spread throughout the atria until it reaches the Atrio-Ventricular Node (AV Node (2)) which will first delay the signal. After complete contraction of the atria the excitation is spreaded via the Bundle of His (3) and the left and right bundle branch (4) in the interventricular septum until it finally reaches the Purkinje Fibers (5) that will lead to a complete ventricular contraction. Image taken from [www.gardenrain.wordpress.com](http://www.gardenrain.wordpress.com).



During the contraction the force of the muscular contraction will be reduced until the pressure of the ventricles falls below the atrial pressure. In order to prevent a backflow the Pulmonary and Aortic Valve will close and since the Tricuspid and Mitral Valves are also still closed, the ventricles again are in an isometric state, this time an isometric relaxation. After repolarization of the ventricles a new circle can begin.

The sound of the valves when snapping shut can be observed and resembles the familiar sound of the heartbeat. Also the electrical signal can be recorded and thus help to assess rhythm disturbances.

### **3. Pathophysiology of the Heart**

Alterations of the above described functions can lead to diseases of the heart. Variations of the rhythm, the frequency or the primary source of excitation are referred to as cardiac arrhythmias.

Arrhythmias can be divided into two groups depending on their origin in the heart as ventricular arrhythmias and atrial arrhythmias. Most of the people sometimes discover arrhythmia in form of one missing beat or an extra strong beat. These forms of arrhythmia can be referred to as harmless or maybe annoying. Ventricular Arrhythmias can be potentially lethal because they can result in cardiac arrest or sudden death within minutes after ventricular fibrillation. But even less severe forms can cause substantial harm in a long term if they affect the gene expression pattern. These long term arrhythmias can also cause hypertrophy or heart failure. Arrhythmia associated with the atria are less detrimental because they are not directly life threatening. Patients with atrial arrhythmia can live many years with the disease without having any severe symptoms. But it is known that atrial arrhythmias can lead to altered gene expression pattern already after minutes on the single cell level, which indicates similar effects in the whole heart. There are several forms of atrial arrhythmia; first one can distinguish between altered excitation patterns that are followed up by the ventricles, such as a moving pacemaker in the atria or premature atrial contraction. In both cases the excitation is transferred to the ventricles. If the frequency of the atrial beat is altered, we can often observe so called AV-blocks that prevent the excitation to jump over to the ventricles. This is the case for atrial tachycardia with atrial beat rates of 150 – 200 per minute, when a partial AV block lets about each second or third excitation pass and the ventricles usually don't follow the atria. Atrial

flutter instead leads to atrial rates of about 250 – 350 beats per minute which in turn causes ventricular rates of about 100 – 150 per minute.

Atrial fibrillation depicted by atrial beat rates of 350 – 600 per minute which can lead to two types of ventricular response, either they display a normal sinus rhythm with about 60 – 70 beats per minute or the rate is increased to about 160 – 180. The reasons for such atrial fibrillation can be found in several excitation origins within the atria and rotating excitation patterns. Another problem here is that the cardiac ejection can be reduced for about 30 % and that the blood flow in the atria is altered. This can easily lead to the appearance of a thrombus. Atrial fibrillation has been classified with respect to the possibility to return to a sinus rhythm into three groups: permanent, when the conversion into a sinus rhythm is not possible; persistent, when the fibrillation can be converted into a sinus rhythm and paroxysmal, when the fibrillation spontaneously returns to a sinus rhythm (Gallagher and Camm, 1997).

The consequences of atrial fibrillation can be quite detrimental but the treatment methods up to date are not very satisfying, since very often only the symptoms are treated to prevent even more detrimental effects such as strokes. The costs of the treatment are high and the effect is often low.

The research on the reasons for cardiac arrhythmia on the cellular level is thus crucial to improve the situation of patients suffering from such heart disease. The reasons for atrial arrhythmias can be manifold and are found among others in cardiac hypertrophy or high blood pressure. But the reasons on the cellular level remain largely elusive. Experimental studies on animal models revealed some role of the small GTP binding protein Rac1 in the development of cardiac disease. It was shown that Rac1 is involved in the onset of dilation and cardiac hypertrophy (Sussman et al., 2000). Rac1 transduces extracellular signals from G-protein coupled receptors and among other signaling pathways activated, its most important function is to regulate cytoskeletal structures. In cardiac myocytes Rac1 is believed to increase ROS production (reactive oxygen species) by activating NADPH (reduced Nicotinamide adenine dinucleotide phosphate) oxidase. Furthermore the overexpression of constitutively active Rac1 has been demonstrated to cause atrial fibrillation in mouse myocytes (Adam et al., 2007). It thus was assumed to be a good model for atrial fibrillation.

## ***B. Cardiac Myocytes***

### **1. Morphology of Cardiac Myocytes**

Cardiac myocytes represent a part of striated muscle cells revealing a cross striation in the microscopic view. Within the heart they form a very specialized syncytium with connections at the short ends building intercalated discs with gap junctions that functionally connect the single cells. These gap junctions ensure electrical coupling of the cells and thus the formation of a functional syncytium.

Ventricular myocytes display a rod shape and clear cross striation. They contain two nuclei whereas atrial cells only got one nucleus. Also the form of atrial cells is different than that from ventricular cell. Atrial cells are thinner and more elongated than ventricular cells but they also have a clear cross striation. This cross striation can be attributed to the sarcomeres in the cells.

The vast majority of the cell volume is taken by the myofibrils that make about 50 % of the cell volume in mouse and rat myocytes, whereas the fraction is higher in atrial cells. The mitochondria, the main energy source take about 20 – 25 % of the total cell volume in atrial cells and about 37 % of the volume in ventricular cells. The transverse tubules (t-tubules) take about 0.2 % of the total volume in atrial cells and in ventricular cells about 1 – 3 % are incorporated by the t-tubules. For the fraction of the total sarcoplasmic reticulum (SR) volume varying data were given independent of the cell type or species, data range from 0.9 – 12.3 % (Bers, 2001).

The morphology of cardiac myocytes is directly linked to its physiological purpose to regularly and continuously contract.

## **2. Physiology of Cardiac Myocytes**

The duty of the heart to pump the blood through the circuit is performed by single cardiac myocytes in the syncytium of the Myocardium. The transition from the electrical signal is transduced into a mechanical contraction. This process is called Excitation contraction coupling (ECC).

### **a) Excitation Contraction Coupling**

Cardiac excitation contraction coupling is strongly dependant on the ubiquitous second messenger  $\text{Ca}^{2+}$  which is translating the electrical activity into the mechanical contraction.

During an action potential  $\text{Ca}^{2+}$  enters the cell via voltage gated  $\text{Ca}^{2+}$  channels, the  $I_{\text{Ca}}$  and activates Ryanodine Receptors (RyR's) in the SR which then activates  $\text{Ca}^{2+}$  release from the SR, which is called  $\text{Ca}^{2+}$  induced  $\text{Ca}^{2+}$  release (CICR). The  $\text{Ca}^{2+}$  then binds to the myofilaments inducing a contraction. After the contraction  $\text{Ca}^{2+}$  is removed from the cytosol by several processes. The most important are the refilling of the stores via a  $\text{Ca}^{2+}$  pump located in the SR (SERCA) and the extrusion out of the cell via the Sodium- $\text{Ca}^{2+}$  exchanger (NCX) in the plasmamembrane. But also mitochondrial uniporter participate in the  $\text{Ca}^{2+}$  removal process but only to a small degree. Fig. 3 depicts the  $\text{Ca}^{2+}$  transport during ECC and the contributing players in the process of ECC. It also depicts the time course of an action potential and the subsequent  $\text{Ca}^{2+}$  signal and the resulting contraction.

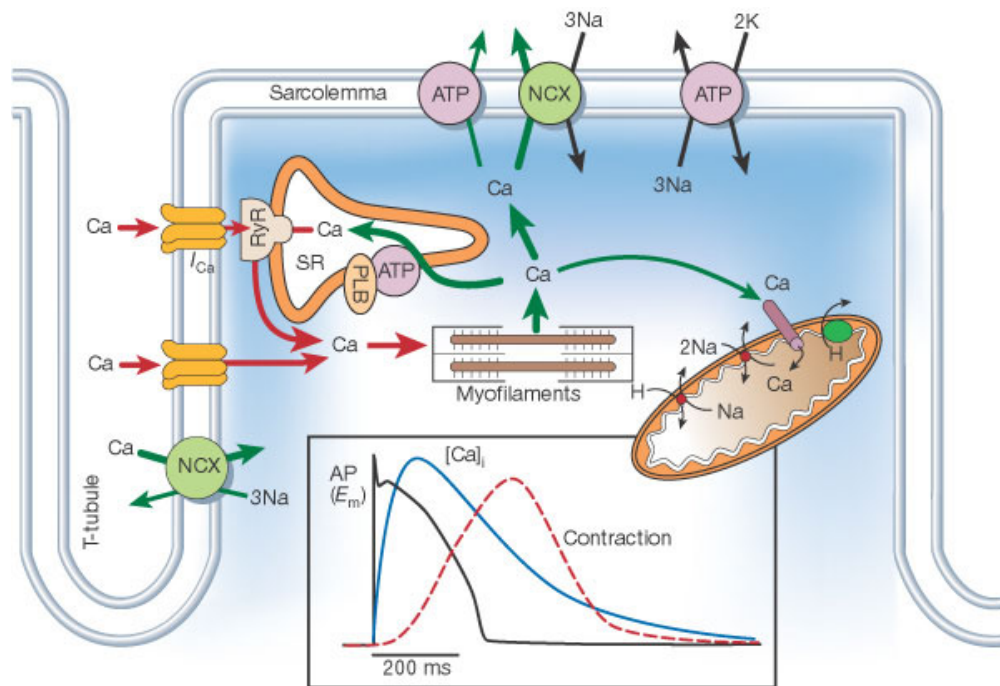


**Figure 3: Ca<sup>2+</sup> transport in ventricular myocytes during ECC.** Ca<sup>2+</sup> enters the cell via L-type Ca<sup>2+</sup> channels that are predominantly located in the t-tubules and leads to CICR from the internal stores by opening of the RyR's. This Ca<sup>2+</sup> causes the contraction due to binding to the myofilaments. Cytosolic Ca<sup>2+</sup> has to be normalized, it is therefore either extruded out of the cell via NCX or Ca<sup>2+</sup> pump or it is pumped back into the SR via the SERCA. Some Ca<sup>2+</sup> is transported into the mitochondria via uniport. Image taken from Bers, 2002 (Bers, 2002).

For ECC in ventricular cells the special morphology of these cells is crucial for CICR. The t-tubules are invaginations of the plasmamembrane that form postnatal by penetrating inward (Di Maio et al., 2007) and contain a large number of proteins contributing to ECC. The t-tubules contain the vast majority of L-type Ca<sup>2+</sup> channels that are responsible for the I<sub>Ca</sub> inducing Ca<sup>2+</sup> release from the stores and a loss of t-tubules subsequently causes alterations in Ca<sup>2+</sup> handling and thus ECC (Brette et al., 2006, Leach et al., 2005, Lipp et al., 1996). The NCX largely contributes to ECC because it transports Ca<sup>2+</sup> out of the cell and thus ensures cytosolic Ca<sup>2+</sup> baseline levels that are crucial for ECC. It has been shown that NCX can modulate the contraction and that is found predominantly within the t-tubules (Fowler et al., 2004, Yang et al., 2002).

The SR as the major Ca<sup>2+</sup> storage organelle is located close to the t-tubules where functional couplings (Moore et al., 1984), the so called dyadic junctions are the sites of CICR. These sites have about 10 – 25 L-type Ca<sup>2+</sup> channels located in the plasmamembrane and about 100 – 200 RyR's on the SR. The opening of the Ca<sup>2+</sup> channels in the membrane causes influx and increase of Ca<sup>2+</sup> in the dyadic cleft (space between SR and plasmamembrane) which then activates a part of the RyR's of the cluster, releasing

$\text{Ca}^{2+}$  from the SR. This  $\text{Ca}^{2+}$  can then bind to troponin C and thus cause a contraction of the cell.

To ensure relaxation  $\text{Ca}^{2+}$  has to dissociate from the troponin. Therefore the  $\text{Ca}^{2+}$  has to be removed from the cytosol by several mechanisms that include extrusion from the cell and transport in to the SR, refilling the internal stores. Removal from the cytosol is achieved by NCX and the sarcolemmal  $\text{Ca}^{2+}$  ATPase. Refilling of the stores is achieved by the activity of SERCA pump, the  $\text{Ca}^{2+}$  ATPase located in the SR membrane. Furthermore  $\text{Ca}^{2+}$  is transported into the mitochondria via uniporters. This fraction of  $\text{Ca}^{2+}$  removal might be irrelevant to ECC since it only contributes with less than 2 % to the  $\text{Ca}^{2+}$  removal but it is important for the activation of certain dehydrogenases increasing the production of NADH and ATP to meet increased energy demands of the cell. The contribution of the described removal mechanisms varies from species to species, e.g. the SR  $\text{Ca}^{2+}$  reuptake contribute with about 92 % to the total  $\text{Ca}^{2+}$  removed in rat myocytes whereas it only contributes with about 70 % in rabbit myocytes (Bers, 2002). Besides the removal of  $\text{Ca}^{2+}$  from the cytosol, the release from the SR has to be terminated in order to reduce cytosolic  $\text{Ca}^{2+}$  concentration. Recent studies have provided evidence that SR  $\text{Ca}^{2+}$  modulates the RyR's and thus terminates SR  $\text{Ca}^{2+}$  release (Zima et al., 2008).

## **b) $\text{Ca}^{2+}$ signaling**

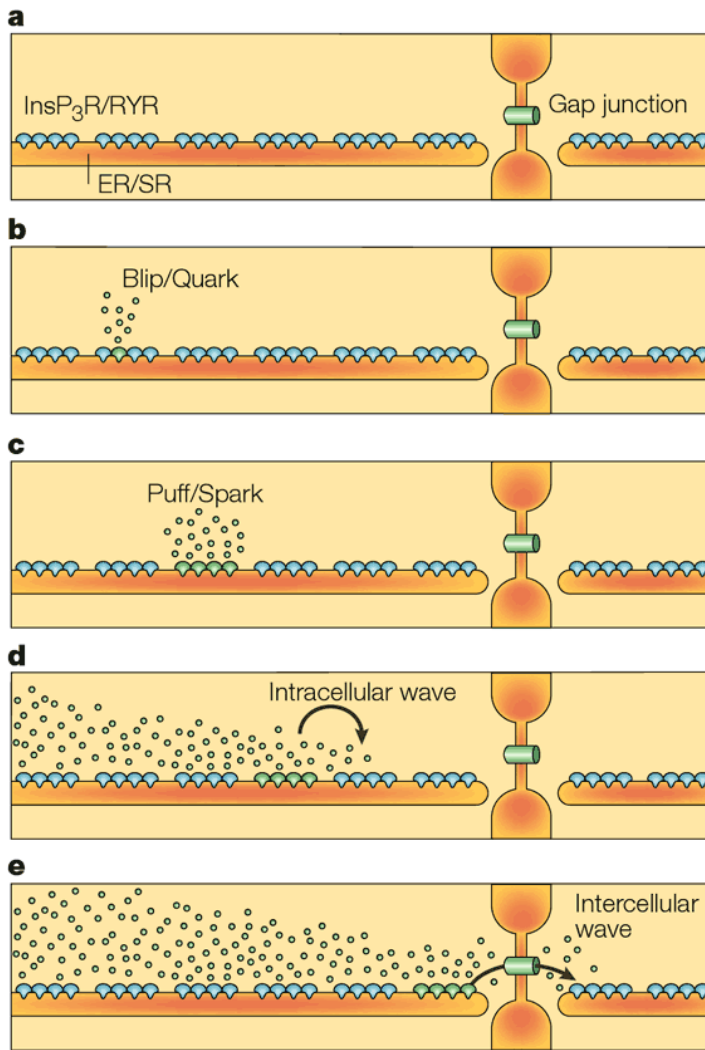
$\text{Ca}^{2+}$  is a universal second messenger involved in various cellular functions. The above described function in ECC reflects one aspect which can be further modulated due to spatial and temporal variations of the  $\text{Ca}^{2+}$  signal.

While a global  $\text{Ca}^{2+}$  signal is the uniform increase of cytosolic  $\text{Ca}^{2+}$  concentration it is known that such a signal is composed of the sum of local release events within a cell. Fig. 5 displays a schematic drawing of the spatial organization of  $\text{Ca}^{2+}$  release events from intracellular stores. Clusters of RyR's represent the  $\text{Ca}^{2+}$  release sites of the SR that consist of a group of single channels located at the dyadic junction.  $\text{Ca}^{2+}$  release from a single RyR is called a quark while the activity of a cluster of RyR's is referred to as a spark. If such a spark activates neighboring clusters via CICR the  $\text{Ca}^{2+}$  signal is spreaded throughout the cell in form of a wave. Since cardiac myocytes are functionally connected via gap junctions at the intercalated discs, the signal can spread to the neighboring cells and thus cause intercellular waves (Berridge et al., 2000). Recent studies revealed that the

intercellular distribution of  $\text{Ca}^{2+}$  is limited to a few cells for spontaneous occurring waves (Baader et al., 2002).

The elementary  $\text{Ca}^{2+}$  signal in cardiac myocytes is a spark and the observation of such an event is only possible with confocal microscopes, which reduce out-of-focus fluorescence and thus are particularly beneficial for thick cells such as myocytes. Sparks are usually described by their amplitude, duration, decay time and their spatial spread but it also is known that these parameters are dependent on some other factors like loading conditions with the  $\text{Ca}^{2+}$  indicator or the filling state of the SR (Niggli and Shirokova, 2007).

While some observations of the fundamental  $\text{Ca}^{2+}$  signals suggested that  $\text{Ca}^{2+}$  derived from the opening of a cluster of RyR's (Lipp and Niggli, 1996, Niggli and Egger, 2002) it was assumed that there are even smaller events underlying a spark. The opening of a single RyR would be a nanoscopic event or a  $\text{Ca}^{2+}$  quark. Using two-photon photolytic activation studies revealed small events that were about 40 times smaller than a spark (Lipp and Niggli, 1998) but computer modeling studies proposed that the release from a single RyR could not be resolved within the noise of a confocal recording (Sobie et al., 2002). Thus the exact properties of a  $\text{Ca}^{2+}$  quark remain elusive since they have not been verified in experimental approaches.



**Nature Reviews | Molecular Cell Biology**

**Figure 4: Spatial organization of  $\text{Ca}^{2+}$  release from internal stores.** RyR's are found in clusters on the SR of cardiac myocytes (a). The  $\text{Ca}^{2+}$  release from a single receptor is referred to as a quark (b) and the release from a cluster of RyR's is called a spark (c). A signal propagating from one cluster to the neighboring throughout the cell is a intracellular wave (d) whereas the propagation of such a wave via gap junctions to the neighboring cell is referred to as a intercellular wave (e). Image taken from Berridge et al. (Berridge et al., 2000).



### **c) Transient Receptor Potential Channels (TRPC's)**

As described above the intracellular  $\text{Ca}^{2+}$  in cardiac myocytes has two origins, SR and the extracellular space. The main entry for  $\text{Ca}^{2+}$  from the extracellular space during ECC is the L-type  $\text{Ca}^{2+}$  channel, but other  $\text{Ca}^{2+}$  channels are found in the plasmamembrane of cardiac myocytes as well. Important players in the regulation of  $\text{Ca}^{2+}$  in cardiac myocytes have been identified in the family of transient receptor potential channels (TRP channels). The superfamily of TRP channels is still growing and a total of 28 members have been identified so far. These members can be further classified by sequence similarities into 7 subfamilies: TRPC (canonical), TRPV (vanilloid), TRPM (from the tumor suppressor melastatin), TRPP (polycystin), TRPML (mucolipin), TRPA (ankyrin) and TRPN (no mechanoreceptor potential C) (Montell et al., 2002).

Functional TRP channels are either homotetramers of 1 type of TRP subunit or heterotetramers of different TRP subunit types. TRP channels form channels that are permeable to  $\text{Ca}^{2+}$  with the exception to TRPM4 and TRPM5. Most of the TRP channels are poorly selective for  $\text{Ca}^{2+}$  and are gated by various stimuli, e.g. temperature changes, chemical or mechanical stress but also the binding of intra- and extracellular messengers, while others appear to be constitutively open.

In the heart members of the TRPC, but also from the TRPV, TRPM and TRPP family have been identified and recently the involvement of TRPC channels in cardiac disease such as hypertrophy has been demonstrated (Nishida and Kurose, 2008, Ohba et al., 2007, Watanabe et al., 2009). TRPC1 was recognized as a store operated  $\text{Ca}^{2+}$  channels (SOC) in cardiac myocytes and was associated in cardiac hypertrophy (Ohba et al., 2007). Furthermore the down regulation of SERCA induced an upregulation of TRPC4 and TRPC5 in failing hearts (Seth et al., 2004).

These studies indicated important regulatory roles of TRP channels in the heart and the involvement in the development of cardiac disease.

### C. *Cell Culture*

In addition to studies on the whole animal or organ level, primary isolated cells have been long standing models to study the detailed physiology but also the pathophysiology in diseased situations. Especially for highly differentiated cells such as smooth muscle cells (Chambers et al., 1999), hepatocytes (Tokiwa et al., 1986) or cardiac myocytes (Eppenberger et al., 1988, Schwarzfeld and Jacobson, 1981) major alteration processes have been described during and/or following acute isolation from the originating tissue.

More than 30 years ago cell isolation procedures for  $\text{Ca}^{2+}$  tolerant rat cardiac myocytes have been introduced (Powell and Twist, 1976) followed a few years later by initial attempts to use such cells in longterm culture (Nag and Cheng, 1981, Schwarzfeld and Jacobson, 1981). All of those studies have reported a significant de- and redifferentiation of cellular and/or subcellular properties of the myocytes. Together with other groups Eppenberger and co-workers have performed seminal work in characterising this process also referred to as *in vitro* remodelling that occurs in cells maintained in medium containing serum (Eppenberger et al., 1988). Further investigations revealed that serum free medium was more appropriate to retain cell morphology. Nevertheless, after a few days even under these conditions, cell dedifferentiation kicked in (Volz et al., 1991). Additionally, newer studies achieved diminished dedifferentiation and characterised remaining alterations of cell morphology and/or physiology (Banyasz et al., 2008, Viero et al., 2008).

Shortly after isolation one of the most pronounced structures of the adult ventricular myocyte, the T-tubular system, has been reported to undergo major remodelling in almost all adult myocytes studied so far. These species include guinea-pig (Lipp et al., 1996), rabbit (Mitcheson et al., 1996) and rat (Banyasz et al., 2008). Nevertheless, this is of particular interest since major steps of cardiac myocyte ECC take place between the plasma membrane and the membrane of the SR, at the dyadic junctions predominantly at the t-tubules. Another important organelle for cardiac function is the SR which primary function is that of a storing organelle for  $\text{Ca}^{2+}$  (Bers, 2002). Not much is known about the structure of the SR in living cardiac muscle cells nor in cultured myocytes, most of the

structural data is either derived from electron microscopy studies (Moore and Ruska, 1957) or indirectly from immunocytochemistry of SR proteins such as SERCA pumps or RyR's.

As a mechanically active cell, cardiac myocytes consume large amounts of ATP which are primarily produced in mitochondria. Beside this, mitochondria serve as a multitude of other functions in the myocytes including the production of reactive oxygen species (Ide et al., 2000, Ide et al., 1999) which appears to be important during many cardiac pathologies and serving as a global and local  $\text{Ca}^{2+}$  buffer. Mitochondria appear to be located on close proximity to local  $\text{Ca}^{2+}$  release sites. This has been suggested for non excitable cells (Quintana et al., 2006) and Michael Duchen has provided seminal work reporting local depolarisations in response to local  $\text{Ca}^{2+}$  release in cardiac muscle cells (Duchen et al., 1998). Despite all of this knowledge the morphology and distribution of mitochondria in cultured adult myocytes and changes thereof are largely unknown but important for their physiology.

Individual cells that have been isolated from tissue or entire organs often serve as single cell *in vitro* models to study their *in vivo* function. For this to be reliable, it is inevitable to gain deep insight into the physiological as well as morphological changes that occur after isolation, a situation that is particularly important for highly specialised cells but too often slightly neglected.

#### ***D. Objectives***

The introduction of improved cell culture systems for adult cardiac myocytes in the recent years (Banyasz et al., 2008, Viero et al., 2008) presented a useful tool for studies on adult cardiac myocytes without the need to freshly isolate cells every day. Culturing of these cells also enables longterm studies applying adenoviral gene transfer to express fluorescent fusion proteins or genetically encoded biosensors. Both will allow the analysis of the physiology and pathophysiology of cardiac myocytes without the necessity to generate transgenic animals for the study of cardiac diseases.

The culture method introduced by Cedric Viero (Viero et al., 2008) was used as the fundament of the present study. It was demonstrated that this method provided sustained cell morphology and physiology of the adult cardiac myocytes and that this method was suitable for the expression of genetically encoded biosensors.

In the present work I wanted to further explore how the culture affects the morphology of the subcellular structures found in these cells. The cells morphology was observed through a confocal microscope with a high spatial resolution and organelle labelling using fluorescent fusion proteins and small molecules dyes. This study aimed to quantify possible residual alterations of the subcellular structures due to the culture and possibly enlighten some of the processes associated with dedifferentiation as a consequence of culturing. The use of fluorescent fusion proteins allows the observation of cell organelles in living cells without the need of fixation, as it would be the case for immunocytochemistry. This approach thus gives information on the real morphology without possible preparation effects due to fixation processes (e.g. the use of chemical fixation). The results from this approach thus might give indications on how the subcellular morphology of cardiac myocytes is arranged in freshly isolated cells, which presumably resemble the situation in vivo better than fixed cell preparations known from electron microscopy studies. Furthermore adaptations to the culture environment can be monitored and analyzed and possible starting points for even further improvements could be identified.

The second part of my thesis focused on the physiology and pathophysiology of isolated cardiac myocytes from adult mice. To study the processes fundamental to ECC, I analyzed  $\text{Ca}^{2+}$  sparks, since it was believed that these local signals represent the fundamental process of ECC in cardiac myocytes. The technique of confocal microscopy with high spatial and temporal resolution set the baseline for the recording of  $\text{Ca}^{2+}$  sparks in two-dimensional time series. This technical tool denotes the possibility to study  $\text{Ca}^{2+}$  sparks in more detail especially with respect to their spatial properties. This required an analysis tool other than a line scan analysis. Therefore a MatLab based spark algorithm was introduced in our group, which first had to be evaluated and was subsequently used to analyze data derived from mouse myocytes. I described the properties of  $\text{Ca}^{2+}$  sparks in myocytes from both

atria and the ventricles and compared the results. These findings set the basis for the analysis of sparks in different mouse models for cardiac hypertrophy.

I have chosen to work with cardiac myocytes from rat and from mice, because at this point the culturing of mouse myocytes is still more difficult than the culturing of rat myocytes. But the long term culturing of myocytes is an important tool for the analysis of different models for cardiac diseases. For the analysis and evaluation of  $\text{Ca}^{2+}$  sparks the cells from mice were preferred, because further analysis of the fundamental  $\text{Ca}^{2+}$  signals in disease models will also require the use of genetically modified animals, which are mostly available in mice.

## IV. Material and Methods

### A. *Adult Rat Cardiac Myocytes*

The isolation and cultivation of ventricular myocytes from adult rats was performed according to the protocol published in Viero et al. (2008), in summary:

For the purpose of preparing and maintaining a primary cell culture system consisting of ventricular myocytes, adult male Wistar rats of age 6 to 12 weeks corresponding to 200 g to 400 g respectively met the conditions of the experiments. After sedation with CO<sub>2</sub>-gas the animals were anaesthetized with an intraperitoneal injection of pentobarbital-sodium (Narcoren, Merial, Germany; 160 mg/kg bodyweight) or a mixture of ketamin (Ursotamin®, Serumwerk, Germany; 968 mg/kg bodyweight) and xylazine (Rompun®, Bayer AG, Germany; 47 mg/kg bodyweight), respectively. The first animals were anaesthetized with Narcoren but due to the characteristic of barbiturates to cause respiratory depression, the anesthetic was switched to the mixture of ketamin and xylazine. Cells isolated from both groups did not show any significant differences in morphology or physiology.

To prevent clotting of the blood, 2.9 mg sodium citrate, dissolved in 250 µl 0.9 % sodium chloride solution were also injected intraperitoneal.

The animals were finally sacrificed by cutting through the arteria carotis communis. After flushing the heart with ice cold Ca<sup>2+</sup>-free solution (Tab.1), it was attached to a modified Langendorff-apparatus to retrograde perfuse the heart with an oxygen saturated Ca<sup>2+</sup>-free solution containing 200 µM EGTA (ethylene glycol tetraacetic acid) for 5 min at room temperature (RT) with a flow rate of 4 ml/min. Subsequently the solution was changed to a Collagenase-mix (Liberase Blendzyme 4, Roche, Germany; 0.35 mg/ml) which digested the tissue within 25 minutes at nominally 37°C. After removing the heart from the Langendorff-apparatus, the ventricles were liberated from the atria, the valves and the vessels and subsequently cut into pieces to further digest the tissue in the enzyme solution. The supernatant was discarded and the pellet suspended in nominal Ca<sup>2+</sup> free solution (Tab.1). The pellets were incubated for 5 min at 37°C and constantly agitated within a water-bath. This procedure was then repeated 2 times in low Ca<sup>2+</sup> solution and one time in high Ca<sup>2+</sup> solution (Tab.1). Finally the pieces were carefully triturated to isolate the

single cells from the tissue pieces. The supernatant, now containing viable cells was then further diluted with high  $\text{Ca}^{2+}$  solution.

Cells were plated on glass-cover slips coated with an extracellular matrix protein mix (ECM; 1.11 mg/ml, Harbour Bio-Products, Norwood, MA, USA or ECM gel 0.33 mg/ml, Sigma, USA) in 12-well plates. First experiments were performed on cover slips coated with ECM from Harbour Bio-Products until it was no longer available and thus ECM from Sigma was used. Cells showed no significant differences on both coatings. The ventricular myocytes were kept in medium M199 with Earle's modified salts and glutamine (Biowest; Nuaille, France) supplemented with 100  $\mu\text{g/ml}$  Penicillin/Streptomycin, 50  $\mu\text{g/ml}$  Kanamycin (PAA Laboratories, Austria) and 870 nM Insulin, 65 nM Transferrin and 29 nM Na-Selenite (Sigma, USA) (ITS supplemented medium) in an incubator at 37°C, 5%  $\text{CO}_2$  atmosphere and saturated humidity for up to 1 week. The medium was changed after plating at 1 hour, day *in vitro* (DIV) 1 and 3.

All measurements were performed in normal tyrode's solution described in table 1 at pH 7.35 if not stated otherwise. Monitoring of the isolation process and cell length measurements were performed with a Nikon Eclipse TS 100 inverted microscope connected to a Nikon Digital Net Camera DN 100.

## **B. Adult Mouse Cardiac Myocytes**

For the purpose of isolating adult mouse myocytes, adult mice of age 6 to 10 weeks or 20 to 25g respectively were sacrificed. The animals were anaesthetized with an intraperitoneal injection of a mixture of Ketamin (Ursotamin®, Serumwerk, Germany; 85 mg/kg bodyweight) and Xylazine (Rompun®, Bayer AG, Germany; 15 mg/kg bodyweight), the preparation of the heart and the subsequent digestion at the Langendorff-apparatus were performed using the protocol for the isolation of rat ventricular myocytes described above. In contrast to this protocol, the enzyme concentration was 0.15 mg/ml and the digestion time was 12 min with respect to the smaller hearts of the mice.

After removing the heart from the Langendorff-apparatus, the heart was divided into the ventricles and the two atria. The ventricles were cut open, but not into separate pieces. The supernatant, still containing the enzyme, was discarded and the heart slowly agitated in nominal  $\text{Ca}^{2+}$  free solution containing 0.045% DNase, which was distributed in a 12-

well plate supplemented with coated glass cover slips. The supernatant was carefully discarded and each well was filled with 1.5 ml fresh nominal  $\text{Ca}^{2+}$  free solution containing 0.045% DNase.  $\text{Ca}^{2+}$  increase was achieved by adding 10 times 150  $\mu\text{l}$  high  $\text{Ca}^{2+}$  solution at intervals of 5 minutes each. When the final  $\text{Ca}^{2+}$  concentration was reached, the solution was exchanged by Medium M199 prepared as described above.

The atria were placed separately in small petri dishes with approx. 3 ml enzyme solution to further digest the tissues for a minimum of 20 minutes in the incubator at 37°C. The digestion was completed when the tissue released viable atrial myocytes. After that the atria were transferred into 500  $\mu\text{l}$  of a nominal  $\text{Ca}^{2+}$ -free solution containing 0.09% DNase. For the  $\text{Ca}^{2+}$  increase 50  $\mu\text{l}$  high  $\text{Ca}^{2+}$  solution was added 10 times at intervals of 5 minutes. The cell suspension was distributed to 6 wells of a 12-well plate with coated coverslips and after 1 hour of settlement, the suspension was exchanged for Medium M199, prepared as described above.

**Table1:** Composition of the solutions used for the isolation of adult ventricular myocytes of rats and mice

	<b><math>\text{Ca}^{2+}</math> free solution</b>	<b>Low <math>\text{Ca}^{2+}</math> solution</b>	<b>High <math>\text{Ca}^{2+}</math> solution</b>	<b>Tyrode's solution</b>
<b>substance</b>	<b>concentration [mM]</b>			
NaCl	134	134	134	135
$\text{CaCl}_2$	0	0.1	0.2	1.8
glucose	11	11	11	10
KCl	4	4	4	5.4
$\text{MgSO}_4$	1.2	1.2	1.2	-
$\text{Na}_2\text{HPO}_4$	1.2	1.2	1.2	-
HEPES	10	10	10	10
DNase	0	0.045%	0.09%	-
$\text{MgCl}_2$	-	-	-	1



### ***C. Adenovirus Constructs and Transfection***

To express fluorescent fusion proteins in cardiac myocytes, a transfection system had to be established since adult cardiac myocytes are end-differentiated cells that are no longer able to proliferate. For such cells most of the commonly used transfection systems such as chemically driven transfection or electroporation are not suitable. Chemically driven systems do not work on highly differentiated cells that cannot divide and electroporation is too inefficient and harmful to cardiac myocytes. The best approach to efficiently transfect cardiac myocytes was to use viral gene transfer systems. Here the two suitable virus systems for adult myocytes tested in our laboratory were lentiviral or adenoviral driven methods, because these viruses efficiently transfect also end-differentiated cells. In our group the adenovirus was chosen because it led to expression after 24 h in contrast to lentiviruses that needed at least 72 h. Also for adenoviral driven gene transfer the transgene virus does not integrate itself into the genome, which ensures that no side effects occur due to the random nature of gene integration into the genome.

Adenoviruses were constructed as described earlier (Viero et al., 2008) using the Transpose-Ad<sup>TM</sup> Adenoviral Vector System (MP Biomedicals, USA), which is a Tn7-based transposition system for generating recombinant adenoviruses. Generation of the adenoviruses was performed by Sandra Ruppenthal and Anke Scholz following the protocol provided by the company, shortly described below and visualized in Fig. 1. First, the gene of interest had to be cloned into a Transpose-Ad<sup>TM</sup> Transfer Vector. HighQ-1 Transpose-Ad<sup>TM</sup> 294 competent cells were transformed with this vector as depicted on the upper part of Fig. 1. Subsequently these cells were plated on LB-plates containing Bluo-gal (300 µg/ml), IPTG (isopropyl-beta-D-thiogalactopyranoside; 40 µg/ml) and antibiotics (chloramphenicol: 20 µg/ml; tetracycline: 15 µg/ml; ampicilin: 100 µg/ml). A positive cell should contain the Transpose-Ad<sup>TM</sup> 294 Vector with the adenoviral genome and a resistance against chloramphenicol, the helper plasmid, coding for the transposase with a resistance against tetracycline and the Transposase-Ad<sup>TM</sup> Transfer Vector with the gene of interest and an ampicilin resistance. As a result of the transposition of the introduced sequence into the virus genome, the LacZ gene on the Transpose-Ad<sup>TM</sup> 294 plasmid was disrupted. Positive recombinants appeared as white colonies which then had to be picked. Here we performed colony-PCR to decide from which cells a DNA-isolation was performed. The isolated DNA from positive colonies was then transformed into DH5α-cells and plated on chloramphenicol-containing plates. To select only those colonies that contained solely the

Transpose-Ad™ 294 Vector with the gene of interest, colonies were distributed on plates with chloramphenicol, ampicillin or tetracycline, respectively. Colonies growing exclusively on chloramphenicol plates were used for Maxiprep DNA-isolation. After linearization with *Pac* I QBI-HEK 293 packaging cells were transfected (see also Fig. 5) to generate the recombinant adenovirus expressing the desired gene product. Viral plaque formation occurred between 7 and 21 days after transfection. The culture medium where the cells were growing in contained the virus and was collected. To increase the yield it was possible to disrupt the cells, also containing virus, by several freezing and thawing steps. The medium was centrifuged to remove cell fragments and other unwanted residues from culturing. This virus containing solution was stored at -80°C and could be directly used for transfection of cardiac myocytes.

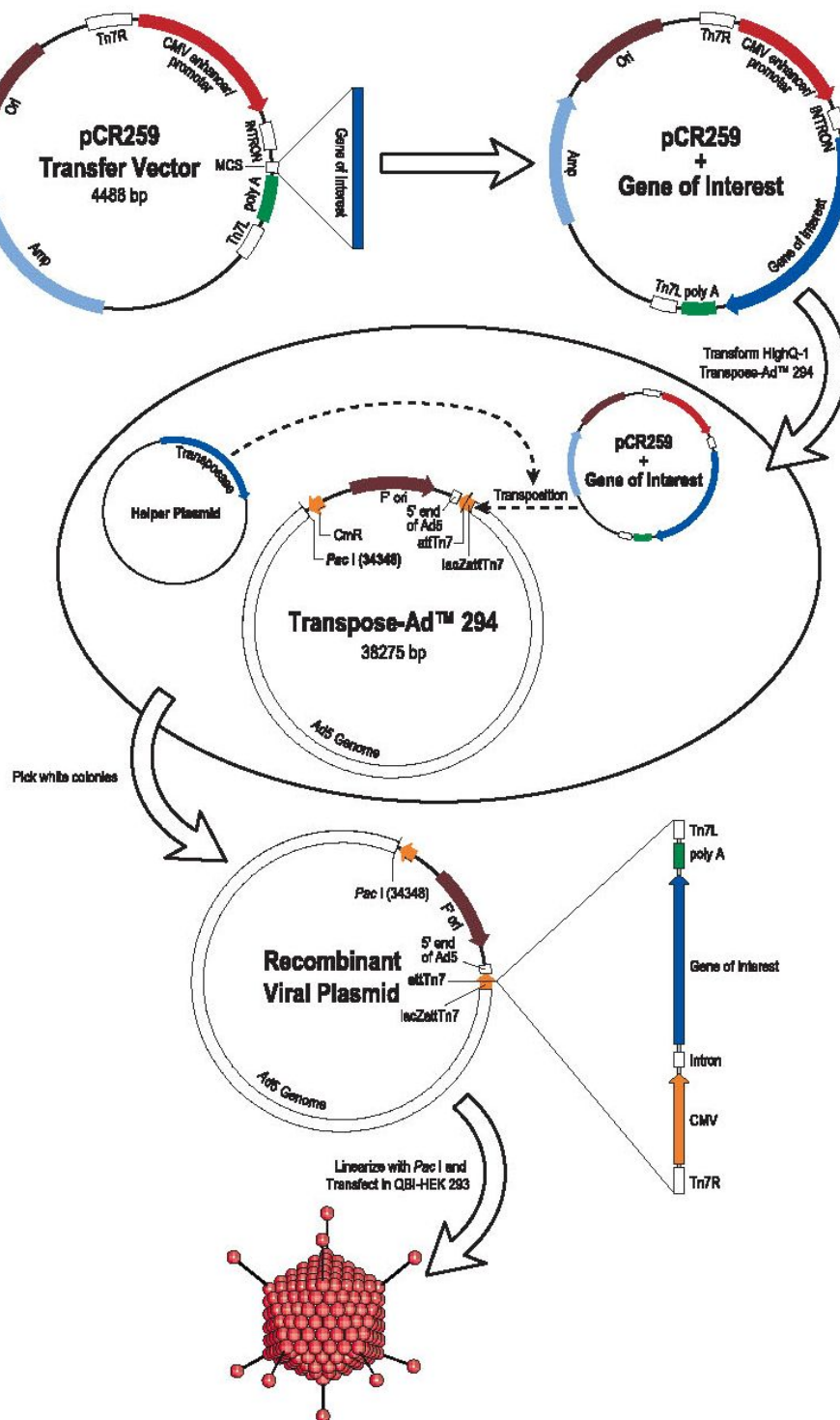


**Figure 5: Generation of recombinant adenoviruses using the Transpose-Ad™ system.** The gene of interest was cloned into a Transpose-Ad™ transfer vector which was subsequently transformed into HighQ-1 Transpose-Ad™ competent cells. After selection and DNA-isolation positive clones were transformed in DH5α cells and after selection, DNA isolation of the positive clones was performed. DNA was linearized using *Pac I* and transfected in QBI-HEK 293 packaging cells, which then generated the viruses. (Figure taken from: Transpose Ad™ Adenoviral Vector System, Application Manual, Version 1.1, Q-Biogene, CA, USA)

Vectors for the following fusion proteins were used for the construction of recombinant adenoviruses also shown in Fig. 6: to label ER/SR dSRed2 was fused between the C-terminal end of the endoplasmic reticulum localisation sequence of Calreticulin and the N-terminal end of KDEL (ER-retrieval sequence); to label mitochondria dSRed1 or eGFP was fused to the C-terminal end of subunit VIII of human cytochrome C oxidase targeting sequence (both constructs have been prepared in our lab and were used for these experiments; no differences were observed between the two fluorescent fusion proteins, which approximately had the same size as depicted in Fig. 6); labelling the Golgi Apparatus was achieved by fusing a YFP to ts045G (temperature sensitive glycoprotein of vesicular stomatitis virus) (Scales et al., 1997); to label lipid rafts within the plasma membrane a YFP was fused at the N-terminal of a GPI sequence (Keller et al., 2001). For the visualization of the filamentous actin a mRuby was fused to the terminus of Lifeact (the first 17 Amino acids of Actin binding protein 140, labelling F-actin) (Riedl et al., 2008). The excitation and emission maxima of the fluorescent proteins are give in table 2 as well as the laser wavelength used for excitation. For all constructs a double dichroic mirror was used which let wavelengths from 510 – 550 nm and > 580 nm pass towards the detector.

**Table 2:** Excitation and Emission Peaks of the fluorescent proteins used for the detection of cell organelles.

<b>Fluorescent Protein</b>	<b>Laser</b>	<b>Excitation Maximum</b>	<b>Emission Maximum</b>
dSRed2	561 nm	563 nm	582 nm
eGFP	488 nm	488 nm	507 nm
YFP	488 nm	514 nm	527 nm
mRuby	561 nm	558 nm	605 nm

All fluorescent fusion proteins used had a DNA sequence length in the range of 738 to 807 bp except for the golgi apparatus with a length of 2385 bp (Fig. 6). The expression of these proteins did not alter the cells physiology or morphology of the cardiac myocytes.

The transfection of the cultured rat myocytes was performed 1 h after the plating of the cells with a multiplicity of infection (MOI) of 5-20 plaque forming units/cells. Cells were

incubated with the viruses for 24 h at 37°C and 5% CO<sub>2</sub> atmosphere and saturated humidity, before the medium was exchanged for a virus free medium.

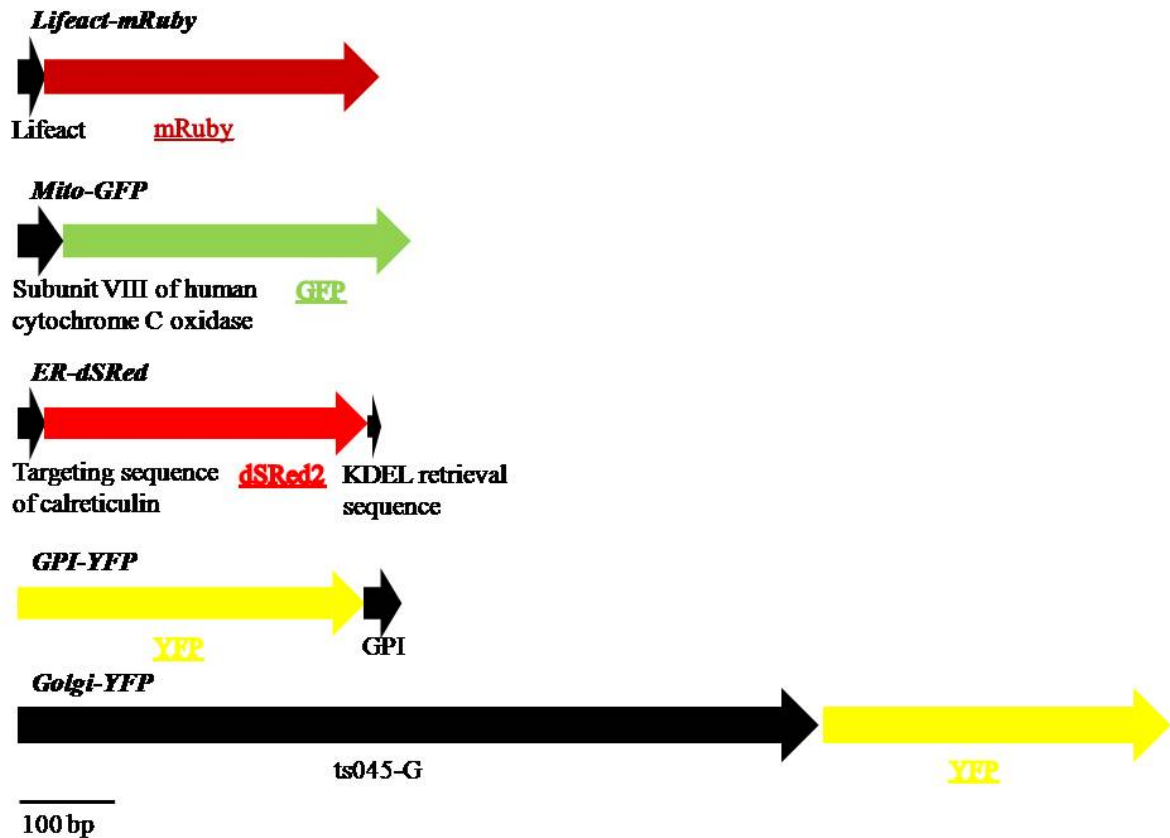


**Figure 6: Schematic design of the DNA-sequence of the fluorescent fusion proteins.** All constructs are drawn from 5' to 3'. Black arrows depict the targeting sequence and the fluorescent proteins (FP's) are shown in corresponding colours (green for GFP, red for dsRed2 and mRuby and yellow for YFP). Lifeact-mRuby, Mito-GFP and Golgi-YFP are C-terminal FP fusions; GPI-YFP is a N-terminal FP fusion and for ER-DsRed the FP is located C-terminal to the localization sequence and N-terminal to the retrieval sequence. The DNA sequence of the FP's have approximately the same size (GFP and YFP: 720 bp; DsRed2: 672 bp; mRuby: 693 bp) as well as most of the targeting sequences (Lifeact: 51 bp; Mito: 87 bp; GPI: 69bp; ER: 51 bp + KDEL: 15 bp) except the sequence for the golgi apparatus with a length of 1665 bp.

#### D. *Fluorescent small molecule dyes*

In addition to the fluorescent fusion proteins fluorescent dyes were used to visualize cell organelles. This enabled us to estimate the impact of the adenoviral gene transfer on the cultured cardiac myocytes and allowed the labelling of sub-cellular structures even in freshly isolated cells. All dyes described below were first dissolved in Pluronic<sup>®</sup> (20% in Dimethylsulfoxide (DMSO); Molecular Probes, USA) to a stock solution of 1 mM. These stock solutions were stored at -20°C and thawed preparing the working solutions.

Labelling of the plasma membrane was achieved using the membrane potential sensitive dye Di-8-ANEPPS (Molecular Probes, USA) with the advantage that it is only very slowly internalized and thus exclusively labeled the plasma membrane accessible from the outside of the cell (S. et al., 1992). Cells were incubated with 2.5  $\mu$ M Di-8-ANEPPS for 10 minutes at room temperature. Excitation wavelength was 488 nm and peak emission was at 650 nm as depicted in Fig. 7. Experiments with Di-8-ANEPPS were performed in nominal  $\text{Ca}^{2+}$ -free solution to reduce moving artefacts. This solution corresponds to normal tyrode's solution without the addition of  $\text{CaCl}_2$ .

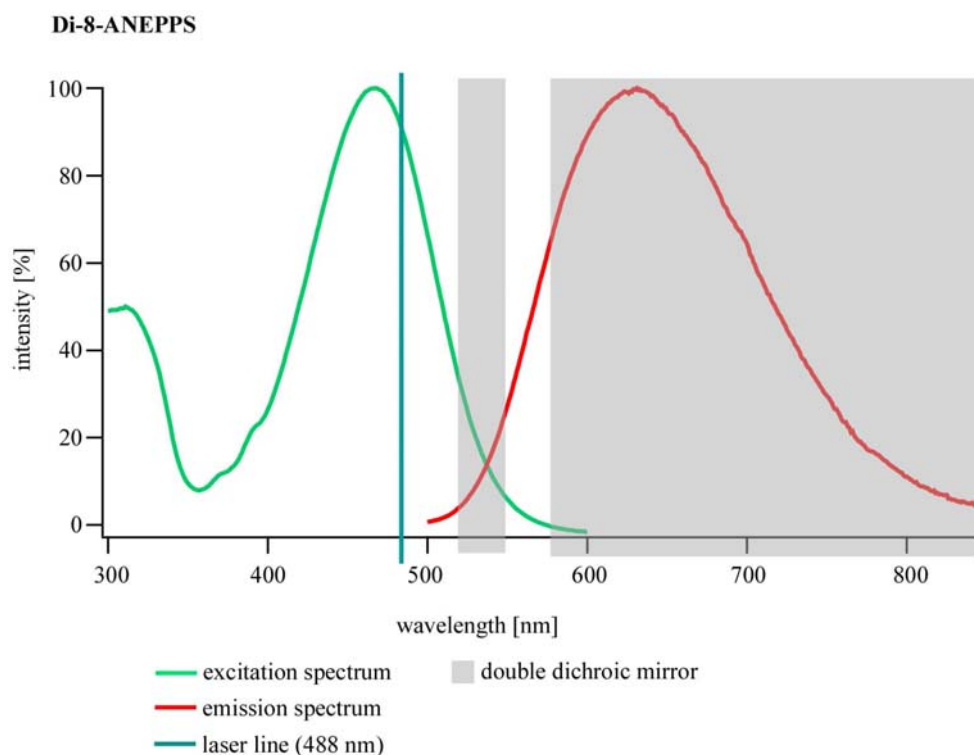


**Figure 7: Excitation and Emission Spectra of lipid bound Di-8-ANEPPS.** The green line depicts the emission spectrum of lipid bound Di-8-ANEPPS. The blue line depicts the excitation wavelength of the laser which was used. The red line depicts the excitation spectrum. The grey underlay indicates the wavelengths that were allowed to pass the double dichroic mirror located between the two spinning discs (see also Fig. 12).

For visualization of mitochondria, MitoTracker<sup>®</sup> Green was used (Molecular Probes, USA) at a final concentration of 1  $\mu$ M for 30 minutes at room temperature. The excitation- and emission- spectra are shown in Fig. 8 together with the laser and the double dichroic mirrors used for these experiments.

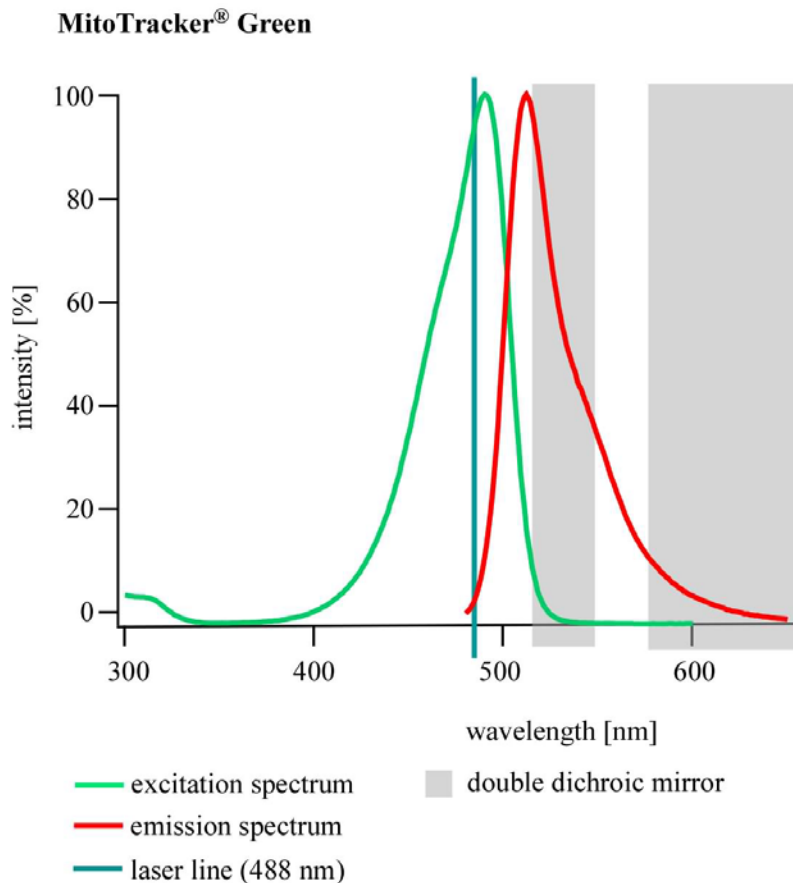


**Figure 8: Excitation and Emission Spectra of MitoTracker<sup>®</sup> Green.** The green line depicts the emission spectrum of MitoTracker<sup>®</sup> Green. The blue line depicts the excitation wavelength of the laser which was used. The red line depicts the excitation spectrum. The grey underlay indicates the wavelengths that were allowed to pass the double dichroic mirror located between the two spinning discs (see also Fig. 12).

ER-Tracker™ Green (Molecular Probes, USA) was used to label the sarcoplasmic reticulum. It is the drug conjugate glibenclamide BODIPY® FL. The cells were incubated for 30 min with a 1  $\mu$ M solution at RT.

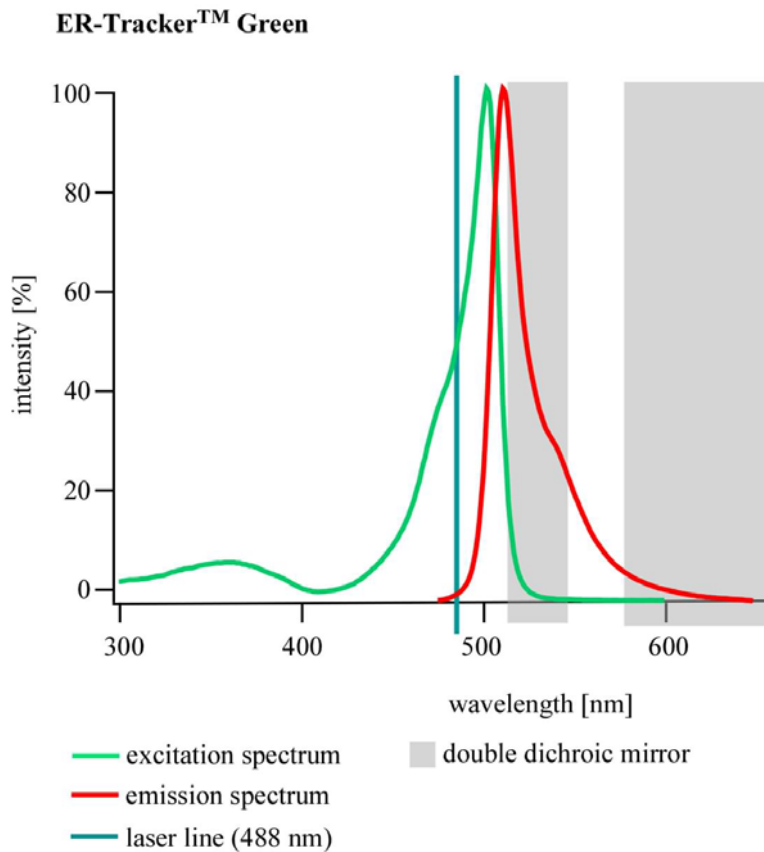


**Figure 9: Excitation and Emission Spectra of ERTracker™ Green.** The green line depicts the emission spectrum of ERTracker™ Green. The blue line depicts the excitation wavelength of the laser which was used. The red line depicts the excitation spectrum of the dye. The grey underlay indicates the wavelengths that were allowed to pass the double dichroic mirror located between the two spinning discs (see also Fig. 12).



BODIPY TR C<sub>5</sub> (Molecular Probes, USA) was the small molecule dye labelling the Golgi apparatus. It is the drug conjugate glibenclamide BODIPY<sup>®</sup> FL and was employed at a final concentration of 5 μM at RT. Incubation was performed to the following protocol: first cells were incubated for 30 min at 4°C, then they were washed 2 times with ice cold tyrode's solution and subsequently warm tyrode's solution had to be added and incubated for 30 min at 37°C and finally a washing step with tyrode's solution finalized the procedure. The dye was excited with a 561 nm laser although the excitation maximum was 589 as shown in Fig. 10.

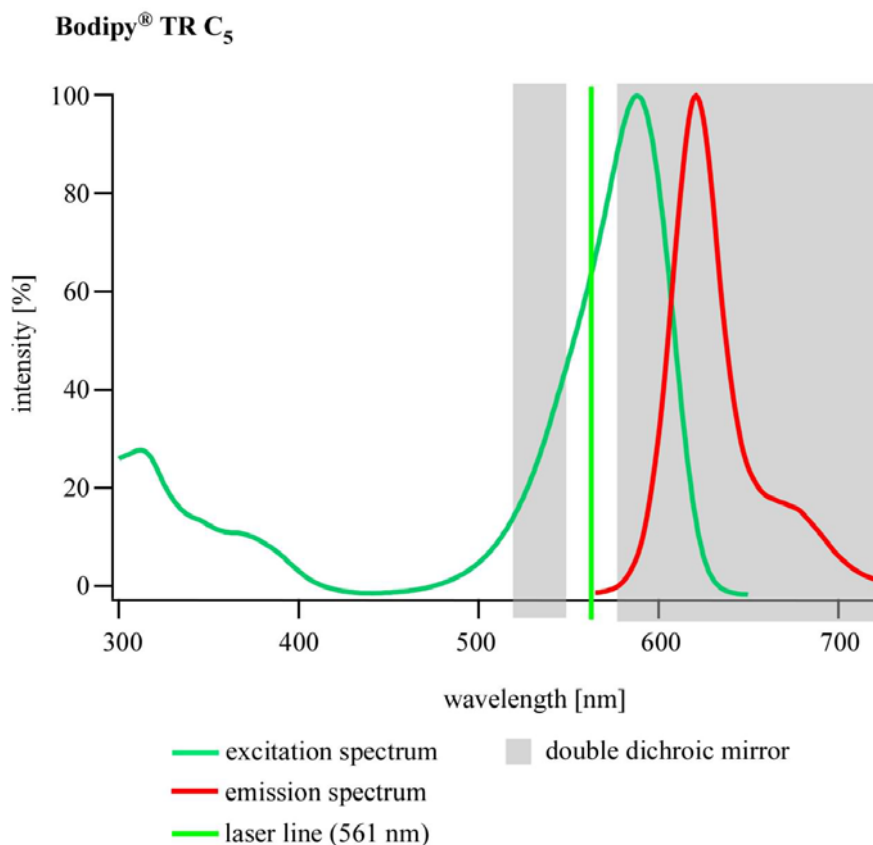


**Figure 10: Excitation and Emission Spectra of BODIPY TR C<sub>5</sub>.** The green line depicts the emission spectrum of BODIPY TR C<sub>5</sub>. The blue line depicts the excitation wavelength of the laser which was used. The red line depicts the excitation spectrum. The grey underlay indicates the wavelengths that were allowed to pass the double dichroic mirror located between the two spinning discs (see also Fig. 12).

Ca<sup>2+</sup> imaging experiments were performed on cells loaded with the Ca<sup>2+</sup> indicator Fluo4-AM (Molecular Probes, USA) at a final concentration of 1.5 μM for 30 min at RT followed by a 20 min deesterification period at RT in tyrode's solution. Excitation and emission spectra for Ca<sup>2+</sup>-bound Fluo4 are shown in Fig. 11.

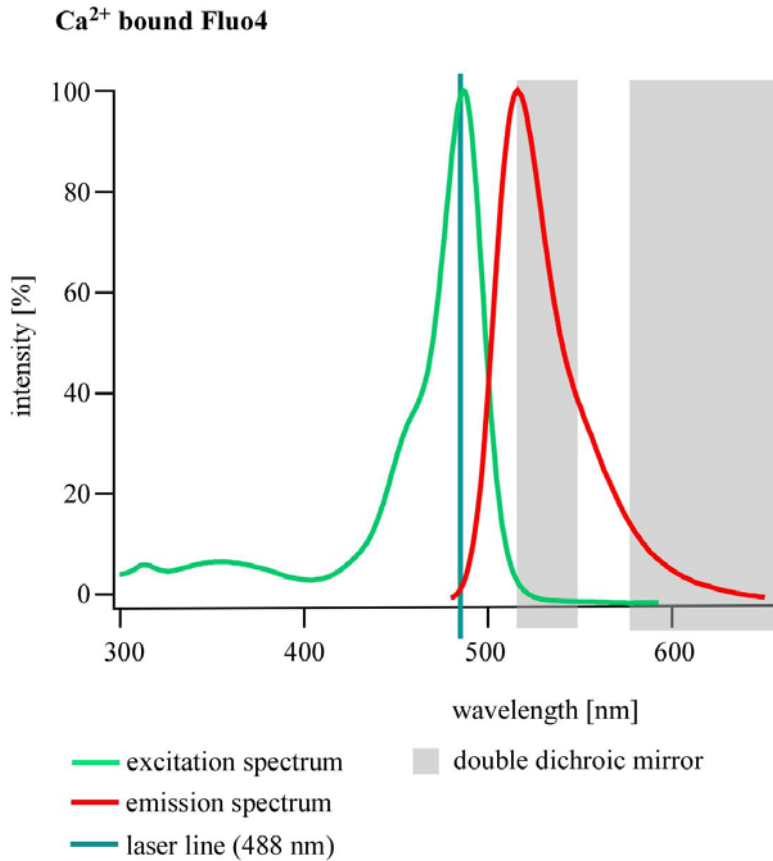


**Figure 11: Excitation and Emission Spectra of Ca<sup>2+</sup> bound Fluo4.** The green line depicts the emission spectrum of Fluo4 bound to Ca<sup>2+</sup>. The blue line depicts the excitation wavelength of the laser which was used. The red line depicts the excitation spectrum. The grey underlay indicates the wavelengths that were allowed to pass the double dichroic mirror located between the two spinning discs (see also Fig. 12).

In control experiments with fluorescent fusion proteins and small molecule dyes the specific labelling was evaluated. Table 3 displays the two methods used for each cell organelle where possible. There was no life cell dye available for actin.

**Table 3:** Labelling methods for the visualization of single cell organelles in isolated and cultured adult cardiac myocytes

Cell Organelle	Fluorescent Fusion	
	Protein	Small Molecule Dye
Endo- / Sarcoplasmic Reticulum	ER-dSRed2	ER-Tracker Green
Golgi Apparatus	ts045G-YFP	Bodipy TR C <sub>5</sub>
Plasma Membrane	GPI-YFP	Di-8-ANEPPS
Mitochondria	Mito-dSRed1	MitoTracker <sup>®</sup> Green
Actin	Lifeact-mRuby	Life cell dye not available

### ***E. Confocal Microscopy***

The morphological studies in adult rat ventricular myocytes in long term culture were performed with confocal microscopy. All morphological experiments required a high spatial resolution which was given by a laser scanning confocal microscope comprising a scanning head (QLC-100, VisiTech International, UK) attached to an upright microscope (Eclipse 600, Nikon, Japan) and two CCD-cameras for detection (Orca-ER, Hamamatsu Photonics, Japan). The QLC-100 is a Nipkow-disc based confocal microscope. The spinning discs within the light path of the microscope consist of an arrangement of micro lenses and pinholes, respectively (Fig. 12). For the excitation of the fluophores two different solid state lasers were attached to the microscope via optical fibers emitting wavelengths of 488 nm (Sapphire 488-30, Coherent, USA) and 561 nm (85-YCA-015, Melles Griot, USA).

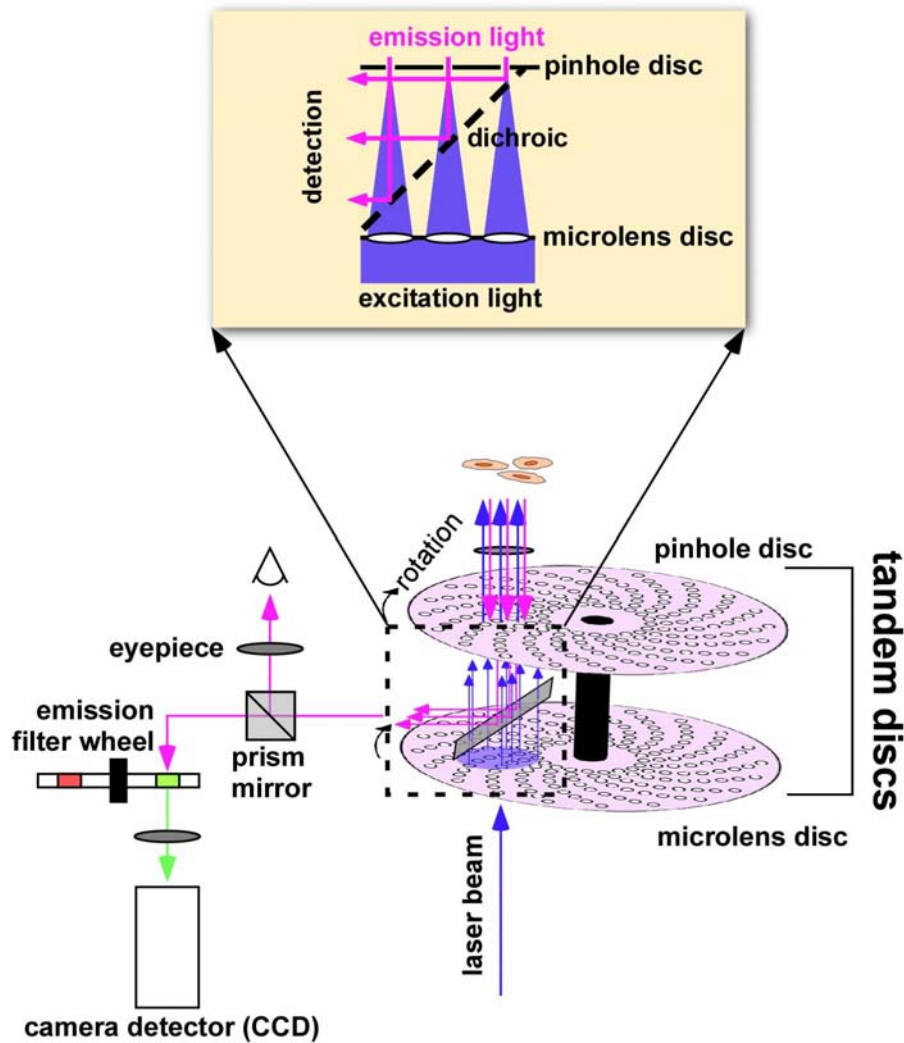


**Figure 12: Beam path of a Nipkow-disc based confocal microscope.** The laser beam (excitation beam; blue) enters the microlens disc where the excitation beams are focused onto the pinholes after passing a dichroic mirror. The emission beams (pink) are guided towards the same pinholes the excitation beams were passing to exclude scattered light from out-of-focus planes within the specimen. The dichroic mirror between the two discs guides the emission beam towards the CCD-camera or the eyepiece. Figure taken from Lipp P and Kaestner L (2006), Wiley-VCH.

Imaging was performed through a 100x water immersion objective (Plan 100x/1.10 W, Nikon, Japan). In order to acquire 3D-images of the sub cellular structures, z-stacks had to be taken with a step size of 0.2-0.3  $\mu\text{m}$  by the use of a piezo-controlled z-stepper (PiFoc, Physics Instruments, Germany). For that purpose the lowest and upmost position of the stack were defined. To achieve the highest possible spatial resolution, no binning was set to the camera, if the labelling intensity was high enough, if this was not the case the binning was set to 2 which lead to a pixel size of 0.066  $\mu\text{m}$  and 0.132  $\mu\text{m}$  (x and y direction), respectively.

The plated cells were transferred to custom made experimental chambers where the loading of the cells as well as the subsequent measurements were performed. Before starting an experiment the settings of the microscope had to be defined. Fig. 13 depicts a screenshot of the VoxCell Software for controlling the microscope (VisiTech International, UK). The properties of the Acousto Optic Tunable Filter (AOTF), camera properties and microscope properties can be stored and reused for the next experiments. First one had to define the AOTF properties, where the laser wavelength and intensity was chosen, and then the camera properties were set. One had to choose the camera and define exposure time and binning rate. Amplification and light mode were by default set to ‘maximum’ and ‘low’, respectively. The microscope properties allowed defining settings for z-stack capture which subsequently were automatically used when the protocol was set up.

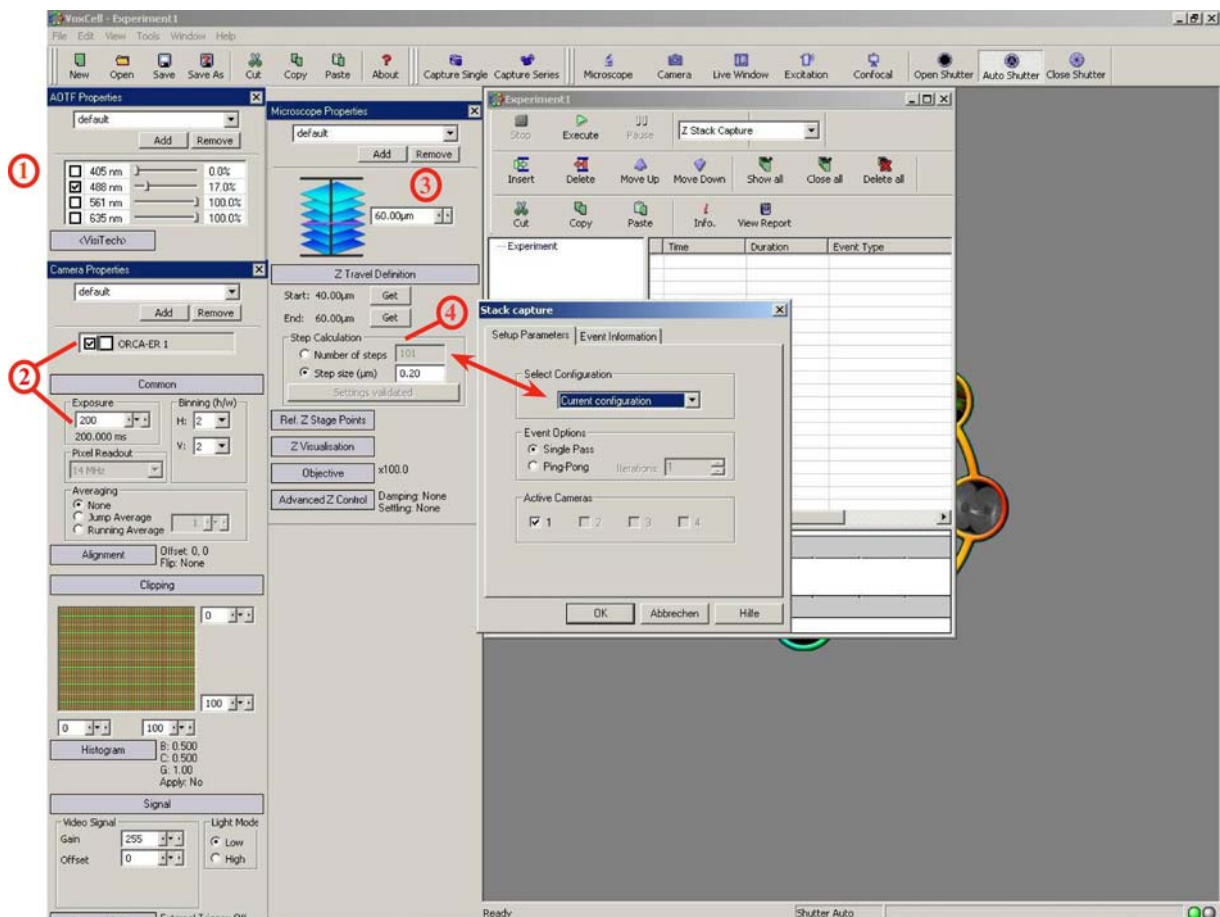


**Figure 13: Software-tool for the QLC-control.** The control software for the QLC was VoxCell (VisiTech International, UK). First the AOTF settings have to be arranged by choosing the laser wavelength and the intensity (1). Then the camera properties are set by choosing the camera, exposure time and binning rate (2). For z-stack-capture the top and the bottom point of the cell have to be defined using the piezo stepper (3). For the protocol, the start- and endpoint have to be set as well as stepsize and number of steps (4). These informations are needed when the protocol is written.

$\text{Ca}^{2+}$  sparks were recorded with a laser scanning confocal microscope comprising a scanning head (VT Infinity, VisiTech International, UK) attached to an inverted microscope (Eclipse TE 2000-U, Nikon, Japan) and a cooled EM-CCD-camera for detection of the signal (Andor iXon DV 887, Andor Technologies, UK). The VT Infinity is a kilobeam 2D-array scanner which enabled fast acquisitions of two-dimensional images by guiding a bundle of 50 x 50 excitation beams to the specimen via a Galvo scanner and the emission beams through pinhole-arrays towards the detection device (Fig. 11 A). This setup allowed a fast acquisition speed and was therefore suitable for the recording of short, local signals such as  $\text{Ca}^{2+}$  sparks.

The setup was controlled by the software VoxCell, provided by the company (VisiTech International, UK) which is shown as a screenshot in Fig. 14. For the recording of local Calcium signals such as  $\text{Ca}^{2+}$  sparks, high acquisition rates were mandatory. 2-dimensional time series were recorded with a speed of about 100 Hz. The binning rate of the camera had to be set to 2, which yielded in a pixel size of 0.5  $\mu\text{m}$  in x and y in combination with the 60x oil immersion objective (Plan Apo 60x/1.40 Oil, Nikon, Japan). The image frame size was set to 256 x 102 pixels to reduce the camera read out time; this frame size turned out to be sufficient to image a single cardiac myocyte. Additionally the scanned area can be reduced by defining the turning points for the scanning mirror. When reducing the area between the two turning points (=scan area) the scanning speed can be reduced. For the recording of spontaneous local  $\text{Ca}^{2+}$ -release events 1500 images were taken which corresponds to a total recording time of approx. 16 seconds (Fig. 14). The laser was set to maximum because the exposure time had to be kept as low as possible.

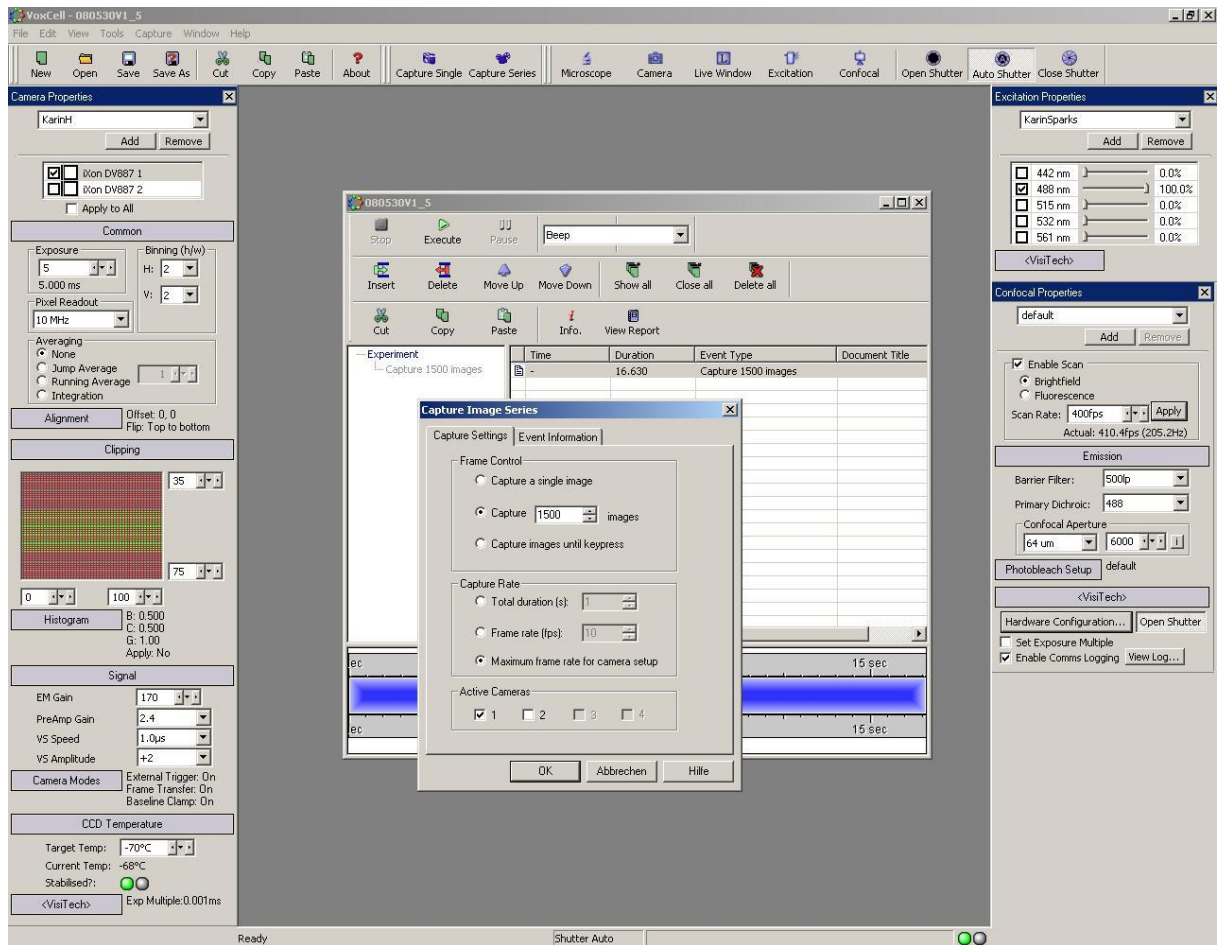


**Figure 14: VoxCell control software for recording Calcium sparks at the Infinity.** The camera settings were defined in the left panel where the camera was chosen, exposure time and binning rate set and the clipping size defined (image frame size). For the camera gain a value of 170 turned out to be ideal for measuring  $\text{Ca}^{2+}$  sparks. The camera was cooled to  $-70^{\circ}\text{C}$ , which had to be observed in the lower left panel. In the right panel the laser line and intensity was set as well as the filter settings (500 nm longpass filter as barrier filter and a 488 nm dichroic mirror). The protocol contained the number of images taken and the acquisition speed was set to maximal possible frame rate for the camera chosen.

Fluorescence Recovery after Photobleach (FRAP) experiments were also performed using the VT Infinity microscope setup. The fluorescence signal was scanned via the conventional beam path described above but in addition an additional beam path was added to enable the bleaching of a defined area of the cell. This was achieved by adding two Galvo scanners in front of the beam expander (Fig. 15A). To bleach a defined area of the cell, the laser beam was guided around the beam expander directly onto the beam combiner via two additional mirrors. The beam combiner led the beam towards the dichroic mirror and subsequently it was directed onto the previously defined region of

interest (roi) (Fig. 15B). In this case the emission was not collected as indicated in Fig. 15B. After bleaching, the settings for the AOTF and the beam path were switched back to the normal imaging mode. The switching time between the two settings was about 70 ms in total which led to a gap of this time frame between bleaching and the recording of the fluorescence recovery.



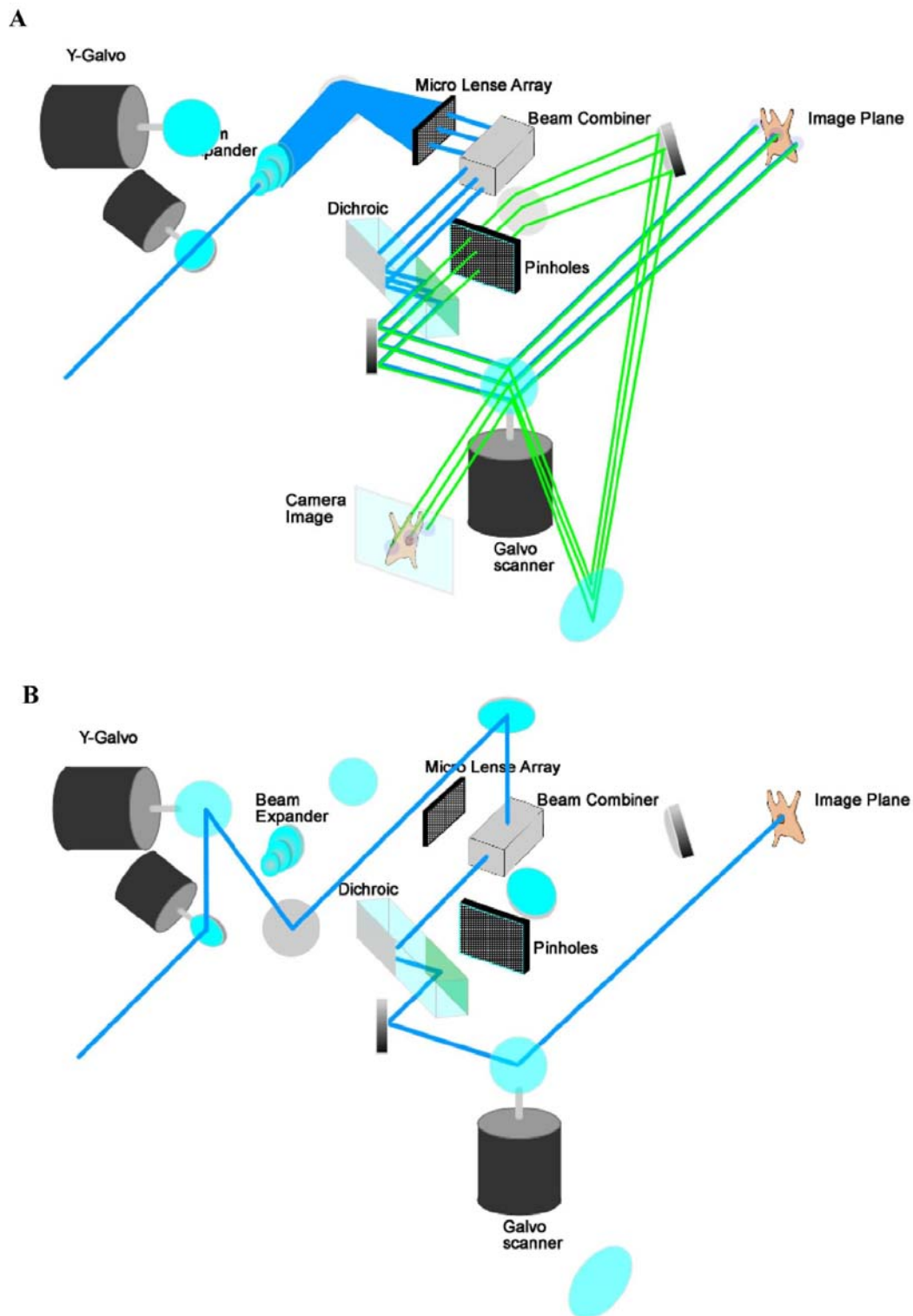


**Figure 15: Beam path of the Infinity for performing FRAP experiments.** Panel A depicts the beam path for fluorescence recordings. It corresponded to the setup used for the measurement of  $\text{Ca}^{2+}$  sparks. It additionally contains two Galvo scanner that can easily build a bypass for the laser beam. In that case the laser is guided around the beam expander and the micro lens array onto the region of interest on the cell (B). Figure provided by VisiTech, International, UK.

The whole procedure of FRAP experiments was navigated via the appropriate software version of VoxCell (Fig. 16). The software enabled the experimenter to set the size and the location of the region of interest to be bleached as well as the intensity and duration of the bleaching process. This bleaching protocol was only performable when no binning was set to the camera because this assured the correct positioning of the roi.

The software used is the same version as used for the imaging of  $\text{Ca}^{2+}$  sparks but with some different settings as shown in Fig. 16. The protocol always started with capturing 20 images at an acquisition speed of approx. 4 frames per second (fps) to get a baseline level of the fluorescence intensity before an area is bleached. Then the AOTF settings were switched to the photobleach setup (Fig. 16.4). Next step was to define the bleaching process by setting duration and roi. The location of the roi could be uploaded either pre-experiment or pre-event. Uploading pre-event was mandatory when bleaching more than one roi. In this case one bleaching step for each roi had to be inserted into the protocol (Fig. 16.5).

After bleaching a region of interest, the settings were switched to the imaging mode by changing the AOTF properties back to baseline. Image capture of 120 images was performed at an acquisition rate of approx. 4 fps to capture the first possible changes after bleaching. Then a time series of 120 images followed at a speed of 0.5 fps to record later changes. Since this protocol setup produced 3 independent files of image series a processing node was inserted to combine these three files and finally a last processing node was inserted to save this combined file as a TIFF-image series (Fig. 16).

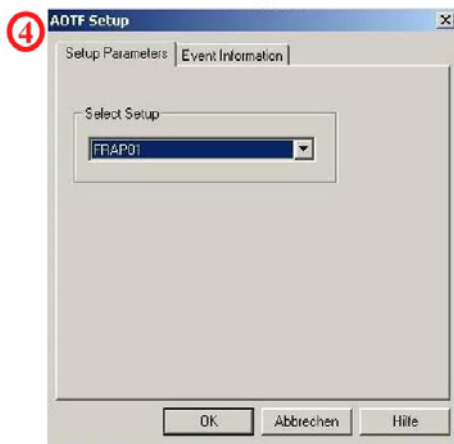
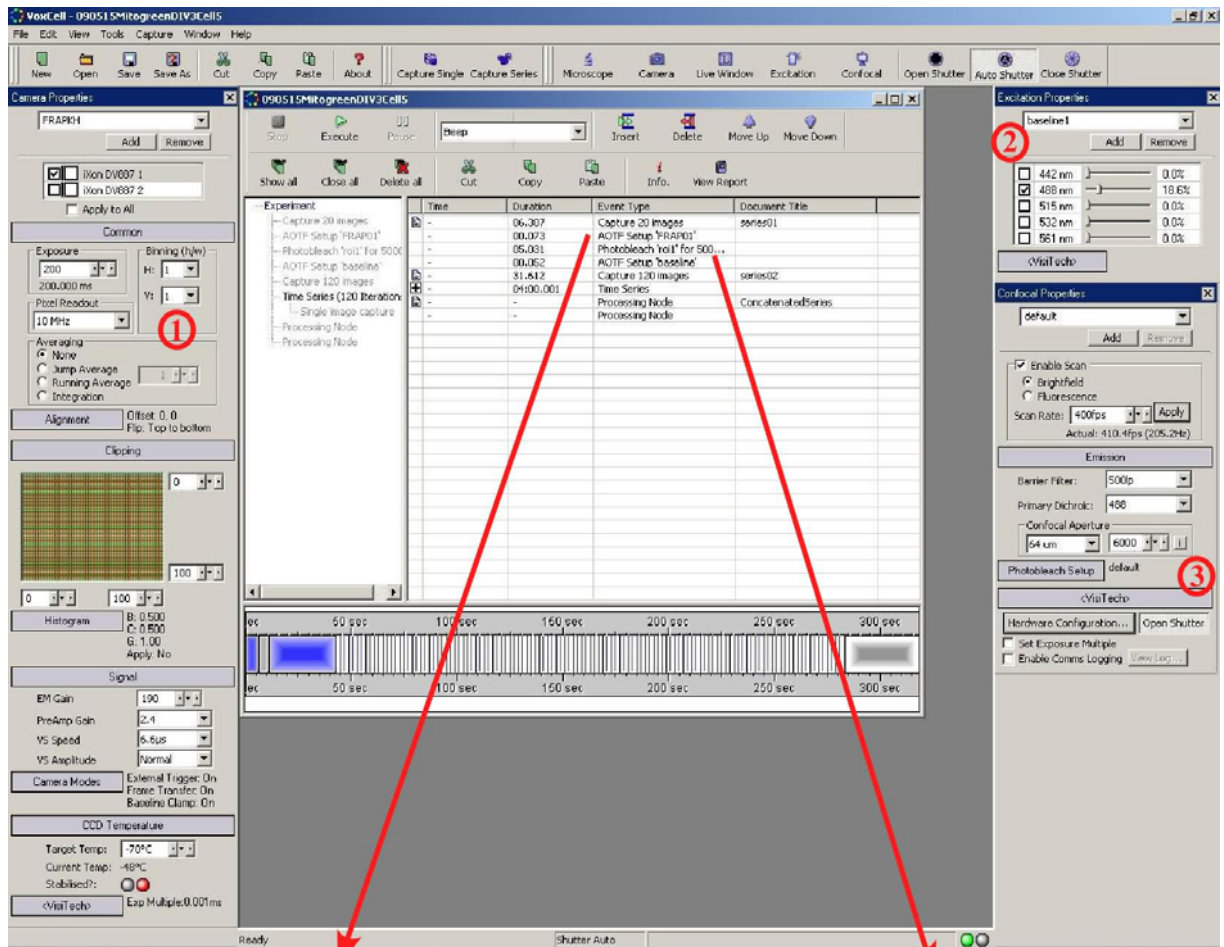


**Figure 16: VoxCell software for FRAP experiments.** On the left panel the camera settings can be adapted. Exposure time for the fluorescence measurements can be set at 200 ms but it is crucial to use no binning to ensure the correct position of the photobleach area (1). For the excitation settings the laser intensity is set at approx. 18 % and saved in the settings. For photo bleaching the intensity of the Argon Ion laser is set to maximum and saved (2). The photobleach setup can be adjusted and stored as default (3). The experiment protocol starts with a time series of 20 images and then AOTF-setup is switched to photobleach (4). Then photobleach can be performed; here the roi can be uploaded pre-experiment or pre-event and the bleaching time can be set (5). For bleaching more than 1 roi, this point had to be repeated for each roi and the roi's had to be uploaded pre-event.

These experiments were performed using a 100x oil immersion objective (S Fluor 100x/1.30 Oil, Nikon, Japan). The focus was set to the lower part of the cell, close to the cover slip to reduce light scattering when bleaching. Cells were loaded with MitoTracker<sup>®</sup> Green, as described above.

For the excitation of the Fluo4 and the MitoTracker<sup>®</sup> Green an air cooled Argon Ion laser was used with the wavelength of 488 (Model 185-F12, Spectra Physics, USA) which was connected to the microscope via an open coupling.

## ***F. Data Analysis***

Images taken from rat myocytes were initially processed in ImageJ (Wayne Rasband, NIH, USA) and subsequently deconvolved using AutoDeblurX (AutoQuant, USA). This program used an adaptive, theoretical point spread function (PSF) to reduce the blurring in the single slices obtained from the confocal microscope. The deconvolved image stacks were then transferred into Imaris 4.3 (Bitplane, Switzerland) for the final 3D rendering.

For cell length measurements and acquisition of fluorescence intensity plots ImageJ was used. Further analysis such as Fast Fourier Transformation of intensity plots and peak values were performed in Igor Pro (WaveMetrics Inc., USA). Also the analysis of the FRAP experiments were performed using Igor Pro and ImageJ.

Statistical values are given as mean values  $\pm$  S.E.M (standard error of the mean). Results were analysed using GraphPad Prism 5 (GraphPad Software Inc., USA), effects were regarded as significant when  $p \leq 0.05$  (marked with one asterisk) or  $p \leq 0.01$  (marked with two asterisks) or  $p \leq 0.005$  (marked with three asterisks). At the beginning of each statistical analysis the distribution of the values was determined. Based on this information and the type of data, e.g. paired or unpaired data, the suitable statistical test was chosen to analyze whether significant changes were found. The n-number of the experiments were given as number of events or measurements per cell and number of cells (events/cells) or solely the number of analyzed cells and were depicted as numbers on the bar graphs.

## ***G. Calcium-Spark Analysis***

To meet the increased performance of confocal microscopes such as the VT Infinity, we developed an algorithm to analyze calcium sparks in cardiac myocytes in time series of two-dimensional confocal images at acquisition rates of 100 Hz. This algorithm was programmed in MATLAB<sup>®</sup> (R2008a; MathWorks<sup>™</sup>, USA) and was first introduced in the Diploma Thesis of Aline Flockerzi.

We developed a three-dimensional approach for such analysis using locally “derivative-like” functions for spark-detection allowing the algorithm to be suitable for temporal and spatial analysis of calcium sparks. We deliberately avoided user-operations by calculating all critical parameter values. All detection criteria were automatically adapted to inherent experimental parameters such as frame rate and pixel size (i.e. camera binning, objective magnification). Beside the image series a dark image series was loaded into the program to generate background corrected image series. Furthermore an Input file had to be generated to feed the program with the desired boundaries for cell detection, spark detection as well as spark properties that were calculated. This file can also be used to run the software in a so called batch mode, which allows the automatic loading of cells to be analyzed.

The algorithm worked in 6 major steps that are also depicted in Fig. 17 as a flow chart of these main steps. First the experimenter had to load the data and metadata (step 1) which could be done using a batch mode that allowed loading of several files with their corresponding metadata. A proper method for cell detection (step 2) ensured that only signals inside the cell were detected and artifacts from outside the cell were excluded. Using a threshold-based method the objects within the field of view were detected and subsequently a size filter deleted all objects but the largest one. A cell mask was created to define the area of spark detection.

These data files were then further processed and filtered with different methods (Gaussian filter, running average filtering, and derivative like function to enhance the signals) and a final thresholding detected the putative sparks (step 3). For user-friendly evaluation of the final results each spark could be visualized as original data and as a 3D-gaussian function thereby data had been double checked.

The experimental fit and the Gaussian fit were used to calculate the spark parameters (e.g. amplitudes, decay time constant, frequency, spatial spread) for further analysis after

defining the particular spark properties such as dimensions, coordinates, gravity and center (step 4).

Additionally the single sparks were clustered according to the sparksite. A phylogenetic cluster analysis was performed by calculating the distance of the single sparks and a dendrogram was compiled. After defining cutoff values for the maximal distance of two sparks within a cluster, the mean values for each output parameter per sparksite were calculated (step 5).

Finally the data were stored in MatLab workspaces and Excel files (step 6).

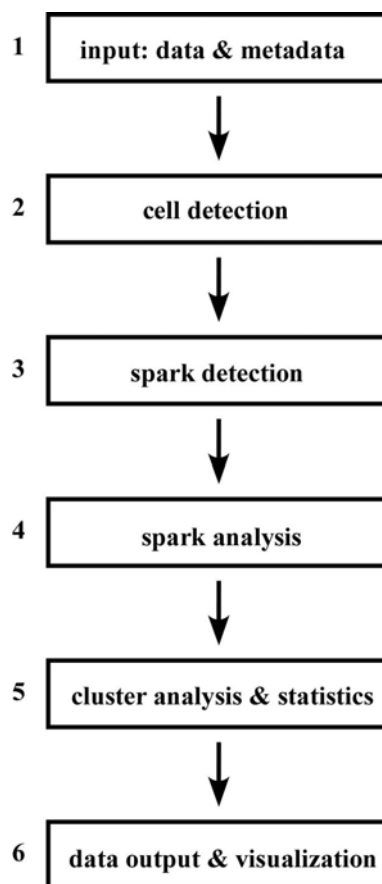


**Figure 17: Flow-chart of the algorithm for the spark-detection.** The algorithm consisted of 6 major steps as depicted in the diagram. It started with the input of data and metadata then cell detection was performed to subsequently detect the single sparks. These were then analysed. Finally cluster analysis and statistics were performed. At the end of the program stands the data output and the visualisation of the results.

## **V. Results**

### ***A. The Morphology of Adult Cardiac Myocytes in Long Term Culture***

The culture of adult cardiac myocytes was highly desirable because it could yield in viable cells for long term experiments in homogeneous populations without other cells found in the heart such as fibroblasts or endothelial cells. The cell culture method previously introduced by Cedric Viero provided a system that enabled us to get a stable culture for one week without the known signs of dedifferentiation when they lose their adult phenotype. The aim of this study was to elucidate how the intracellular structures of cultured myocytes were affected by the culturing procedure. Therefore cells were observed at defined time points during the cell culture period. Freshly isolated cells were compared to cells at DIV 1, at DIV3 and at DIV6. For all cell organelles two separate labeling methods were used, as outlined in Table 2.

#### **1. Plasmamembrane and Transverse Tubular System**

The loss of the adult phenotype of cardiac myocytes in culture also referred to as dedifferentiation, is detectable in cardiac myocytes in various forms such as a loss of the t-tubular system. Although it was known that detubulation occurs as a part of dedifferentiation of the cardiac myocytes in culture it remained unclear how that process occurs. Some approaches studied the detubulation during long term culture and also tried to quantify this process (Banyasz et al., 2008) but the reasons remained elusive. Detubulation studies using formamide as a detubulation agent showed that after detubulation the t-tubules remain within the cell (Brette et al., 2002). Here I wanted to evaluate how detubulation occurs during dedifferentiation.

To approach this, the plasma membrane was labeled with two methods utilizing adenoviral gene transfer of a fluorescent fusion protein (GPI-YFP construct) and the small molecule dye Di-8-ANEPPS. With both methods it was clearly visible that the t-tubules gradually disappeared during several days in culture (Fig.18A + C). At DIV6 there were no t-tubules visible with either method. The comparison of both approaches revealed that there were more structures labeled in cells expressing the fluorescent fusion protein. I calculated the relative t-tubule length by first measuring the thickness of the cell and then

the length of 4 t-tubules, which were clearly connected to the membrane. Since for all cells z-stacks have been recorded it could be assured that the complete length of the t-tubules was measured, because one could slide through the cells allowing following the single tubules. The values were then calculated as the relative length in relation to the thickness of the cell. Measuring the relative t-tubule length depicted that even in freshly isolated cells the relative length was only 62 % in relation to the cell diameter, so even in fresh cells the t-tubules did not completely cross the cells. Furthermore, the relative t-tubule length was reduced during the time in culture until there were no longer detectable (Fig. 20). During the one week of culturing t-tubules were significantly longer in cells expressing GPI-YFP than in Di-8-ANEPPS labeled cells, which was most obvious at DIV1 where the relative t-tubular length was 25 % in cells labeled with Di-8-ANEPPS in contrast to 48 % in cells expressing the fusion protein. The double labeling in Fig.18B depicts an example for the observed differences of the both labeling methods. Whereas Di-8-ANEPPS only labeled structures that were still clearly connected to the outer plasma membrane, the fusion protein was also found in deeper regions of the cells and in fragments that were clearly disconnected from the outer shell, which was affirmed by sliding through the z-axis of the cell.



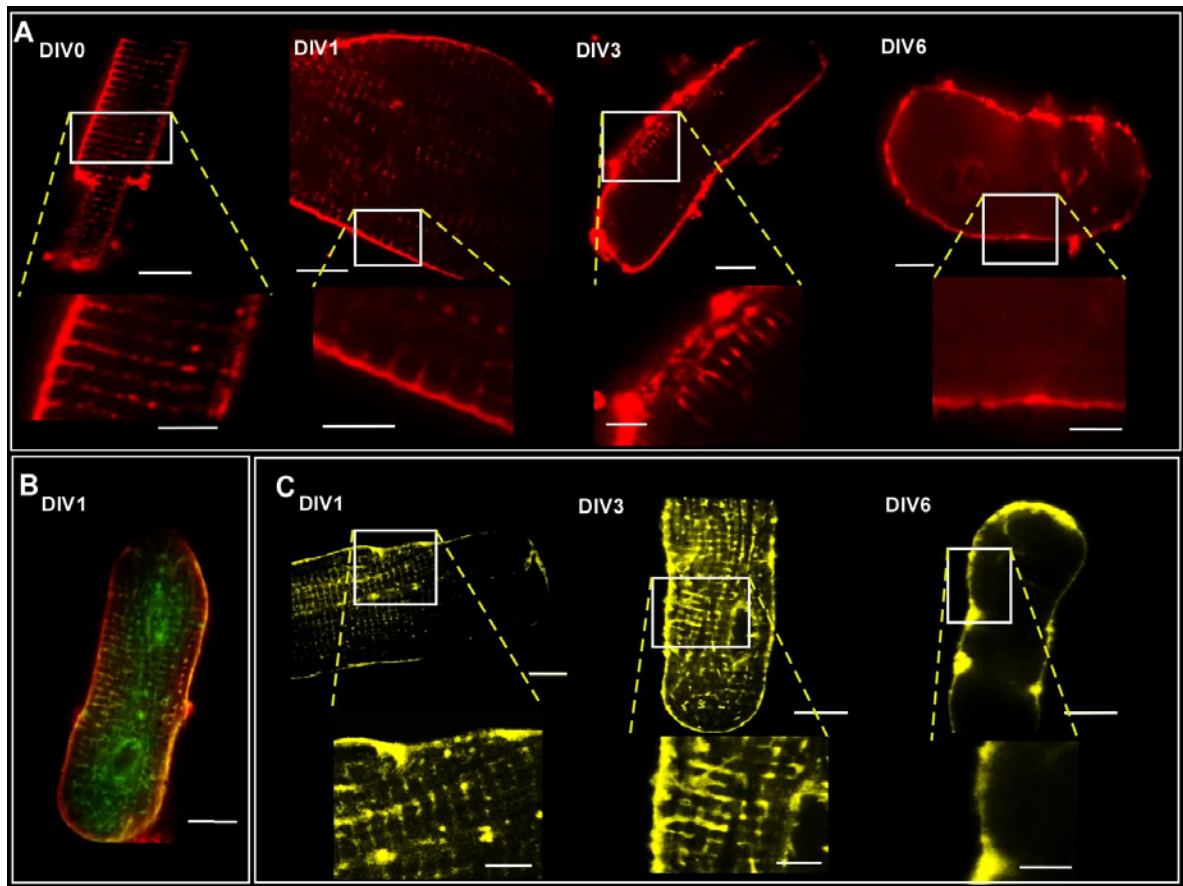


**Figure 18: Labeling of the plasma membrane during long term culture.** Row A depicts cells labeled with Di-8-ANEPPS, after 1 day *in vitro* (DIV), t-tubules appeared shorter than in freshly isolated cells and at DIV3 only short residues directly underneath the plasma membrane were visible and no t-tubules were left after DIV6. Row C displays examples of cells expressing the fluorescent fusion protein. At DIV1 and DIV3 there seemed to be more structures within the cells labeled with the fusion protein than in cells labeled with Di-8-ANEPPS and also some t-tubules were clearly disconnected from the plasma membrane. A double labeling (B) clearly showed the overlap of both labeling methods (yellow color) but also the structures labeled only with the fusion protein (green); the Di-8-ANEPPS staining was visualized with red color. Scale bars: 10 μm and 5 μm for the enlargements.

The shortening of the t-tubules came along with a shrinkage of the cells which was observed in cultured cells, where length and width were measured and subsequently utilized to calculate an approximation of the cross section of the cells assuming a rectangular shape (Fig. 19). Freshly isolated cells had a cross section of 2841 μm<sup>2</sup> and cells that have been cultured for 1 week shrunk to a cross sectional size of 1495 μm<sup>2</sup>. Also the number of cells was reduced as already described by Cedric Viero who found that the initial 80% viable cells (i.e. rod shaped, living cells) were reduced to a number of about 42% of viable cells at DIV6. These numbers gave the percentage of rod shaped cells from

all living cells (round and rod shaped cells; approx. 5000 per ml). The total number of cells was not counted on a routine basis but was also reduced during the time in culture.

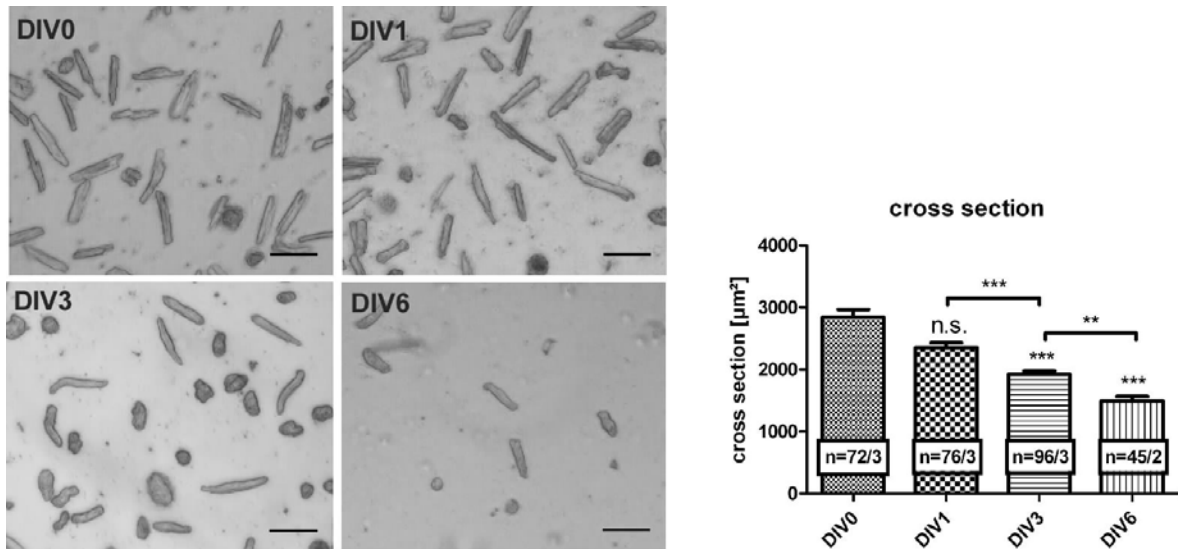


**Figure 19: Cross section of adult cardiac myocytes cultured for up to 1 week.** Cells were imaged during their time in culture and the cross section was calculated after measuring length and width using ImageJ. Cells reduced their cross sectional size significantly. Scale bars: 80  $\mu\text{m}$ . N-numbers were given for cells/animals.

These findings raised the question to why t-tubules disappear during the time in culture. A change of the cytoskeleton might have been a reason for the change of the t-tubular structure. Therefore CytochalasinD which is known to act on actin (Cooper, 1987) was added to the culturing medium directly after the plating of the cells.

This intervention improved the maintenance of the t-tubules in such a manner that cells that have been treated with CytochalasinD had about 15 – 20 % longer t-tubules in comparison to Di-8-ANEPPS-labeled cells not treated with CytochalasinD as depicted in the diagram in Fig 20. Also the cells expressing the fluorescent fusion protein showed an improved maintenance, whereas here the improvement was most obvious in cells at DIV3 where t-tubules in CytochalasinD treated cells were about 40 % longer than in untreated cells. Even after one week in culture the t-tubules were not completely lost after treatment with CytochalasinD but were reduced to a length of 8,6 % for cells labeled with Di-8-ANEPPS an GPI-YFP in contrast to untreated cells where no t-tubules were visible at DIV6 with either labeling method.

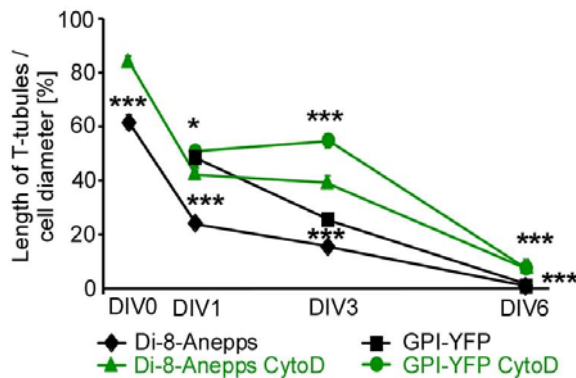


**Figure 20: Relative length of t-tubules in ventricular myocytes cultured for up to 1 week with and without CytochalasinD in the culture medium.** The relative t-tubular length is given as percentage of the cross section of the cell. The relative t-tubular lengths of untreated cells (without CytochalasinD) are shown in black whereas those of treated cells (with CytochalasinD) are shown in green. Di-8-ANEPPS stained cells had significantly longer t-tubules in treated cells at DIV0, DIV1 and DIV3. Cells labeled with the fluorescent fusion protein showed the same relative t-tubular length in both cells, treated and untreated, but at DIV3 treated cells had much longer t-tubular residues. Only cells treated with CytochalasinD showed short residues of the t-tubules at DIV6. The asterisks mark the significant differences observed between groups labeled with Di-8-ANEPPS with and w/o addition of CytoD, which were highly significant at each observed DIV. Cells labeled with the GPI-YFP fusion protein were also highly significant at all days but partially to a lesser degree. (Experiments were performed in 10 to 21 cells from 3 to 8 rats).

## 2. Mitochondria

During the time in culture mitochondria were observed using MitoTracker<sup>®</sup> Green and the fluorescent fusion protein Mito-GFP. In freshly isolated cells, the mitochondria were found within the whole cell and they were visible as single mitochondrial packages arranged along the longitudinal axis of the cells. They were clearly separated from each other on the cross axis of the cells which was visible as a cross striation pattern as depicted in Fig. 21. This pattern was also visible at DIV1 but started to change from DIV3 on. The single packages seemed to fuse and finally they were visible as tubular structures along the longitudinal axis of the cells at DIV6. Fig. 21A depicts 3D reconstructions of z-stacks recorded from cells labeled with MitoTracker<sup>®</sup> Green or the fusion protein Mito-GFP at DIV0, DIV1, DIV3 and DIV6.

Cells labeled with the fluorescent fusion protein showed this pattern as well, although only cells that have been cultured for 3 or more days could be observed (Fig. 21B) since the fluorescent fusion protein which labeled the mitochondria had a long maturation time in comparison to other fusion proteins.

This pattern was quantified by Fast Fourier Transformation (FFT) using ImageJ and IgorPro. First the gray level at a defined line, either longitudinal or crosswise was measured in ImageJ as shown in Fig. 21C and the values from this intensity plot were taken to calculate the power spectrum. From these power spectra the predominant peak was picked and the corresponding spatial frequency could be extracted from the plot. The inverted value of the spatial frequency gave the spatial distance of the fluorescence intensity peaks. The average values from these calculations were visualized in bar graphs for the longitudinal and the transverse frequency (Fig. 21D). The average package distance (along the transverse axis) was found to be 1.8  $\mu\text{m}$  at DIV0 and DIV1, which corresponds to the sarcomere length. This value tremendously increased between DIV1 and DIV3 to a value of about 4  $\mu\text{m}$ , which then remained constant at this level (Fig. 21D).

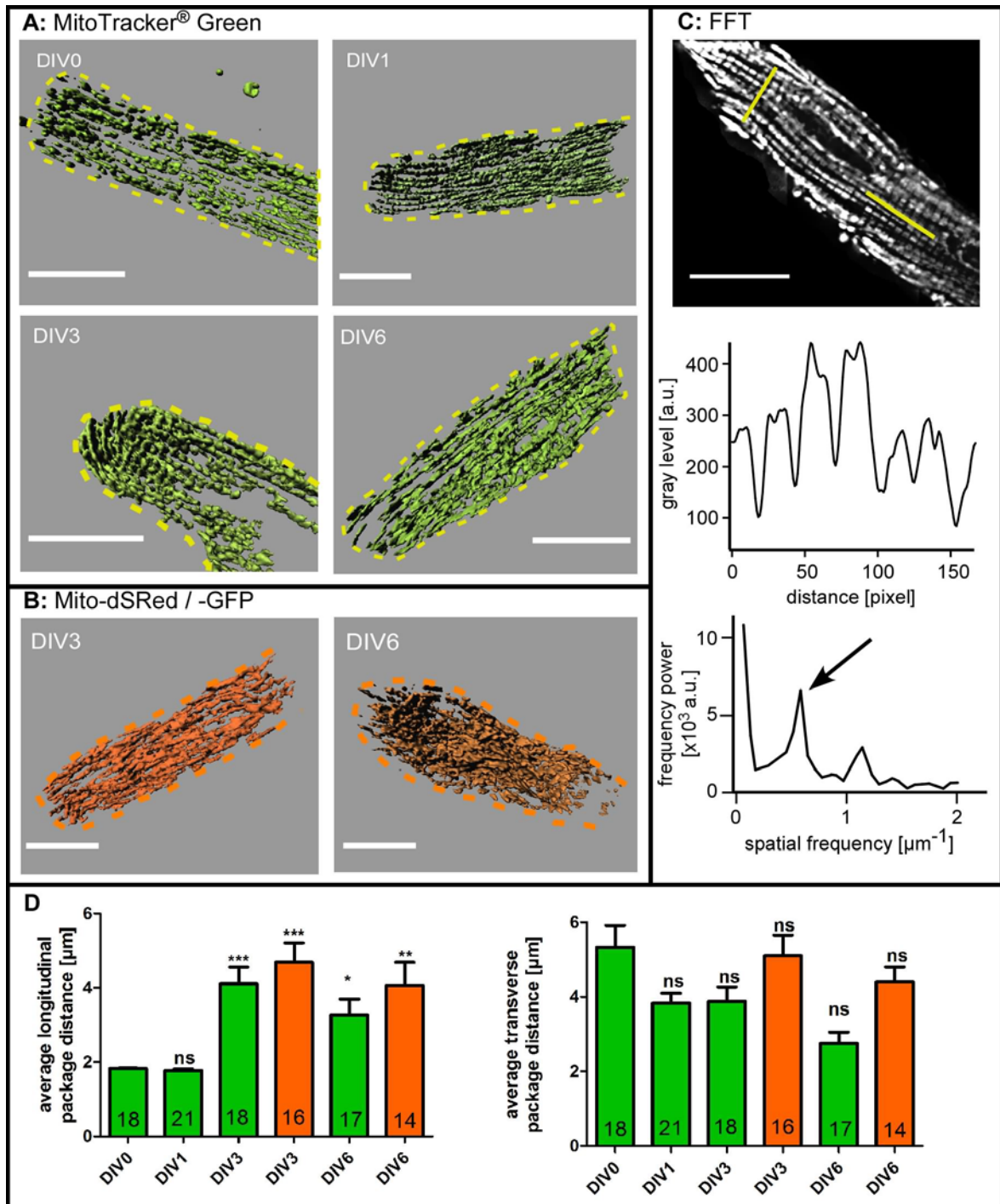


**Figure 21: Mitochondria in ventricular myocytes during the time in culture.** 3D-reconstructions of cells labeled with MitoTracker<sup>®</sup> Green (A) during 1 week of culture. The initially single packages of mitochondria seem to fuse. This could also be observed in cells expressing the fluorescent fusion protein (B). To quantify these qualitative data, a Fast Fourier Transformation (FFT) has been performed, on longitudinal and on cross axis. The average package distance on the cross axis was unaltered whereas the package distance along the longitudinal axis was increased from about 1.8  $\mu\text{m}$  at DIV0 and DIV1 to about 4  $\mu\text{m}$  after DIV3 (D). Scale bars: 20  $\mu\text{m}$ . Experiments were performed in cells from 3 to 8 rats.

To clarify whether the mitochondria really fuse during the time in culture cells labeled with MitoTracker<sup>®</sup> were used to perform Fluorescence Recovery After Photobleach (FRAP) experiments. It is known from experiments using cells with long tubular mitochondria such as HEK cells or fibroblasts, that showed a recovery of the fluorescent signal after bleaching as depicted in Fig. 22. In these cells it was visible that the fluorescence increase within the bleached area was taken from the neighboring part of the mitochondria.

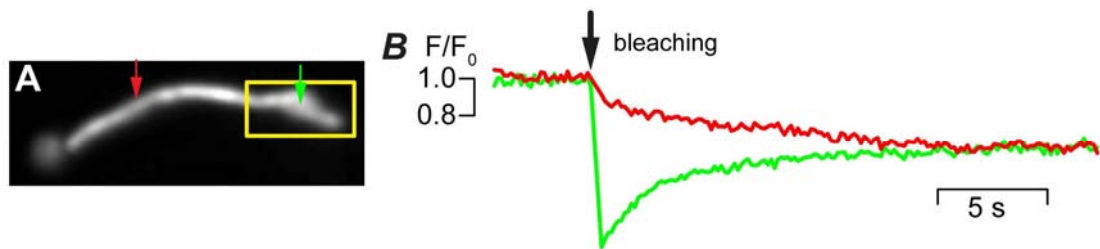


**Figure 22: FRAP in HEK cells and the fluorescent signal recorded.** A part of a mitochondrion of a HEK cell was bleached (depicted as yellow box in **a**) and the fluorescent signal at this point (depicted with a green arrow) as well as close to the bleached area (depicted with a red arrow) were imaged. The fluorescence recovery at the bleached area corresponds to the fluorescence loss of the neighboring area of the mitochondrion as shown in **b** where the green time course corresponds to the bleached area and the red time course to the close-by, unbleached area. The black arrow in **b** depicts the time of bleaching. Data provided by Peter Lipp.

FRAP experiments in HEK cells showed a recovery of the fluorescent signal in the bleached area, which proved that the mitochondria were connected. Based on this, FRAP experiments were performed in cardiac myocytes, since such experiments could provide information whether the single mitochondria packages observed in freshly isolated cardiac myocytes indeed fuse during the time in culture or if they just move close together (beyond resolution limit) and simply appeared to be fused as observed with the confocal imaging of the morphology of the mitochondria in cardiac myocytes.

For this an apparent single mitochondrial package was bleached and the time course of the fluorescence recovery was analyzed. Fig. 23 depicts an example cell recorded at DIV0 with its corresponding fluorescent time course and the time course of the neighboring mitochondrion. Cells at DIV0, DIV1, DIV3 and DIV6 were recorded and the recovery time constant was analyzed using IgorPro.

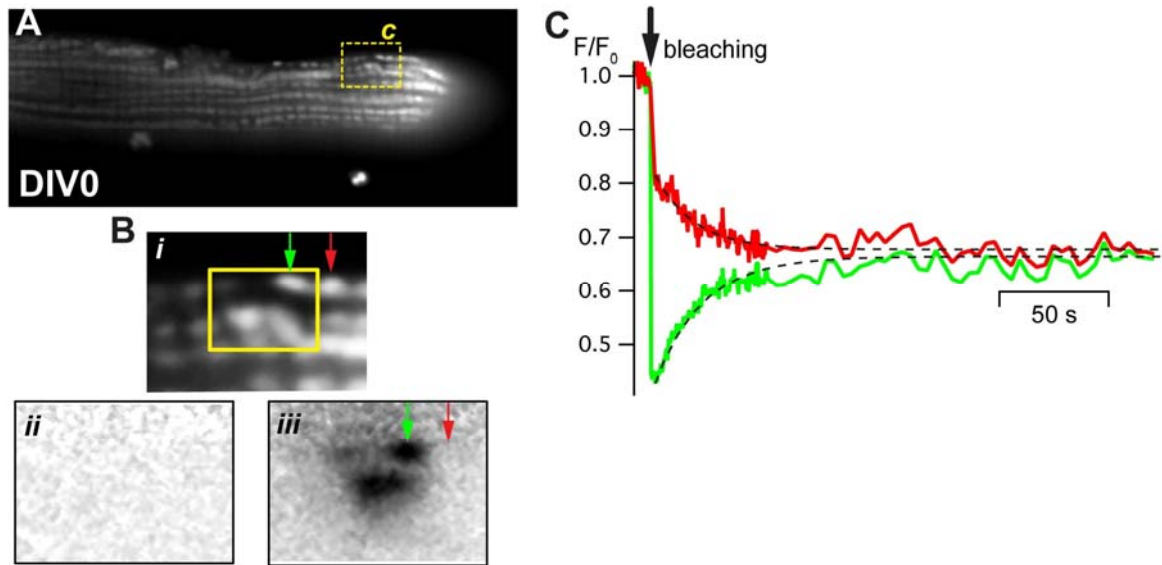


**Figure 23: Fluorescence Recovery After Photobleach (FRAP) in single mitochondria of cardiac myocytes at DIV0.** A freshly isolated cardiac myocyte was loaded with MitoTracker<sup>®</sup>Green and imaged (**A**). The yellow dashed box marks the area of the cell where bleaching was performed. A defined area, which was believed to be a single mitochondrial package, was bleached (**B**; magnification of the yellow dashed box in **A**, highlighted with a green arrow while the yellow box depicts the bleached area) and the fluorescence recovery of this area recorded (**C**, green line). Next to the bleached mitochondrion was an apparent separated mitochondrion (**Bi**, highlighted with a red arrow), that was not bleached as depicted in the normalized images **Bii** and **Biii** whereas **Bii** was taken before bleaching and **Biii** after bleaching. These images displayed the values of the fluorescence intensity divided by the baseline value ( $F/F_0$ ); an area of baseline intensity was shown as almost white image and fluorescence decrease was visible as darker areas as seen in **Biii**. The time course of the neighboring mitochondrion (**C**, red line) revealed a fluorescent loss after bleaching the neighboring mitochondrion.

As control cells fibroblasts were analyzed as described above. The time courses at each DIV observed were depicted in Fig. 24A where the time course of the fluorescent signal recorded in a fibroblast was shown in comparison to the signals recorded in cardiac myocytes. The red lines indicated the exponential fit performed in IgorPro to calculate the recovery time constant. The values from cardiac myocytes were significantly different from those found in fibroblasts but they did not differ among each other except the cells at DIV6 that had a significantly faster recovery of the fluorescent signal.

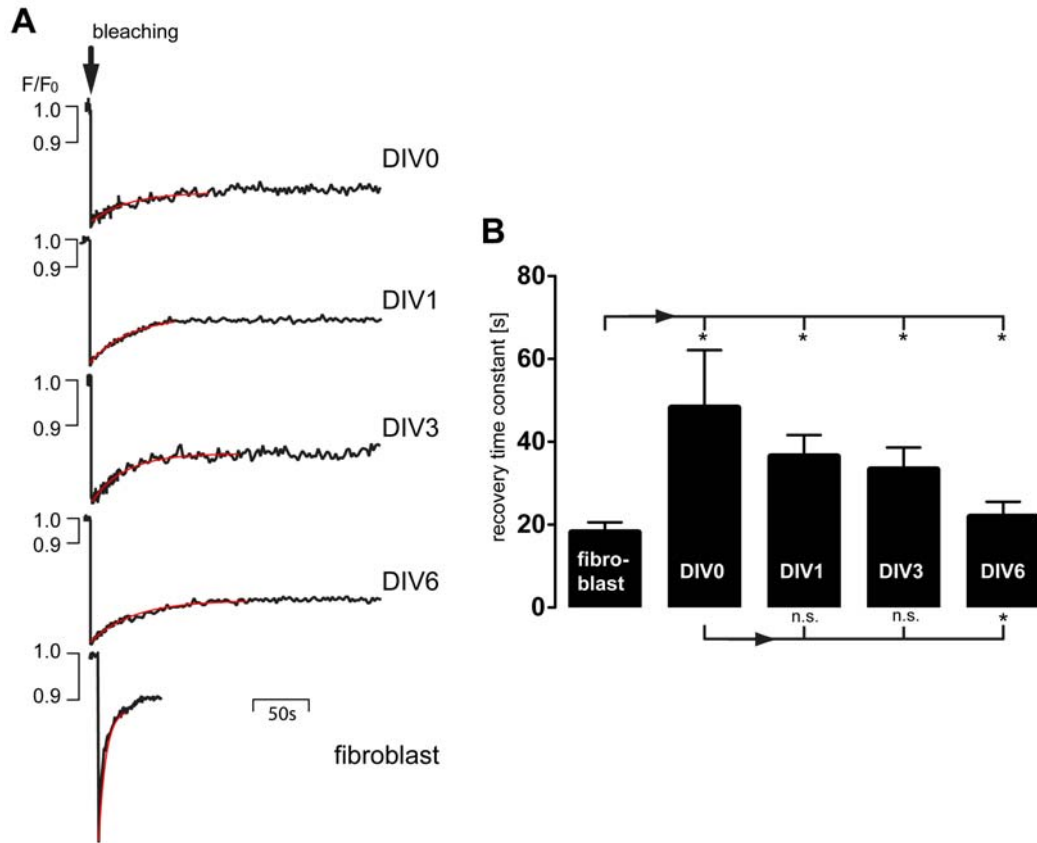


**Figure 21: FRAP in single mitochondria of cardiac myocytes in comparison to fibroblasts.** Mitochondria in cardiac myocytes at DIV0, DIV1, DIV3 and DIV6 as well as fibroblasts were bleached and the fluorescent time course was recorded (**A**; depicting representative traces). The red lines depicted the exponential fit that was used to calculate the recovery time constant. The averages of these calculations were drawn in the diagram in **B**. All values of the cultured cardiomyocytes differed significantly from the fibroblasts but not from each other except the cells at DIV6. Experiments were performed in 12 to 24 cells from 3 to 4 rats.

### 3. Endoplasmic/Sarcoplasmic Reticulum

The sarcoplasmic reticulum (SR) was labelled with a dSRed fluorescent protein fused to the endoplasmic reticulum localisation sequence of Calreticulin and contained the retention sequence (see Fig. 6). Confocal images were taken during one week of culture. It was not possible to obtain fluorescent images with the small molecule dye ER-Tracker™ Green, because experiments performed with this dye revealed that it unspecifically labelled the mitochondria.



From DIV1 onwards the SR was visible as a very fine network evenly spread throughout the cell (Fig. 25A) except of the labelling around the nucleus which was slightly more prominent for all cells. While the network was found evenly distributed throughout the whole cell during the time in culture its structure did change. Quantification of this change was achieved by performing FFT as described for the mitochondria. The intensity profile on the longitudinal and the transverse axis was analyzed.

On the longitudinal axis, the SR had an average spatial distance of about 2  $\mu\text{m}$  at DIV1. This distance increased during the time in culture until it reached a value of about 5  $\mu\text{m}$  at DIV 6. Also the spatial distance on the transverse axis increased from an initial value of 2.8  $\mu\text{m}$  to a final value of about 7  $\mu\text{m}$  at DIV6 (Fig. 25B+C). These data showed that the highly structured appearance of the SR was reduced during the time in culture and while it was still evenly spread throughout the cell with exception of the more prominent staining around the nuclei at DIV6 it was less organized (the higher intensities seen in Fig. 25A for DIV6 were due to areas out of the focal plane).

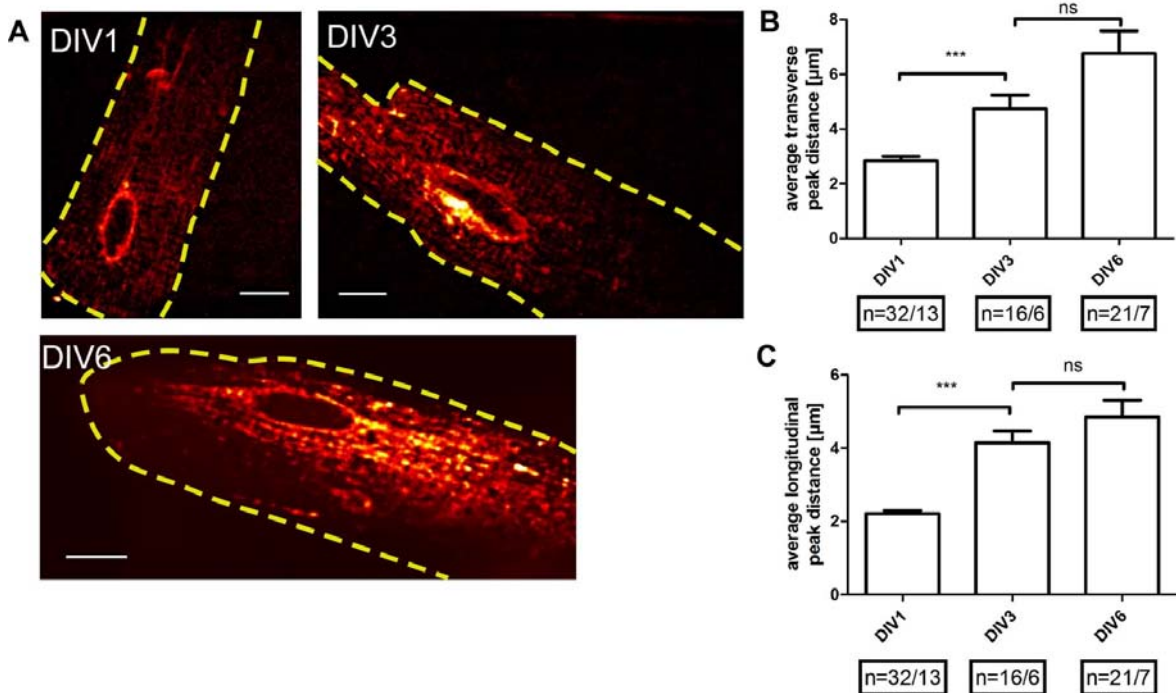


**Figure 25: Visualization of the ER-/SR-network in cardiac myocytes cultured for one week.** The ER/SR was visible as a fine network evenly distributed within the cells with a more prominent staining around the nuclei. While the distribution remains unaltered, the organization seems to change during the time in culture (A). FFT of the intensity plots taken on the longitudinal and transverse axis of the cells showed that the distance of the tubules increased during the time in culture in both directions (B + C).

#### 4. Golgi Apparatus

The Golgi apparatus was visualized using a YFP fluorescent protein fused to ts045G and observed from DIV1 ongoing until DIV6. No images were taken with the dye BODIPY TR C<sub>5</sub> because it was not possible to detect any fluorescence in cells loaded with the dye.

At DIV1 the Golgi apparatus was visible as a fine dot-like structure evenly spread throughout the cell in the original image and in the 3D-reconstruction (Fig. 26A+B). During the time in culture a major rearrangement occurred when the organelle accumulated in the perinuclear region at DIV6 (Fig. 26A+B). By laying a 10 pixel wide band of interest right next to the nuclei the intensity distribution could be analyzed (Fig. 26B). A ratio of the mean intensity at the perinuclear area and the mean intensity at the cytosol was calculated to quantify the intensity distribution of the fluorescent protein within the cell. At DIV1 and DIV3 the intensity was evenly distributed throughout the cell whereas at DIV3 the intensity curve showed a rather peak like structure (Fig. 26C). At DIV6 the reorganization of the organelle was also visible in the plot of the fluorescence intensity. The whole Golgi apparatus was accumulated around the nuclei and almost no fluorescence could be detected within the rest of the cytosol.

To analyze whether this alteration of the Golgi apparatus in cultured cardiac myocytes was connected to a possible alteration of the cytoskeleton the organelle was imaged in cells that have been treated with CytochalasinD. These cells showed a very similar rearrangement of the Golgi apparatus, although here the redistribution started earlier than in untreated cells where there was no significant difference between the intensity distribution at DIV1 and DIV3 (Fig. 26D). Cells treated with CytochalasinD had a more prominent orientation of the Golgi vesicles towards the nuclei depicted in the bar graph of quotients of the mean intensities (Fig. 26D) where already at DIV3 a significant difference was visible.

When comparing treated with untreated cells, there were no significant differences found at DIV1 and at DIV6 (Fig. 26). Cells cultured for 3 days without the supplementation with CytochalasinD showed no rearrangement whatsoever, but cells treated with CytochalasinD showed already a rearrangement of the Golgi vesicles that started to accumulate around the nuclei. After 1 week in culture with both settings the Golgi apparatus was accumulated in the perinuclear regions of the myocytes.

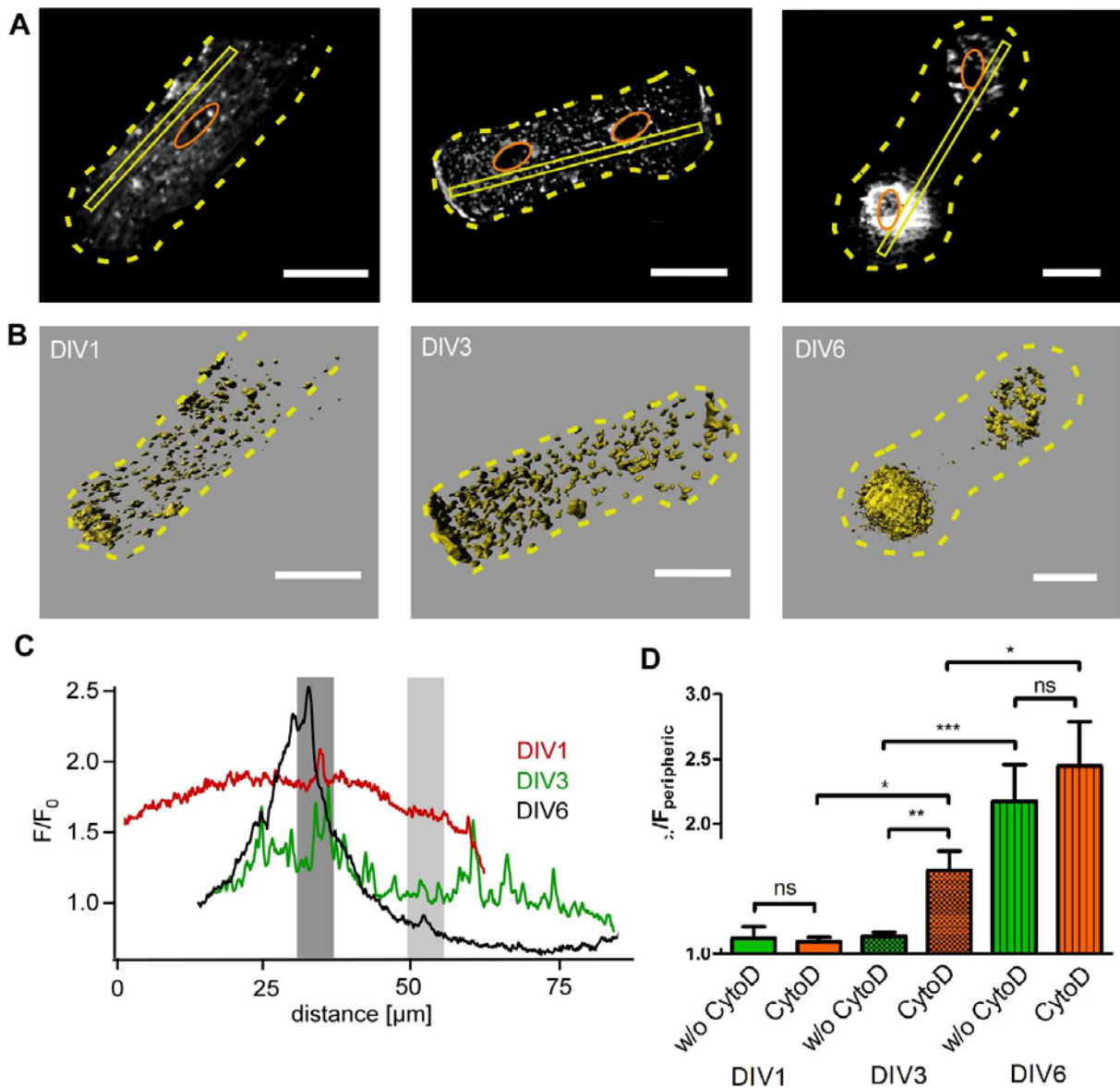


**Figure 26: Redistribution of the Golgi apparatus during the time of culture.** At DIV1, DIV3 and DIV6 z-stacks from Golgi apparatus were taken (A) and after deconvolution 3D-rendered (B). The 3D-reconstructions showed the redistribution of the Golgi apparatus which was first seen as evenly spread vesicle like structure in cardiac myocytes. At DIV6 it was only found at the perinuclear area. The middle slice of each stack was taken to draw a line in the cell and measure the mean intensity of the cytosolic and the perinuclear fluorescence signal (C). The ratio of these values was unaltered until DIV3, but increased significantly between DIV3 and DIV6 (D) within cells that have not been treated with CytochalasinD. Cells treated with CytochalasinD showed already a shift of the Golgi apparatus at DIV3 in contrast to the untreated cells until the complete Golgi apparatus was accumulated around the nuclei. Cells were taken from 8 to 10 rats.

## 5. Actin filaments

The actin filaments of the cultured cardiac myocytes were observed by expressing Lifeact-mRuby, a fluorescent fusion protein to label the F-actin in cells. There was no adequate dye available to detect the actin filaments, all dyes available were not membrane permeable and could only be used in fixed cells and therefore were not viable for live cell imaging.

The expression level of the fusion protein reached a detectable level after 3 days and therefore no data were available for cells at DIV1. After 3 days, cells showed a good expression and the actin filaments were visible as packages along the longitudinal axis with a clear cross striation (Fig. 27A). This fusion protein labeled the filamentous actin which were densely packed in cardiac myocytes due to the morphology of these cells and the structure of the sarcomeres (Cooke et al., 1987, Craig and Padrón, 2004). With a FFT-analysis the package distance was analyzed and the distance was 1.7  $\mu\text{m}$  at DIV1 and 2  $\mu\text{m}$  at DIV6. These mean values were comparable to the sarcomere length and they did not differ significantly from each other (Fig. 27B).

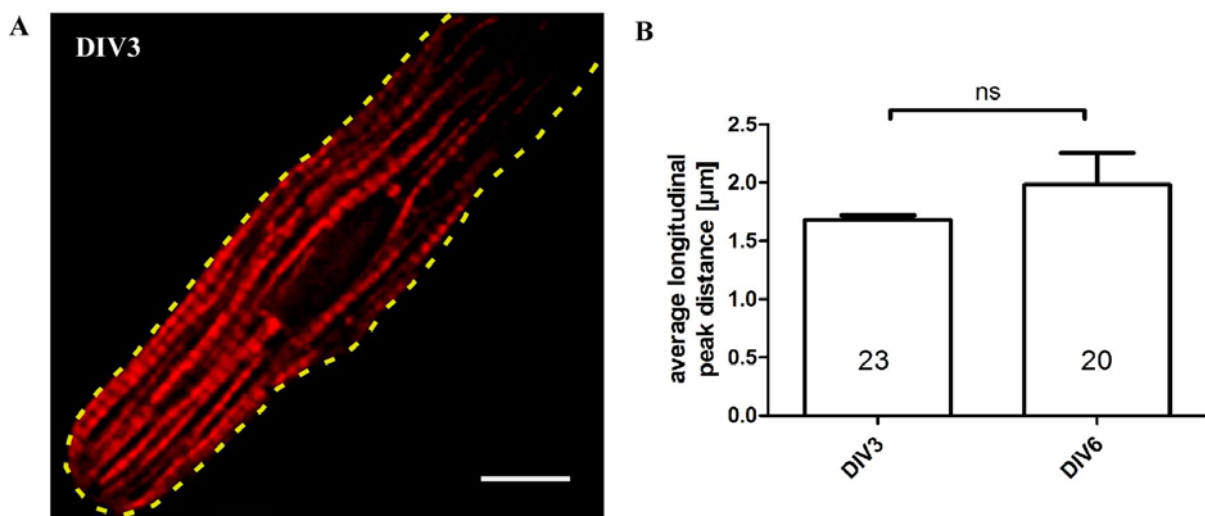


**Figure 27: The cytoskeleton in cardiac myocytes visualized with the fluorescent fusion protein Lifeact-mRuby.** The actin filaments were visible as packages along the longitudinal axis of the cell and showed a clear cross striation. The yellow dashed line indicates the cell border and in the middle of the cell a black area is visible, which was the location of one of the nuclei. This cell at DIV3 represents the cells at DIV3 as well as at DIV6, since no major changes occurred. The packages distance was analyzed with FFT and was found to be 1,7 and 2  $\mu\text{m}$  at DIV3 and DIV6, respectively. Scale bar: 10  $\mu\text{m}$ . Cells were taken from 4 to 5 animals.

## ***B. The Physiology of Adult Mouse Myocytes – Ca<sup>2+</sup> Sparks***

### **1. Evaluation of the MatLab Algorithm**

To test the MatLab algorithm we had to evaluate how many sparks actually are detected by the program and how accurate the data calculated by the software were. Since this required that the number of sparks their location and temporal data are known, we created a model cell with model sparks which then could be analyzed by the program. The output parameter could then easily be compared to the input data.

First a model spark was created by averaging real sparks. These data were taken from 22 sparks (22 spark sites, 9 ventricular myocytes and 3 animals) and averaged. The averaged data were fitted according to the algorithms used within the spark detection and analysis software. Fig. 28 shows a 3D reconstruction of the mathematical phenomenological description of a spark on a time course of 280 ms.

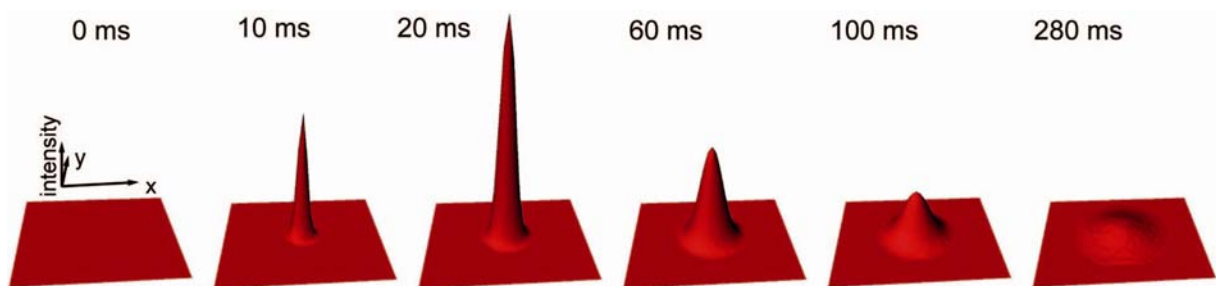


**Figure 28: The 3d reconstruction of the mathematical description of a model spark.** The figure depicts the time course of the model spark in a 3d reconstruction. The time course was 280 ms. The model spark was calculated by averaging 22 real sparks (22 spark sites, 9 ventricular myocytes from 3 animals) and fitted according to the analysis algorithm.

After having constructed a model spark, a model cell had to be calculated. Here we used the information from ventricular myocytes to create an image series of 500 images with a size of 250 x 150 pixels and an image depth of 16 bit. The background was set to 1000 and the resting fluorescence values in the cell to 2000; both values were found to be typical for ventricular myocytes. Within this cell 100 model sparks with the same amplitude were placed at random positions with no spatial or temporal overlap. The outcome was a simulated image series with randomly arranged sparks with constant amplitude on a noise

free background. Fig. 29 depicts a volume render of this model cell with model sparks; it also shows the randomly placed sparks with constant amplitude.

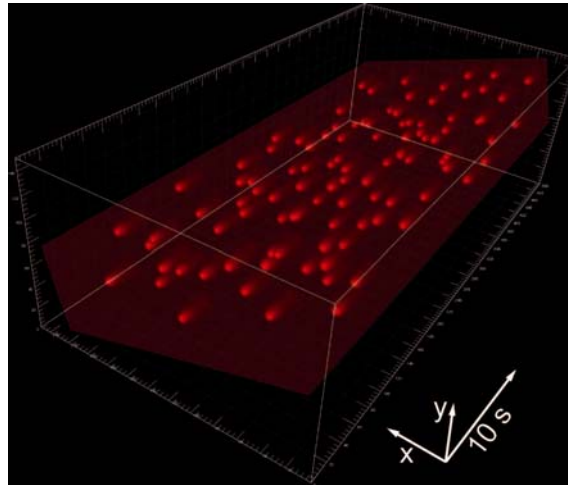


**Figure 29: Volume render of a noise free model cell with model sparks.** The model cell was calculated basing on data from real cells (ventricular myocytes) with a background of 1000 and baseline fluorescence within the cell of 2000. No noise was added in this example. 100 previously calculated model sparks with constant amplitude were randomly simulated into the cell, whereas no spatial or temporal overlap was allowed.

The noise found in the signal of real cells derived from different sources and thus we added noise in our model cell with sparks. We included a sum of electronic noise as the Gaussian component but also an intensity dependent noise reflecting the Poisson component of the noise signal. The noise was calculated from realistic values found in our experimental data and the technical specifications of the EM-CCD-camera we used for these experiments (ANDOR iXon DV 887, Andor Technologies, UK) as well as the typical photon counts per pixel. The 3D surface rendering of the model cell including model sparks at a single time point is depicted in Fig. 30A displaying the noise added to the baseline fluorescence. We also compared the time course of a real spark with the time course of a model spark with noise. As shown in Fig. 30B the two time courses were superimposable and thus we concluded that the calculated noise reflected accurately the experimental situation.

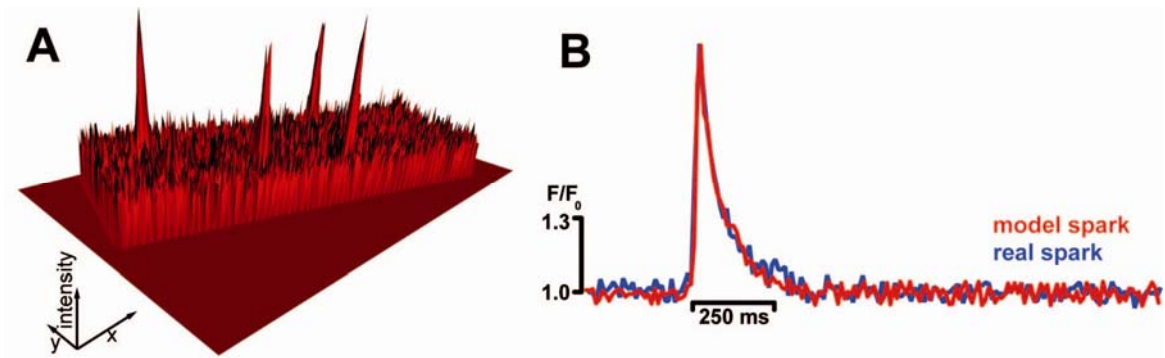


**Figure 30: 3D surface render of a model cell with noise and model sparks.** We added noise to the model cell as a sum of Gaussian noise (electronic noise) and Poisson noise (intensity dependent noise) which was visualized as a surface rendering in **A**. The superimposition of a model spark with the calculated noise and a real spark revealed a high overlap and thus the calculated noise reflects very close the experimental situation (**B**).

The simulation of a model cell with realistic noise and a model spark that could be adapted and varied as favored, set the basis for the evaluation of the algorithm. We were able to construct different data sets to be analyzed by the algorithm, allowing us to evaluate the accuracy of the program. 3 data sets have been constructed based on our model cell with noise. The first contained 100 sparks with constant amplitude, the second cell had 100 sparks with amplitudes that showed a Gaussian distribution and the third data set was filled with 100 sparks with declining amplitudes. For all three data sets the sparks were randomly distributed without spatial or temporal overlap. Fig. 31 displays the volume renders of the three data sets. The algorithm could detect 100% of the sparks in the model cell with sparks of constant amplitude and in the cell with spark amplitudes that followed a Gaussian distribution. In the third data set which contained 100 sparks with declining amplitude, 91% of the sparks could be detected.

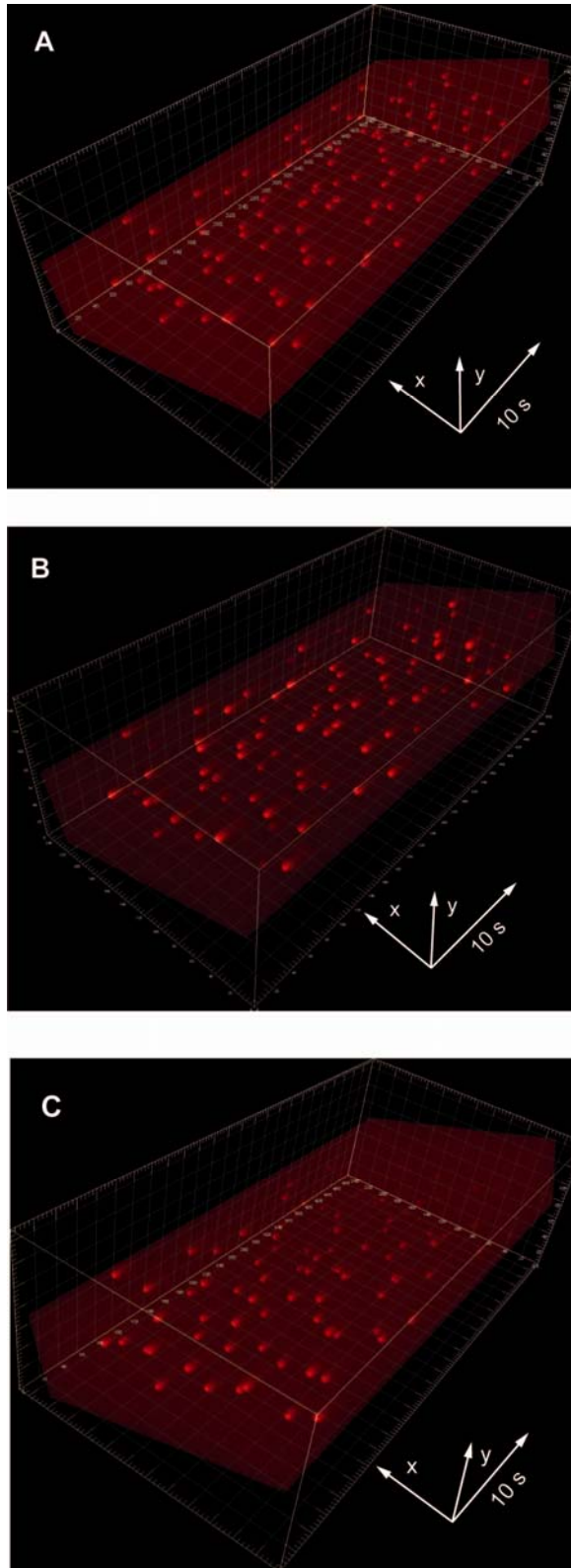


**Figure 31: Data sets for the evaluation of the detection characteristics of the algorithm.** 3 data sets have been constructed to evaluate the detection characteristics of the algorithm. **A** depicts the first data set where sparks displayed a constant amplitude, **B** was the volume rendered data set with sparks having Gaussian distributed amplitudes and **C** was the volume rendered model cell containing sparks with decaying amplitudes. For **A** and **B** 100% of the sparks were detected whereas in data set **C** 91% of the sparks have been successfully detected.



## 2. Characterization of $\text{Ca}^{2+}$ Sparks in the Major Compartments of the Heart

The preparation technique for the isolation of adult cardiac myocytes enabled us to isolate individual cells from the three major compartments of the heart separately, because the atria were cut off the ventricles, they were digested separately.

During the measurements the cells were not stimulated, neither hormonally nor electrically. Only the spontaneous  $\text{Ca}^{2+}$  sparks have been recorded and analyzed. Fig. 32 shows the surface rendering of a single  $\text{Ca}^{2+}$  spark recorded in a myocyte derived from the left atrium and the corresponding time course of the fluorescent signal.

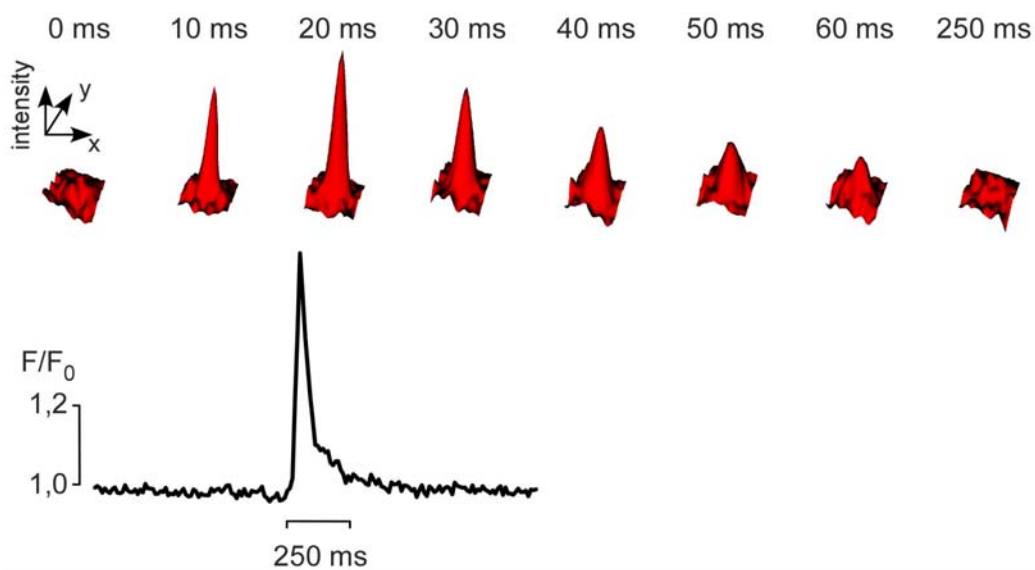


**Figure 32: Exemplary spark taken from an atrial myocyte visualized in a surface rendering and in the corresponding time course.** A single  $\text{Ca}^{2+}$  spark was recorded in a myocyte from the left atrium and visualized as a surface rendering. The corresponding time course is depicted below. The sparks showed a very quick onset and a comparably long decay phase of the signal.

The MatLab algorithm enabled us to compare the amplitudes, the decay time constant and the spatial spread (spark area was calculated with full width at half maximum = FWHM in x and y direction), as well as the spatial anisotropy which was depicted as the ratio of  $\text{FWHM}_x / \text{FWHM}_y$  (1 = round shape;  $>1$  = oval shape) with high accuracy due to the high number of analyzed sparks. For all parameters the mean value per spark site was calculated to rule out false emphasis due to varying activity of different spark sites. The

fact that even subtle changes in the  $\text{Ca}^{2+}$  handling could be detected was also due to the high number of analyzed cells and thus sparks.

When comparing the different compartments of the heart it became clear that some differences existed between the different cell types as depicted in Fig. 33 in the bar graph diagrams. While the spark decay time constant in cells derived from the left and the right atria were not different, the decay time constant of ventricular myocytes was significantly higher. The sparks of all cell types did significantly differ in amplitude, having the highest value in the left atria and the lowest in ventricular cells. The spatial spread was not altered in any compartments of the heart. The anisotropy factor was significantly lower in sparks from the right atria.

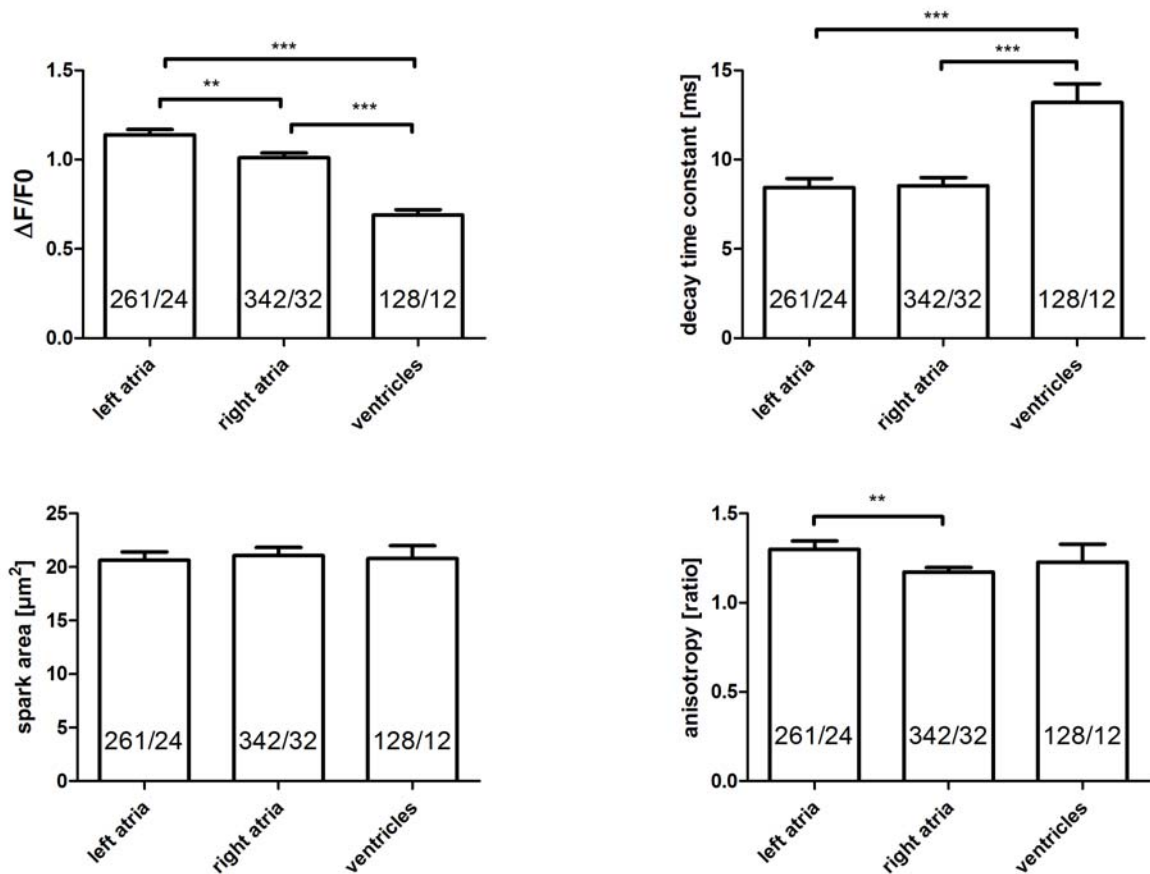


**Figure 33: Spark parameters measured in the three different compartments of WT mouse hearts.** In the upper left diagram the values for the amplitudes of the different compartments were displayed. Sparks from the left atria had the highest amplitudes and those from the ventricles had the lowest values. The decay time constant, displayed in the upper right bar graph diagram, was the same in the left and right atria but significantly longer in ventricles. The spatial spread was not altered in any compartments of the heart. The anisotropy factor was significantly lower in sparks from the right atria. Recordings were performed in 3 to 5 animals.

### **3. The Impact of TRPC1/C4 Double Knock-Out Mutant With and Without Chronical $\beta$ -Stimulation on $\text{Ca}^{2+}$ Sparks**

TRP channels are expressed in almost every human tissue including the heart. Novel studies found evidence that the upregulation of certain TRP channels is involved in the development of cardiac hypertrophy and heart failure. TRPC1 is believed to act as a store-operated  $\text{Ca}^{2+}$  channel (SOC) in cardiac myocytes while TRPC4 is believed to be upregulated due to reduction of SERCA in heart failure (Watanabe et al., 2009). TRPC1/C4<sup>-/-</sup> mice (double knock out (double-KO) of TRPC1 and TRPC4) were provided by the Freichel group (Experimental Pharmacology, Saarland University).

Here it was to discover the effect on the basal  $\text{Ca}^{2+}$  handling by analyzing the spark parameters in cells isolated from these animals.

In a first set of experiments, animals without an implanted minipump were analyzed to discover whether the double-KO itself had an impact on the  $\text{Ca}^{2+}$  sparks. These experiments were performed as blinded studies, so the experimenters did not know the genotype of the animals nor were they allowed to participate in the cell isolation procedures. 4 wild type animals and 3 TRPC1/C4<sup>-/-</sup> animals were analyzed whereas only the mean values for the spark sites were statistically compared. As depicted in the diagrams of Fig. 34, the spatial spread was unaltered in left atrial and ventricular sparks in double-KO animals in comparison to WT mice and anisotropy was increased in left and right atrial sparks. The decay time constant remained unaltered in all compartments. The amplitudes of sparks measured in left atrial cells were increased and decreased in sparks from ventricular cells.

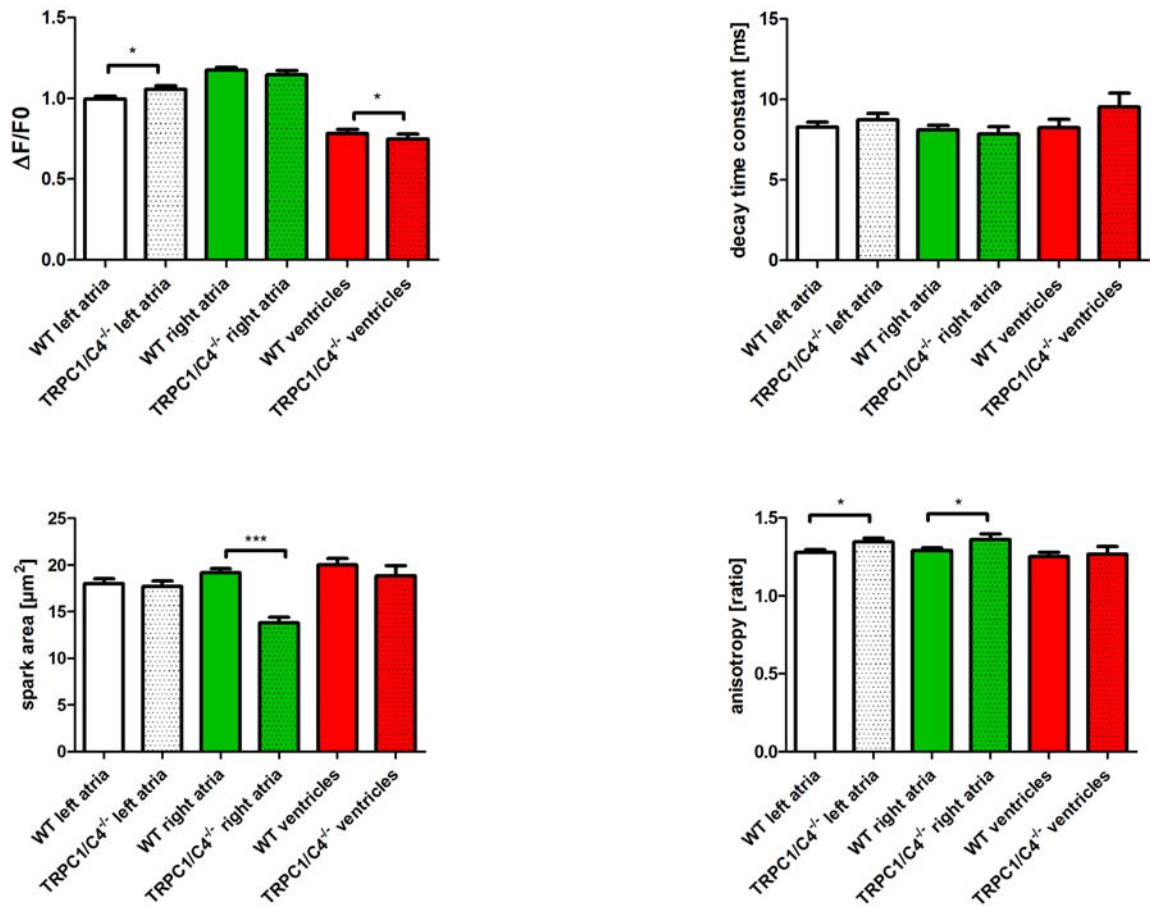


**Figure 34: The impact of heart specific TRPC1/C4 double knock out on Ca<sup>2+</sup> sparks in the three compartments of mouse hearts.** Ca<sup>2+</sup> sparks were measured in TRPC1/C4<sup>-/-</sup> cardiac myocytes from the three major compartments of the heart and compared to WT data. No alterations could be observed in decay time constant, spark area in right atrial cells was significantly reduced and anisotropy was significantly increased in left and right atrial cells. The amplitudes in left atrial cells and ventricles were altered, while left atrial sparks had increased amplitudes and ventricular sparks decreased amplitudes in the double-KO. Statistics were based on the following n-numbers (spark sites/cells/animals): in WT: left atria: 728/27/4; right atria: 754/38/4 and ventricles: 232/12/3 and in the KO-animals: left atria: 509/22/2; right atria: 274/28/3 and ventricles: 126/9/3.

After having analyzed the impact of the double-KO on the Ca<sup>2+</sup> sparks, it was to discover whether Iso, which was used as agent to induce cardiac hypertrophy (Anderson et al., 2008) has an effect on the fundamental Ca<sup>2+</sup> in hearts from WT animals and from double-KO mice. Subcutaneously implanted osmotic minipumps achieved a chronic β-adrenergic stimulation of the mice. The minipumps were filled with isoproterenol (Iso), an agonist for β-adrenergic receptors, widely used for the induction of cardiac hypertrophy in research (Anderson et al., 2008), to achieve a dose of 30 mg/kg/day during 7 days.

Unpublished work from the Freichel lab revealed that there were alterations found in animals treated with Iso in comparison to animals of the control group that were chronically infused with NaCl. Iso induced a hypertrophy that was more pronounced in wild type mice (WT) than in double-KO mice.

As a control group animals were analyzed that had an implanted osmotic minipump filled with isotonic NaCl-solution. These animals should not have displayed any alterations from the infusion but possible impacts deriving from the implantation of the minipumps could be ruled out when the results from the Iso treated animals were compared to this control group.

In WT animals alterations of the  $\text{Ca}^{2+}$  sparks could be observed between the control group and the Iso treated group, where the amplitudes were reduced due to Iso treatment and the spatial spread was significantly increased after the chronic treatment. The anisotropy was not altered. The double-KO animals displayed some alterations due to the Iso treatment as depicted in the bar graph diagrams in Fig. 35. The amplitudes remained unaltered, but the decay time constant was significantly reduced in cells from animals lacking the TRPC1 and TRPC4 channels when treated with Iso in comparison to the animals infused with NaCl solution. No alterations of the spatial spread in either direction could be observed.

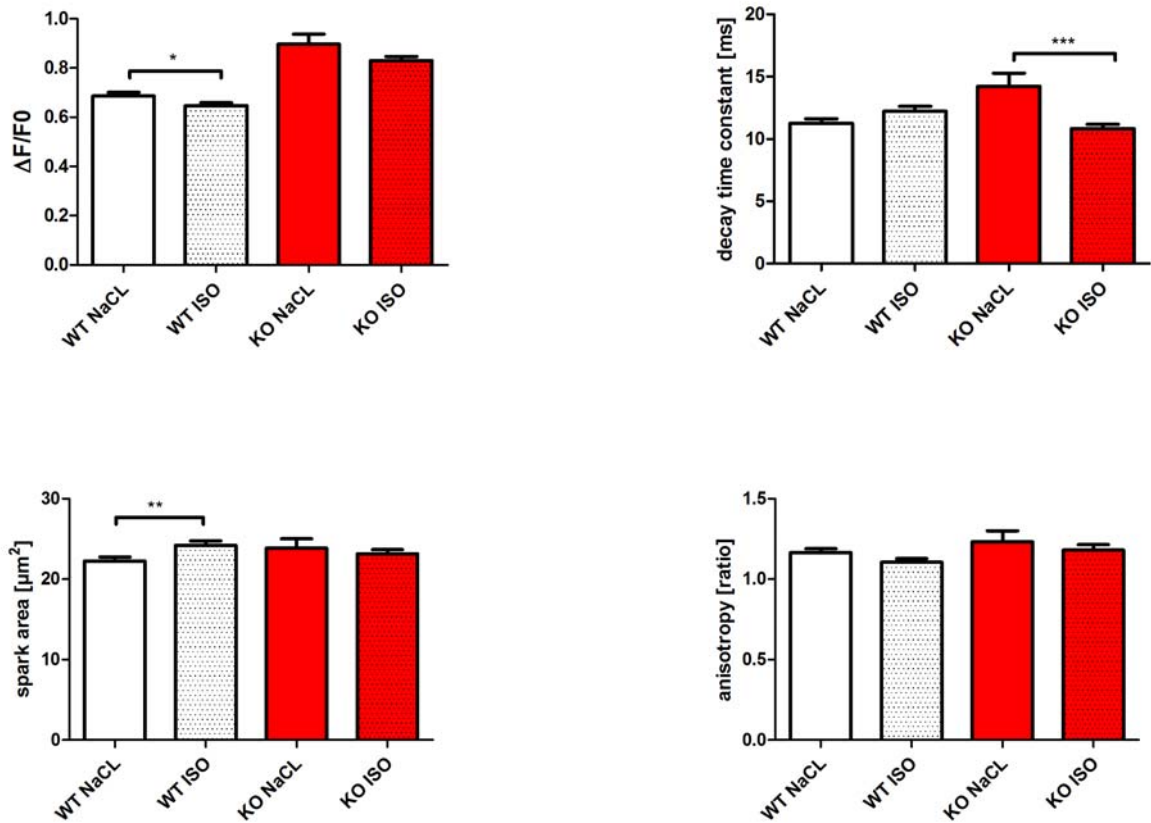


**Figure 35: The impact of chronic isoproterenol infusion on the basal  $\text{Ca}^{2+}$  signals in ventricular myocytes.** The amplitudes were unaltered in double-KO mice but were significantly reduced in WT animals after chronic Iso treatment. The decay time constant remained unaltered in WT animals but was significantly reduced in double-KO animals after Iso treatment. The double-KO animals displayed no alterations of the spatial spread and anisotropy of the  $\text{Ca}^{2+}$  sparks but Iso treated WT cells had increased spatial spread but not anisotropy of the sparks. Statistics were based on the following n-numbers (spark sites/cells/animals): in WT with NaCl: 521/41/3 and with Iso: 519/40/4; in the KO-animals with NaCl: 130/26/3 and with Iso: 557/38/3.

#### 4. The Impact of Over Expression of Rac1 in Mouse Hearts on $\text{Ca}^{2+}$ Sparks

The chronic cardiac overexpression of constitutively active Rac1 is believed to be a mouse model for atrial fibrillation (AF) because the Rac1 GTPase contributes to the pathogenesis of AF (Adam et al., 2007). Functional studies revealed the role of Rac1 in AF formation but the impact on basal  $\text{Ca}^{2+}$  remained unclear and thus studies on the cellular level have been performed from which the results of  $\text{Ca}^{2+}$  spark analysis are presented here.

Rac1 overexpressing mice were based on FVB/N background and therefore the control experiments have been performed also on this mouse strain. The Rac1 overexpressing animals showed great alterations of the heart morphology. These animals had an extremely enlarged right atrium, as depicted in Fig. 36, where the right atrium was approximately three times as large as the ventricles. The isolation of myocytes from such heart usually yielded in lower cell numbers when compared to WT heart.

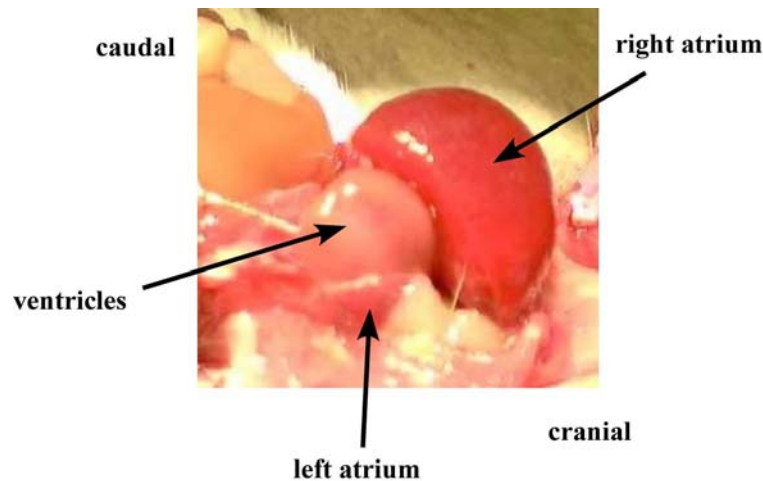


**Figure 36: Hypertrophy of the right atrium in mouse hearts overexpressing Rac1.** The left atrium had a normal size as well as the ventricles but the right atrium was approximately three times larger than the ventricles.

The  $\text{Ca}^{2+}$  sparks of the myocytes from these hearts displayed some alterations in comparison to the wild type (WT) mice as depicted in Fig. 37. The amplitudes of sparks observed in cells derived from each compartment of the Rac1 overexpressing hearts were significantly higher than those observed in WT cells, while the amplitudes in the atria were significantly lower than the ones found in the ventricles.

The decay time constant was not significantly altered in any compartment of the hearts but trends were visible indicating that in left atrial myocytes the decay time constant could have been reduced. More experiments would elucidate this finding. The spatial spread was reduced for the Rac1 overexpressing cells in left and right atria. The anisotropy remained unaltered in the single compartments of the hearts, but a difference between right atrial cells and ventricular cells developed in Rac1 overexpressing cells.

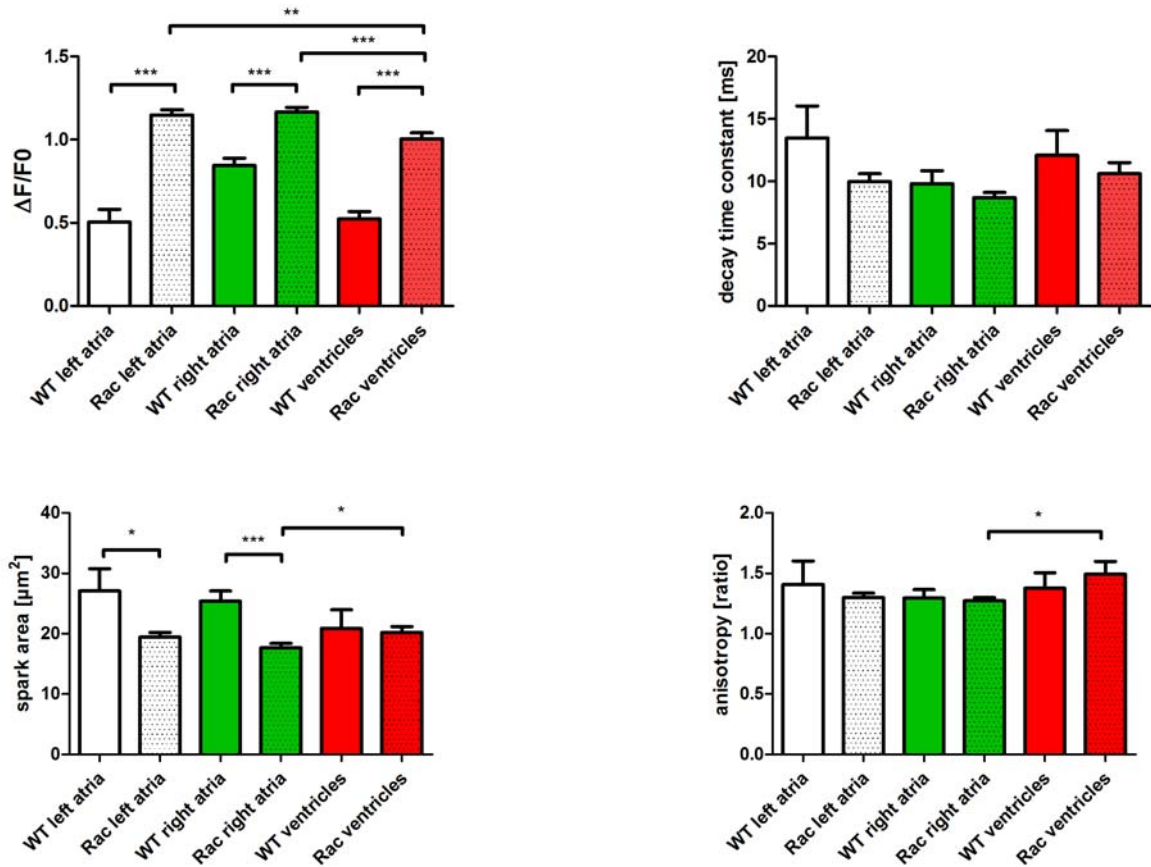


**Figure 37: Spark properties from Rac1 overexpressing cells in comparison to WT cells.** The amplitudes were significantly increased in all three compartments of the heart but the decay time constant was not altered. The spatial spread was reduced in left and right atrial cells but not in ventricles. These data were calculated from 3 to 4 animals for WT and RAC1 overexpressing mice (Rac) each, whereas the n-numbers were as followed (spark sites/cells): WT left atria: 5/3; WT right atria: 12/3; WT ventricles: 6/4; Rac left atria: 27/4; Rac right atria: 18/3; Rac ventricles: 19/4.



## **VI. Discussion**

### ***A. The Morphology of Adult Cardiac Myocytes in Long Term Culture***

The aim of this study was to investigate the effect of long term culture on adult cardiac myocytes in terms of the subcellular morphology. In our group a culturing method has been established which represents a novel approach to keep cardiac myocytes in longterm culture without major alterations of the cells. In conventional culturing methods, the cells were altered due to the adaption to the culturing method (Ellingsen et al., 1993, Horackova and Byczko, 1997, Nag and Cheng, 1981, Poindexter et al., 2001). In our culture method dedifferentiation was largely suppressed in terms of overall morphology (shape and cross striation) and physiology (contractility and global  $\text{Ca}^{2+}$  handling). This study also reported the possibility of adenoviral driven gene transfer in these cells by expressing genetically encoded biosensors (Viero et al., 2008). Such an improved culture system is essential to study longterm effects of chronic electrical or hormonal stimulation on cardiac myocytes or under otherwise controlled conditions. For such studies a culture system is desirable which reduces remodeling of the cells and yields in cells with reproducible alterations that can be handled as baseline characteristics.

The main goal of the presented work was to investigate and describe whether or not cardiomyocytes change their subcellular morphology in our culture method. Thus I investigated the structures of several organelles of the cardiac myocytes (i.e. plasmamembrane, mitochondria, Golgi apparatus and sarcoplasmic reticulum) during longterm culture.

I used two labeling methods for the investigation of the subcellular structures in the living cells. First I expressed fluorescent fusion proteins, because with such a method a highly specific labeling was achieved and interdependencies were ruled out. A drawback of the adenoviral driven gene transfer and the expression of fusion proteins is that the organelles could be imaged from DIV1 onwards but not in freshly isolated cells. When possible, I labeled the structures as well using small molecule dyes. This facilitated a complementary approach to label the cell organelles and it enabled me to investigate the structures in freshly isolated cells.

## 1. Plasmamembrane

In ventricular myocytes the plasma membrane is distinctly different from that found in most other cells regarding its particular morphology. In ventricular cells a highly organized network of so called t-tubules (invaginations of the membrane) is found. The t-tubules serve as enormous increase of the cell surface and previous studies also showed that a large number of key proteins necessary for excitation contraction coupling are found predominantly in the t-tubules (Orchard and Brette, 2008). L-type  $\text{Ca}^{2+}$  channels are located in the t-tubules at the dyadic junctions (Scriven et al., 2000) and the loss of t-tubules in ventricular cells leads to altered  $\text{Ca}^{2+}$  signaling due to inhomogeneities of the  $\text{Ca}^{2+}$  inward current (Lipp et al., 1996).

From all cells labeled with either the fluorescent fusion protein or the small molecule dye, z-stacks have been recorded. Especially with cells labeled with Di-8-ANEPPS this turned out to be difficult, because these cells tended to contract during a measurement. I assumed that the combination of the dye with the energy from the excitation laser induced contractions of these cells. I therefore removed the  $\text{Ca}^{2+}$  from the tyrode's solution to calm the cells. This yielded in cells that were more quiescent. Nevertheless it was difficult to use these data for 3D-rendering and thus the analysis was performed on the z-stacks.

To quantify the assumed loss of t-tubules the relative t-tubular length was calculated by measuring the length of t-tubules connected to the plasmamembrane without truncations in relation to the cell diameter. Therefore a middle slice of a cell was chosen, where the two nuclei were visible to assure consistent procedure. Additionally the t-tubules could be tracked in those cases when they were not completely visible in the observed slice, because z-stacks of the cells were taken.

In cells labeled with Di-8-ANEPPS a loss of t-tubules was observed until none were left at DIV6. The fact that no residues were found in the center of the cell together with the finding that all visible t-tubules were clearly connected to the plasmamembrane indicated that this dye indeed only labeled those t-tubules accessible from the outside as already indicated by Banyasz et al., 2008. In this study a loss of t-tubules during 5 days in culture was described and they assumed degradation process.

The GPI-anchored fluorescent protein was intended to label all plasmamembrane found within a cell and thus possibly disconnected t-tubules should have been visible with this technique. Indeed more labeling was observed in these cells, particularly at DIV1 and

DIV3. These findings depicted in Fig. 18 strengthened the assumption that the t-tubules get detached from the plasmamembrane and thus having no contact to the extracellular space but still being present within the cells. These fragments could no longer participate in excitation contraction coupling in a way that they were electrically disconnected from the plasmamembrane but they may have served as functional compartments where  $\text{Ca}^{2+}$  signaling was possible and where functional junctions of the SR and the membrane of the compartment might have been present. I analyzed data from Cedric Viero with our new spark algorithm and sparks were detected throughout the cell during the week in culture without the indication of a preference towards the membrane. The spark parameters, displayed in the bar graph diagram in Fig. 38, indicated that the  $\text{Ca}^{2+}$  was altered but CICR seemed to be still possible, indicating the presence of compartments capable of  $\text{Ca}^{2+}$  handling to some degree.

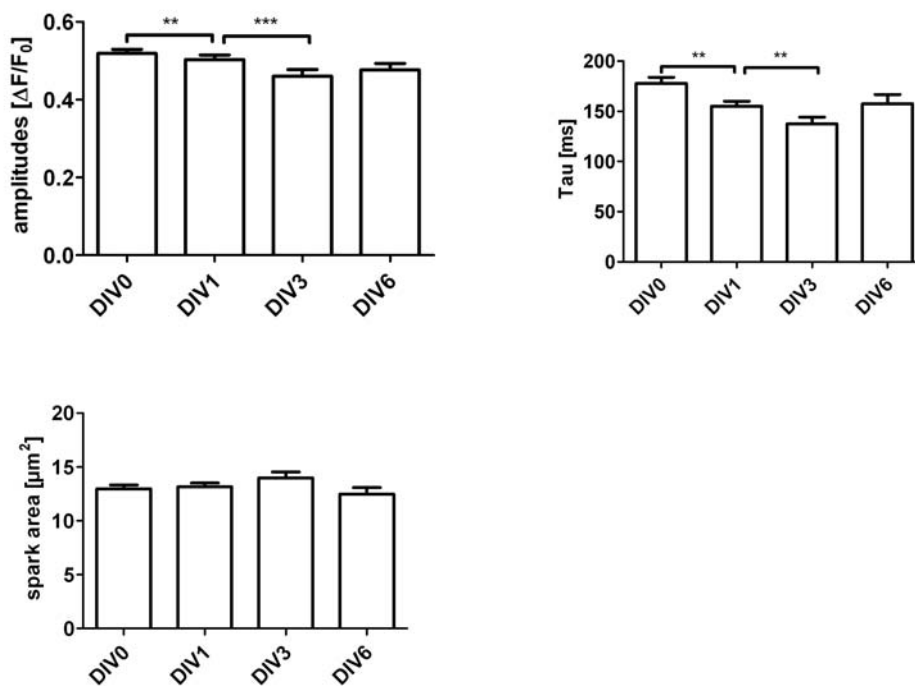


**Figure 38: Spark parameters from cultured cardiac myocytes.** Data were recorded by Cedric Viero and I analyzed them with the new spark algorithm. Amplitudes and decay time constant (tau) initially reduced and recovered at DIV6 whereas no changes of spark area was observed.

Detubulation experiments using formamide as detubulation agent revealed that t-tubules were disconnected from the plasmamembrane but remained inside the cell (Brette et al., 2002). In this study it was shown that the t-tubules disconnected from the plasmamembrane due to formamide wash-out and resealed afterwards which led to a loss

of synchronous  $\text{Ca}^{2+}$  release after electrical stimulation which was also demonstrated in guinea pig ventricular myocytes where a loss of t-tubules led to non-uniform  $\text{Ca}^{2+}$  release (Lipp et al., 1996).  $\text{Ca}^{2+}$  transients in detubulated ventricular myocytes had a slower recovery and initially occurred only at the periphery of the cells. It has also been demonstrated that dyads at the surface remained unaltered after detubulation but the dyads in the depth of the cells were probably disrupted (Brette et al., 2005, Brette et al., 2002, Brette et al., 2004).

The relative t-tubular length found in cells labeled with the fluorescent fusion protein was significantly longer than those observed in Di-8-ANEPPS stained cells. It has been demonstrated (see Fig. 18 and 20) that more structures were labeled with the GPI-YFP than with the dye and thus it might have appeared that these t-tubules were longer. The cells observed during the week in culture were captured within an ongoing process of detubulation as demonstrated with these data and some of the t-tubules that have just been constricted from the plasmamembrane were probably still in very close proximity of the outer membrane. If the space between two fragments was below the resolution limit of the microscope they were observed as not truncated. Electrophysiological experiments from our lab, where the capacitance of the cells was measured, indicated a loss of surface area during the time in culture (Martin Oberhofer, oral communication) and thus strengthen the findings made in Di-8-ANEPPS labeled cells. In some cells the both labeling methods have been performed in parallel to elucidate whether both methods labeled the same structures. Both methods labeled the outer leaflet with its t-tubules but it was very obvious that the fusion protein labeled more structures than the Di-8-ANEPPS during the culture of the cells which was already detectable at DIV1. While Di-8-ANEPPS was restricted to the plasmamembrane and its invaginations that were still connected and accessible from the outside, the fusion protein also labeled disconnected but intact t-tubular residues within the cells.

In conventional culture cardiac myocytes undergo a process of dedifferentiation where they lose the adult phenotype (Nag et al., 1996, Poindexter et al., 2001) including a loss of t-tubules. Here the aim was to quantify the loss of t-tubules. Therefore the cells have been labeled with two methods, first with Di-8-ANEPPS and second with the GPI-YFP fusion protein. Di-8-ANEPPS is a membrane potential sensing dye and was chosen for these experiments because it is retained in the outer leaflet of the membrane due to its lipophilic structure and thus was preferred over Di-4-ANEPPS, which tends to be internalized more

easily and is more phototoxic (Rohr and Salzberg, 1994). The characteristics of this dye allowed to exclusively monitor plasmamembrane which was still accessible from the outside. The complementation of these experiments was achieved by using the fluorescent fusion protein which localized at the GPI anchor which is found within the lipid rafts of the plasmamembrane. Such a GPI anchored protein would be associated to membrane if it is still in contact to the extracellular space or not and thus it was hypothesized that t-tubules could be labeled even if they were disconnected from the plasmamembrane.

Detubulation of cardiac myocytes was described as early as these cells were cultured and was found to be connected to a disorganization of the myofibrils which underwent rearrangement during cell culture and in some cases was even extruded via exocytosis (Eppenberger et al., 1988, Nag and Cheng, 1981, Nag and Lee, 1997, Nag et al., 1996). A major role in this process was attributed to actin. Thus CytochalasinD was added to the culture medium to improve the maintenance of the myocyte morphology because it has been demonstrated to improve the maintenance of the t-tubular structure of ventricular myocytes in culture (Leach et al., 2005). CytochalasinD is a naturally occurring organic molecule which binds to actin and inhibits association and dissociation of the actin filaments (Cooper, 1987). It has been shown previously that CytochalasinD stabilizes actin and thus reduces dedifferentiation by maintaining t-tubule density (Leach et al., 2005). These findings could be confirmed and the supplement improved the maintenance of the tubules reflected in the relative t-tubule length observed in cells with either labeling method. The fragments measured in cells labeled with Di-8-ANEPPS were significantly longer from DIV0 onward and there were even some residues found in cells at DIV6. The differences observed at DIV0 demonstrated that the dedifferentiation process already started directly after isolation of the cells because between isolation and first measurements lay about 3 hours which were sufficient for variations in the t-tubular length observed with Di-8-ANEPPS to occur. Even though CytochalasinD represents a potent stabilization agent of the membrane it cannot prevent the remodeling process observed here completely.

## 2. Mitochondria

Mitochondria are often referred to as the power plants of the cells because they represent the main source of chemical energy in form of ATP, but they are also involved in various other processes such as  $\text{Ca}^{2+}$  signaling, cell differentiation and cell death. Mitochondria vary largely in number, size and organization among different cell types. In cardiac ventricular myocytes they are highly organized and the arrangement of mitochondria is related to the overall cell structure and the arrangement of the myofibrils (Birkedal et al., 2006).

The mitochondria were labeled with two labeling methods as described before. No differences between the two methods could be observed as depicted in Fig. 21. The mitochondria of cultured cardiac myocytes were well organized in freshly isolated cells and visible as single packages along the longitudinal axis. The fluorescent images revealed a cross striation which was most probably due to the t-tubules being located in between and separating the single packages. It was observed that this cross striation was lost during the week in culture until there were only few single packages visible but more longitudinal tubes. This observation was consistent in both labeling methods. The length of a single package was found to be 1.8  $\mu\text{m}$  at DIV0 and DIV1, which corresponds to the sarcomere length in ventricular myocytes and which was described as well in earlier confocal microscopy studies (Birkedal et al., 2006). This value was increased to about 4  $\mu\text{m}$  at DIV3 and DIV6, which was more than doubling the distance. This led me to the conclusion that the single packages fused in such a way that 2 or 3 mitochondrial packages apparently fused to become one.

Electron microscopy studies of the mitochondria in the heart of adult rats revealed that they had a flattened morphology with a length of about a sarcomere, being arranged in longitudinal columns in the clefts between the myofibrils (Segretain et al., 1981), which corresponds to my findings here. Newer studies indicated that dependent on the location in the cell, the single mitochondria can have different shapes due to their location within the cell (e.g. close to the membrane or the nucleus or between the myofibrils) and thus different dynamics (Hom and Sheu, 2009). It was also shown in this study that they do contain all proteins necessary for fission and fusion, which was often observed in other cell types but rarely found in cardiac myocytes. Therefore I hypothesized that the mitochondria fused during the time in culture as soon as there was no structure hindering them to get in close contact. This was based on the finding that the distance of the gaps between the

single mitochondria increased while t-tubule density was reduced, giving way for the fusion of the mitochondria.

The alterations of mitochondrial morphology in ventricular myocytes indicated that they fused during one week in culture but the confocal studies alone could not proof this assumption. There was still the possibility that the mitochondria moved very close together but actually not fused and functionally connected, which would not have been detectable with morphological studies using a confocal microscope.

Further experiments were performed to answer the question whether the mitochondria really fuse or just move very close together, beyond resolution limit. For that purpose FRAP experiments have been performed on cells labeled with MitoTracker<sup>®</sup> Green. This type of experiments allowed to check whether two mitochondria were connected or not by measuring the fluorescence recovery in a bleached area of the mitochondrion. From experiments in HEK cells depicted in Fig. 22, which have single, relatively long and thin mitochondria, it has been shown that the bleached area from a long mitochondrion showed recovery while the neighboring area showed fluorescence loss after photobleach (FLAP). Such a behavior is exclusively possible when there is a connection between the two observed areas. This phenomenon was also found in cardiac myocytes, were the bleached, apparently single mitochondrion showed a recovery of the fluorescence and the neighboring mitochondrion lost some of its fluorescence, presumably giving it to the bleached neighbor. Fibroblasts shown as control cells had a relatively fast recovery which was significantly faster than the times observed in myocytes, because the mitochondria were connected in these cells. Cardiac myocytes at all observed DIV's showed recovery of the fluorescence signal which had a recovery time that was not significantly different but displayed a trend towards a faster recovery at DIV6. At DIV0 and DIV1 there were also mitochondria observed that showed no recovery at all and it was thus concluded that the mitochondria in ventricular myocytes had heterogeneous morphology, some have connections with their neighbors others not.

Electron microscopic images taken from cultured cardiac myocytes at DIV0 revealed that even in freshly isolated cardiac myocytes there were mitochondria that have been clearly separated (vast majority of mitochondria observed) but some mitochondria were already fused or connection via a thin connection as depicted in Fig. 39, an electron

microscopic image taken by Dr. Ludwig Edelman. This image also revealed that the mitochondria of a single cell displayed heterogeneous morphology.

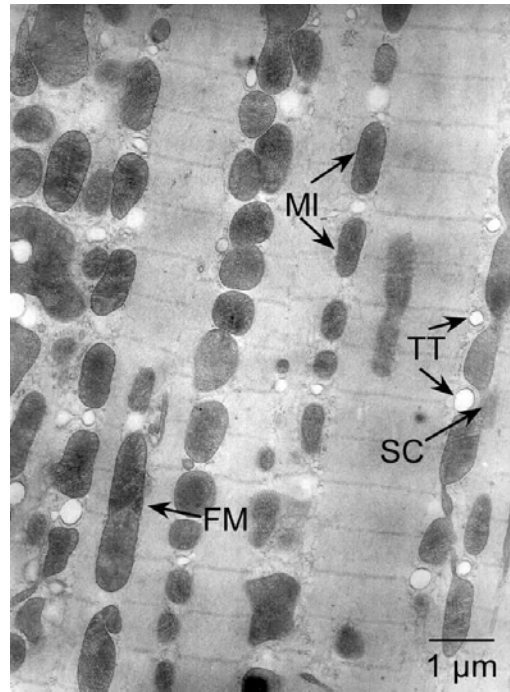


**Figure 39: Electron microscopic image of a freshly isolated cardiac myocyte.** The mitochondria, depicted with MI, displayed various morphological states. While apparently single packages were found (MI), some mitochondria were completely fused (FM) and others had only a small connection (SC), e.g. when a t-tubule (TT) was located between two mitochondria. Image provided by Dr. L. Edelman.

These findings indicated that there were some mitochondria that were already connected to their neighbors at DIV0 and that these connections allowed an exchange between the single packages. It was assumed that there were already small functional connections in freshly isolated cells that were not visible with confocal microscopy. While the mitochondria seemed to fuse to some extent during the days in culture the recovery was faster, because the exchange was much better due to the better connections, i.e. larger exchange rate was possible when two mitochondria completely fused.

The experiments performed here revealed that first mitochondria adapt to the alterations of the morphology in long term culture by fusing but functional connections could be observed also in freshly isolated cells. To get quantitative data on the level of fusion of single mitochondria, a different experimental design would be necessary. In contrast to the already performed FRAP experiments, future studies will have to focus on more mitochondria within a single cell to be bleached. This would give an insight on the fraction



of mitochondria that do have functional connections and on the quality of these functional connections, i.e. whether the connections are small ‘tubes’ between two mitochondria as depicted in the electron microscopic data or if mitochondria are completely fused.

### **3. Endoplasmic/Sarcoplasmic Reticulum**

The sarcoplasmic reticulum (SR) of muscle cells is a specialized form of the smooth endoplasmic reticulum (SER). The SR differs from the SER in two ways, first in the composition of proteins it contains and second in its function. While the SER is predominantly involved in several metabolic processes synthesizing molecules, the SR especially stores  $\text{Ca}^{2+}$  and controls the cytosolic  $\text{Ca}^{2+}$  concentration.

The localization target of the fluorescent fusion protein was a combination of two proteins found in the ER, localization sequence of calreticulin and the ER-retrieval sequence KDEL; both proteins were also detected in the SR (Allen and Katz, 2000, Gatti et al., 2001). It is believed that the ER and the SR form a continuous network where the two parts are not clearly separated.

The sarcoplasmic reticulum was found to be a fine tubular network that was well organized and evenly spread throughout the cells except for the perinuclear area, where the labeling appeared to be more prominent. This highly organized pattern found in cells at DIV1 which was less pronounced at DIV3 and DIV6 (see Fig. 25). Early electron microscopy studies revealed that the endoplasmic reticulum was found distributed in the whole cell with contacts to the plasma membrane and especially the nuclei (Moore and Ruska, 1957). The finding that the organized structure got lost during the time in culture could be associated with the loss of t-tubules, since it has been shown before that the sarcoplasmic reticulum in cardiac myocytes was found next to the t-tubules, running alongside with them (Segretain et al., 1981).

The SR is the major  $\text{Ca}^{2+}$  storing organelle in myocytes and is crucial for ECC. It controls  $\text{Ca}^{2+}$  levels in the cytoplasm by coordinating  $\text{Ca}^{2+}$  storage, release and reuptake and thus regulates the contraction of the cell (Rossi and Dirksen, 2006, Rossi et al., 2008). Since in this study the SR remained distributed throughout the cells with minor alterations of its morphology, it still could participate in  $\text{Ca}^{2+}$  signaling within the cells although the t-tubules and thus the dyadic junctions were lost after one week in culture. Although ECC

was no longer possible  $\text{Ca}^{2+}$  release from the stores could still be performed just as found earlier in our group when  $\text{Ca}^{2+}$  sparks in cultured cardiac myocytes were analyzed. These studies showed that even at DIV6 the sparks were found within the depth of the cells indicating a functioning SR (unpublished data from Cedric Viero). The situation in detubulated ventricular myocytes is comparable to the situation found in atrial myocytes lacking a t-tubular network.  $\text{Ca}^{2+}$  sparks in atrial cells can be classified in two groups, the first group with sparks that occur at the periphery of the cells and sparks that occur in the depth of the cell, whereas the second group displayed slower and smaller sparks (Mackenzie et al., 2001, Woo et al., 2003). The sparks observed in ventricular myocytes that have been cultured in our lab also displayed two populations, one with shorter the other with longer decay time constants. Also the global  $\text{Ca}^{2+}$  handling in these cells closely resembled the situation observed in freshly isolated cells (Viero et al., 2008).

#### **4. Golgi Apparatus**

In contrast to earlier studies where the Golgi apparatus was described as an accumulation of stacks located at the perinuclear region of the cells in electron microscopy studies (Rambourg et al., 1984, Suzaki and Kataoka, 1999) in my experiments this organelle was observed as vesicular structures evenly spread throughout the whole cell. This discrepancy might be attributed to the labeling method with the fluorescent fusion protein. The targeting sequence was the sequence of ts045-G, which is a marker for exocytotic membrane transport from the ER via the Golgi apparatus (Scales et al., 1997). Therefore it was assumed that this fusion protein could not label the whole Golgi apparatus but only the vesicular structures involved in transport.

While this evenly spread pattern was found at DIV1 and DIV3, the Golgi apparatus was accumulated around the nuclei at DIV6 (see Fig. 26). The fact that at DIV6 no fluorescence could be detected elsewhere in the cytosol also supported the specificity of the fluorescent fusion protein in labeling exclusively the Golgi apparatus. The rearrangement of the organelle between DIV3 and DIV6 was thought to be connected to the alterations of the cells that also caused the t-tubular loss. A change of the cytoskeleton might have hindered the Golgi apparatus to move within the cell forcing the organelle to remain at the perinuclear region.

The Golgi apparatus in cells treated with CytochalasinD also displayed a rearrangement of the organelle but in these cells the onset of this alteration started already between DIV1 and DIV3. Since CytochalasinD acts on the actin filaments avoiding the polymerization and depolymerization which fixes the actin at the given state (Cooper, 1987), the Golgi apparatus is probably also no longer able to move towards the plasmamembrane explaining the premature reorganization observed in CytochalasinD treated cells.

## **5. Actin Filaments**

The confocal studies on the subcellular morphology of cultured myocytes revealed a great involvement of the actin filaments in dedifferentiation. The addition of CytochalasinD into the culture medium improved the maintenance of the structure of the cells and thus it was assumed that actin filaments were crucial for the maintenance of the cell morphology. It has been demonstrated before that contractile arrest causes degradation of actin filaments and thus active tension is crucial for the maintenance of the actin filaments (Sharp et al., 1993). Little is known about the structure of actin in living cells because until recently no live cell labeling for the actin filaments were available. Studies from fixed cells demonstrated that f-actin is located at the I-band of the myofibrils and that it is a possible player in myofibril formation which undergo de- and regeneration in long term culture (Eppenberger et al., 1987, Eppenberger et al., 1988).

Here we provided live cell imaging of the actin filaments, where the actin filaments were observed as packages along the longitudinal axis displaying a clear cross striation. The distance of the single packages reflected the sarcomere length and was not altered during the time in culture and thus it could be concluded that the actin filaments did not get lost during one week of culture (see Fig. 27).

Actin usually undergoes very dynamic polymerization and depolymerization processes. With the techniques used in this study, it was not possible to monitor dynamic processes in an appropriate way and thus it was not possible to learn more about the dynamics of actin in cultured cardiac myocytes. It might have been the case that the actin became less dynamic during the time in culture which could have resulted in difficulties transporting the Golgi apparatus as described before or supporting the t-tubules, but would not have been visible in the morphology of the actin as it was observed here. These questions remain elusive and require further experimental designs.

These findings indicated a good maintenance of the cells cytoskeleton and contractile filaments as far as the structure of actin was concerned even without the supplementation of the culture medium with CytochalsinD. The cross striation observed and quantified remained unaltered which was in accordance with earlier findings from Cedric Viero who showed a conservation of the general morphology.

## ***B. The Physiology of Cardiac Myocytes***

### **1. MatLab Spark Algorithm**

The developments in confocal microscopy techniques allowed the fast acquisition of two-dimensional time series of living cells with a speed of 100 to 200 Hz. But until recent it was not possible to analyze three-dimensional data and thus one had to use line scan analysis, which also led to a loss of information from the single  $\text{Ca}^{2+}$  release events observed here. The spatial spread for instance could only be detected in one direction, meaning that the real spatial shape could only partly be calculated. Besides the limitations due to the loss of spatial information, such analysis was very user dependent and time consuming. It thus was highly desirable to have a tool that could reduce user dependent judgments and thus unbiased results. Recent development brought up two approaches to detect and analyze  $\text{Ca}^{2+}$  sparks in two-dimensional time series of cardiac myocytes. Banyasz and Colleagues (Banyasz et al., 2007) developed a tool for spark detection. But this approach still required some user interference and preparation of the recorded images to assure a good detection result. In the same journal issue as Banyasz et al. Bray and colleagues (Bray et al., 2007) introduced a detection and analysis tool, which was also written in MatLab like our software but which was largely dependent on the quality of the input data.

Since the mentioned detection algorithms still had drawbacks like the need for preprocessing of the data, our lab introduced a new algorithm for the detection and analysis of  $\text{Ca}^{2+}$  sparks negotiating such limitations. Our MatLab-based Algorithm to detect and analyze  $\text{Ca}^{2+}$  sparks in two-dimensional time series of cardiac myocytes was introduced in the Diploma thesis of Aline Flockerzi (Flockerzi, 2007). We developed a tool to analyze cells from various origins, with minimized user dependent influence on the data.

The first step towards an improved algorithm was to enable the loading of unprocessed data derived directly from the microscope; this ruled out any influence of the user. To enter the metadata needed for analysis an input file had to be prepared by the user, which contained all the information necessary for the detection and analysis, e.g. image size, minimal cell size for the cell detection, acquisition speed and pixel size. This data file was an excel sheet containing the metadata for all data sets that were to be analyzed and thus could also be used in the batch mode. This way all data collected for example during one day could be loaded within one step, so there was no need for the user to load each data set separately.

Furthermore a tool has been implemented that could detect whether two or more distinct sparks were derived from the same spark site and thus from supposedly the same cluster of RyRs. This so called cluster analysis allocated each detected spark to its spark site and in a further step the mean values for the spark sites were calculated for all parameters presented here. This function also gives the frequency values for sparks per cell and sparks per spark site, but I decided not to further analyze these values because the data shown here were exclusively derived from spontaneous  $\text{Ca}^{2+}$  sparks. It was not discernible in which activity state was at the moment of recording. That could mean a cell could be recorded just after the occurrence of a wave or right before the onset and this would possibly lead to varying spark frequencies. Furthermore, the spark frequency of a cell is also dependent of the condition of the cell itself and its plasmamembrane. My subjective impression implicated that on one cover slip with cells from the same preparation, different activity states could be observed. Some cells displayed no spontaneous  $\text{Ca}^{2+}$  release events whereas others had a very high  $\text{Ca}^{2+}$  spark rate that just passed into  $\text{Ca}^{2+}$  waves. I therefore believe that the analysis of spark frequency within cardiac myocytes makes sense in synchronized cells, e.g. in field stimulated cells but not in cells with spontaneously occurring sparks. Although only a few parameters have been presented in this work, the algorithm allows broadening the parameters extracted.

This program allowed the detection of even subtle changes of  $\text{Ca}^{2+}$  sparks since a larger amount of data could be analyzed than previously possible. The accuracy tested on modeled cells and sparks was above 90% even with noise added to the data sets (see Fig. 31). Furthermore it can be adapted to various experimental settings, e.g. different microscopes. It is easy to use because the user only has to create the input data file which

contains the metadata and no preprocessing of the data is necessary. Thus the algorithm is very robust.

## **2. Characterization of Ca<sup>2+</sup> Sparks in the Major Compartments of the Heart**

The elementary Ca<sup>2+</sup> signal underlying ECC is a Ca<sup>2+</sup> spark and has been studied for many years in various cell types from different species (Niggli and Shirokova, 2007). Depending on the source of origin, e.g. the channel responsible for the Ca<sup>2+</sup> release, such elementary signals have been given different names (Berridge, 2006) as depicted in Fig. 4 but they all have in common that they are produced by opening of a small group of channels, creating a local Ca<sup>2+</sup> signal. The extensively studied elementary signal observed in cardiac myocytes is a Ca<sup>2+</sup> spark. Although Ca<sup>2+</sup> sparks have been studied in various cell types (Cheng and Lederer, 2008), the data for cardiac myocytes is more focused on signals from ventricular myocytes and to my knowledge no direct comparison of the different compartments of the heart (i.e. left and right atrium and ventricles) have been performed so far.

We used a fast confocal microscope and the analysis software described above to analyze Ca<sup>2+</sup> sparks from the three compartments of mouse hearts, the left and the right atria and the ventricles. The amplitudes, decay time constant and spatial spread in x and y direction have been analyzed and compared.

The amplitudes of the sparks observed in atrial cells were significantly higher than those found in ventricular cells with values of about 1 to 1.1 F/F<sub>0</sub> in left and right atria, respectively, and 0.7 F/F<sub>0</sub> in ventricular sparks (Fig. 33). It has been reported before that the sparks measured in atrial cells displayed higher amplitudes and longer time courses compared to sparks from ventricular cells (Sheehan et al., 2006, Woo et al., 2003, Woo et al., 2005). Earlier studies reported varying spark amplitudes even within ventricular cells only (Lipp and Niggli, 1998, Pratusевич and Balke, 1996). Modeling studies provided indications that the real spark amplitude was always higher than the ones found in experimental measurements (Chandler et al., 2003, Rios et al., 2001, Smith et al., 1998). Izu and coworkers provided data from confocal imaging studies displaying larger amplitudes than previously demonstrated (Izu et al., 2001), but it has to be noted that these data were not automatically detected and thus smaller signals were probably lost because

the human eye cannot distinguish very small sparks from the noise of the recording. The underestimation of the  $\text{Ca}^{2+}$  amplitude is most probably due to the techniques used for imaging. I tested the impact of the concentration of the  $\text{Ca}^{2+}$  indicator on the spark parameters. Therefore I tested 3 different Fluo4 concentrations, 0.5, 1.0 and 1.5  $\mu\text{M}$ . These measurements showed that the amplitudes depend on the indicator concentration, displaying a decrease of amplitudes with increasing indicator concentration. The difference in amplitudes between cells loaded with 0.5  $\mu\text{M}$  Fluo4 and cells loaded with 1.5  $\mu\text{M}$  Fluo4 was 35%. The higher fluo4 concentrations probably buffered the  $\text{Ca}^{2+}$  released and thus inhibited further CICR resulting in smaller amplitudes. When comparing result derived from different study designs it is thus indispensable to consider the possibly varying loading conditions with the  $\text{Ca}^{2+}$  indicator. These findings also indicated that CICR might play a more pronounced role in spark formation in ventricular cells than in atrial cells.

Confocal microscopy is characterized by the fact that a defined plane of the cell is imaged with the exclusion of out of focus light. When imaging  $\text{Ca}^{2+}$  sparks it is possible that one collects data deriving from a plane above or below the focal plane, which means that only a part of the spark is recorded and data might be blurred. It is difficult to exclude these out of focus sparks completely. It is assumed that the amplitude of  $\text{Ca}^{2+}$  sparks roughly represents the amount of released  $\text{Ca}^{2+}$  during the rise time of a spark which indicates that more  $\text{Ca}^{2+}$  was released from spark sites in atrial myocytes in comparison to spark sites in ventricular myocytes. It remains elusive whether an increased spark amplitude is due to higher SR  $\text{Ca}^{2+}$  contents or to the opening of a larger number of RyR-openings within a cluster.

The decay time constant found in sparks from atrial cells did not vary between the left and the right atria but the decay time constants found in sparks from ventricular myocytes was significantly higher (Fig. 33). This indicates that the  $\text{Ca}^{2+}$  removal mechanisms in atrial cells differ from those found in ventricular myocytes. These mechanisms include on one hand the termination of the  $\text{Ca}^{2+}$  signal and the removal of excess  $\text{Ca}^{2+}$  from the cytosol on the other hand. The  $\text{Ca}^{2+}$  spark is terminated when the SR  $\text{Ca}^{2+}$  content reaches a critical threshold which was shown to be independent of initial SR  $\text{Ca}^{2+}$  content and release flux (Brochet et al., 2005, Zima et al., 2008). Furthermore a CICR desensitization can contribute to the termination of a  $\text{Ca}^{2+}$  spark (Gyorke and Gyorke, 1996). But also active removal processes such as the activity of the sodium- $\text{Ca}^{2+}$ -exchanger (NCX) transporting the  $\text{Ca}^{2+}$  out of the cell or the sarco-/endoplasmic reticulum ATPase (SERCA)

refilling the stores can influence the decay time constant of a spark. In contrast to ventricular cells the atrial cells do not display a t-tubular system. The contribution of the NCX being located in the plasmamembrane, predominantly in the t-tubules, is thus lower than in ventricular cells, at least for those sparks occurring in the depth of the cells. It thus can be concluded that the role of the SERCA is more dominant in atrial cells than in ventricular cells because it has to be the largest contributor for the  $\text{Ca}^{2+}$  removal in atrial cells, where the NCX is not available in the depth of the cells. The differences in contraction durations from ventricular and atrial preparations have been the reason for Luss and colleagues to analyze the expression levels of certain  $\text{Ca}^{2+}$  regulating proteins in atria and ventricles in different species (Luss et al., 1999). They demonstrated that expression levels of SERCA in atria were higher in comparison to ventricles and additionally the expression of phospholamban (PLB), which modulates the SERCA pumps, was lower in atria. This strengthened the finding of enhanced  $\text{Ca}^{2+}$  removal in atrial cells. It has to be noted that the decay time constant of 13 ms was below the values described before, where constants of 20 ms (Cheng et al., 1993) and 15 to 20 ms (Wang et al., 2002) have been described. The reasons for the different findings remained elusive. To investigate the influence of the detection algorithm on the spark data a comparative study of different algorithms could help. Experimental data and modeled data could be analyzed with different methods, e.g. two-dimensional vs. three-dimensional approaches and of course the different three dimensional approaches described above (see VI.B.1.).

The spatial spread of the  $\text{Ca}^{2+}$  sparks which was given as the area and an anisotropy factor in this study was larger as described in earlier studies. The FWHM for all compartments was twice as large as described in earlier studies where values of 2  $\mu\text{m}$  were observed (Cheng et al., 1993, Gomez et al., 1996, Lukyanenko and Gyorke, 1999, Wang et al., 2002). Variations due to different concentrations of the indicator were unlikely since my experiments with varying Fluo4 concentrations did reveal a strong influence on the amplitudes but the effect on the spatial spread was not comparable. The values found in cells loaded with 0.5  $\mu\text{M}$  Fluo4 had the same spatial spread as cells loaded with 1.5  $\mu\text{M}$  Fluo4. Unclear is whether these different values observed derived from the technical setup which could be evaluated by first analyzing data derived from other microscopes and second by calculating the spark values with other detection and calculation methods.

Taken together the  $\text{Ca}^{2+}$  sparks from atrial cells were larger in amplitude, thus releasing more  $\text{Ca}^{2+}$  from a cluster of RyR's than ventricular myocytes, indicating higher SR  $\text{Ca}^{2+}$



content and/or an increased open probability for RyR's. The signals from atrial cells had a shorter decay time constant, which indicates a faster  $\text{Ca}^{2+}$  removal processes from the cytosol in this cell type.

These data give a description of the spontaneous  $\text{Ca}^{2+}$  sparks recorded in the three major compartments of the mouse heart and thus facilitate a direct comparison of the different signals. This sets the baseline for further analysis of different cardiac diseases such as hypertrophy or atrial fibrillation.

### **3. The Impact of TRPC1/C4 double Knock-Out in the Heart on $\text{Ca}^{2+}$ Sparks with and without chronic $\beta$ -stimulation**

The TRP (transient receptor potential channels) superfamily is composed of several subfamilies of which the TRPC channels are expressed in the heart (Nishida and Kurose, 2008). It is still unclear which subtype of the TRPC channels is involved in cardiac hypertrophy but there is a consensus that TRPC channels do increase the  $\text{Ca}^{2+}$  influx and thus facilitate hypertrophy (Nishida and Kurose, 2008). TRPC1 has been reported to be involved in the development of hypertrophy in rats where its expression was increased and the  $\text{Ca}^{2+}$  signaling was altered (Ohba et al., 2007). TRPC4 as a player in the development of cardiac hypertrophy was determined after knockdown of SERCA2a, which led to upregulation of the transcription of TRPC4, TRPC5 and the  $\text{Na}^+$ - $\text{Ca}^{2+}$ -exchanger (NCX) and subsequent hypertrophic responses (Seth et al., 2004).

Functional TRP channels are known to form oligomers of one or of several types of TRP subunits as functional units. Both TRPC1 and TRPC4 have been proposed to be involved in receptor- and/or store-operated channel formation (Watanabe et al., 2009).

These two members of the TRP family (TRPC1 and TRPC4) are supposedly involved in the development of hypertrophy in the heart. The analysis of the fundamental  $\text{Ca}^{2+}$  signals underlying ECC was to elucidate whether the TRP channels have an effect on these small  $\text{Ca}^{2+}$  release events with and without the induction of a hypertrophic response after chronic  $\beta$ -stimulation. The hypertrophic responses were induced by chronic  $\beta$ -adrenergic stimulation with Iso in WT mice and in mice with double-KO mice of TRPC1 and TRPC4.

The double-KO itself without the chronic  $\beta$ -adrenergic stimulation did not show any alteration in  $\text{Ca}^{2+}$  handling observed in  $\text{Ca}^{2+}$  sparks in ventricular myocytes except some

changes in the amplitudes observed in sparks from left atrial cells and ventricular cells as depicted in Fig. 34. Since the other parameters such as decay time constant and spatial spread remained unaltered it could be concluded that TRPC1 and TRPC4 play a role in normal  $\text{Ca}^{2+}$  handling in intact cardiomyocytes. The alterations of the spark amplitudes in ventricular cells could be interpreted as a small contribution of TRPC1 and TRPC4 to the  $[\text{Ca}^{2+}]_i$ . Unpublished data from our group demonstrated, that the basal  $\text{Ca}^{2+}$  concentration in the cytosol of TRPC1/C4<sup>-/-</sup> animals was significantly reduced in comparison to WT animals and also the SR- $\text{Ca}^{2+}$  load was reduced as depicted in Fig. 40. The application of caffeine to elucidate the SR- $\text{Ca}^{2+}$  load also revealed that NCX and SERCA function were unaltered due to the knock-out of the two TRPC channels. Furthermore, the contractility and the cell length in resting state were reduced. These data strengthened the notion that TRPC1 and TRPC4 contribute to the maintenance of the resting  $[\text{Ca}^{2+}]_i$ , probably by altering the membrane potential and thus increasing the driving force for  $\text{Ca}^{2+}$  entry.

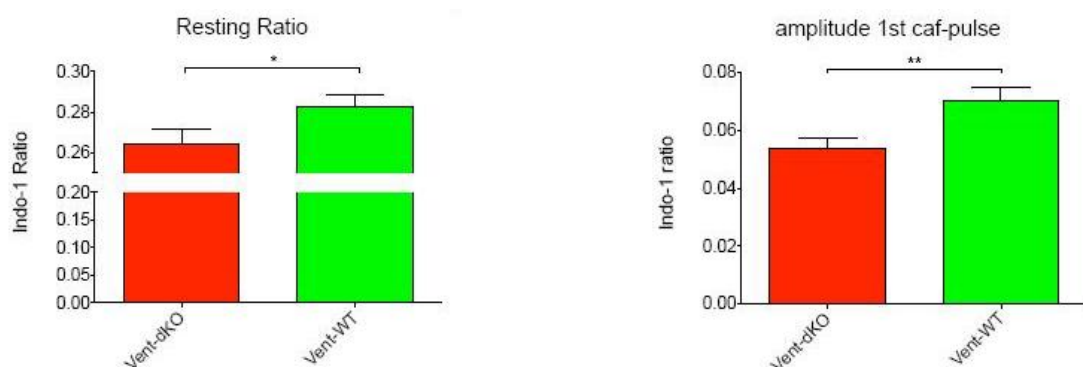


**Figure 40: Resting  $\text{Ca}^{2+}$  level and SR- $\text{Ca}^{2+}$  content of TRPC1/C4<sup>-/-</sup> ventricular myocytes from animals in comparison with WT animals.** The left bar graph diagram depicts the resting  $\text{Ca}^{2+}$  level measured in Indo-1 loaded myocytes. The ratio in double-KO animals was significantly lower, depicting lower  $\text{Ca}^{2+}$  concentrations. The bar graph diagram on the right side depicts amplitude evoked by caffeine application, which was also reduced due to the double-KO, indicating a lower SR- $\text{Ca}^{2+}$  content. dKO=TRPC1/C4<sup>-/-</sup>; WT=wildtype. Unpublished data from Prof. Dr. Peter Lipp.

Although the cells had reduced basal  $\text{Ca}^{2+}$  levels and reduced SR- $\text{Ca}^{2+}$  content in both atria from double-KO animals as depicted in Fig. 41, the spark amplitudes were increased in left atrial cells (see Fig. 34). The spark amplitudes in cells from right atria displayed no alterations due to the double-KO. This indicates that the TRPC1 and TRPC4 do not have a significant influence on spontaneous occurring  $\text{Ca}^{2+}$  release from the SR. The slightly

increased spark amplitudes observed in the left atrium might indicate an increased open probability of the RyR's in the SR, which might be modulated partly by TRPC channels.

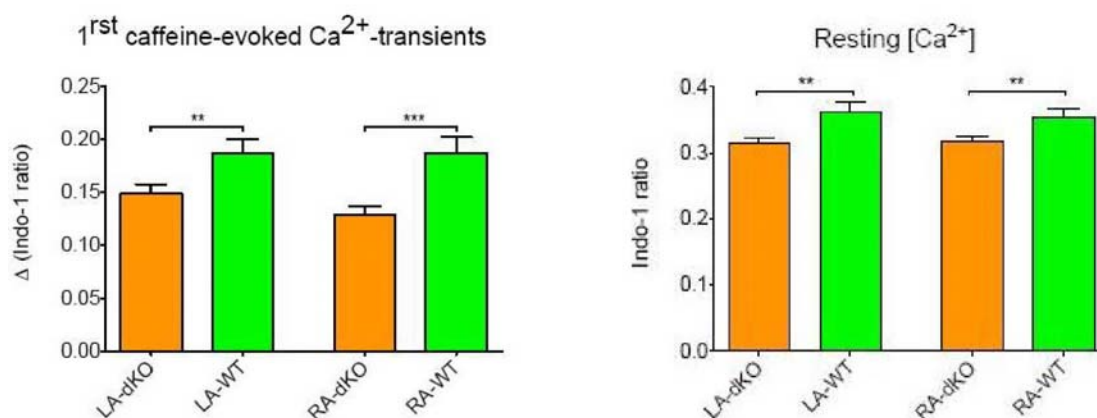


**Figure 41: Resting Ca<sup>2+</sup> level and SR-Ca<sup>2+</sup> content of TRPC1/C4<sup>-/-</sup> atrial cells from animals in comparison with WT animals.** The left bar graph diagram depicts the resting Ca<sup>2+</sup> level measured in Indo-1 loaded myocytes. The ratio in double-KO animals was significantly lower, depicting lower Ca<sup>2+</sup> concentrations. The bar graph diagram on the right side depicts amplitude evoked by caffeine application, which was also reduced due to the double-KO, indicating a lower SR-Ca<sup>2+</sup> content. La= left atria; RA= right atria; dKO=TRPC1/C4<sup>-/-</sup>; WT=wildtype. Unpublished data from Prof. Dr. Peter Lipp.

The data from animals that have had an implanted minipump with isotonic NaCl could not approve the findings in ventricular cells. Here the amplitudes from WT mice were even smaller than those found in double-KO mice. Such variations had to be attributed to the impact of the initial implantation of the minipump itself. It was assumed that the procedure of the implantation and the debris underneath the skin had some impact on the cardiac myocytes, whereas the details of this impact remained unclear. Further analysis performing sham-operations would enlighten these findings by performing the procedure of a minipump implantation without actually implanting a pump. Experiments on the Ca<sup>2+</sup> handling and contractility of myocytes derived from such animals would elucidate the influence of the procedure on the physiology of the cardiac myocytes.

Double-KO mice and WT mice were chronically infused with the β-stimulator isoprenaline for a duration of 1 week and subsequently the ventricular cells were analyzed with respect to their spark properties. The chronical β-adrenergic stimulation of WT mice

with Iso infusion did cause a decrease of spark amplitude and the spark area. This indicated that the basal  $\text{Ca}^{2+}$  handling expressed in  $\text{Ca}^{2+}$  sparks was affected by Iso stimulation in such a way that more  $\text{Ca}^{2+}$  was released from the stores. That might also have influenced the spatial spread of the  $\text{Ca}^{2+}$  spark. In contrast to the findings in WT mice, sparks observed in double-KO mice were not altered in amplitude and spatial spread, but the decay time was significantly reduced due to Iso stimulation. This demonstrated that not more  $\text{Ca}^{2+}$  was released from the stores but the removal from the cytosol was enhanced. This would indicate an increased activity of either the SERCA pump or the NCX or both. It has been demonstrated in earlier studies that the silencing of SERCA2 induces upregulation of TRPC4 and TRPC5, indicating that a deficiency of the SR is compensated by  $\text{Ca}^{2+}$  entry via the plasmamembrane (Seth et al., 2004). Further analysis of the removal mechanisms could enlighten whether this process also works vice versa and whether a knock-out of TRP channels can cause the upregulation of other regulatory proteins for  $\text{Ca}^{2+}$  handling.

These observations approved the finding that TRPC1 and TRPC4 do have an impact on  $\text{Ca}^{2+}$  handling mechanisms in cardiac myocytes in hypertrophic mice (induced by isoproterenol). It was also demonstrated that this influence is not only present in hypertrophic animals but also in healthy animals.

#### **4. The Impact of Overexpression of Rac1 in Mouse Hearts on $\text{Ca}^{2+}$ Sparks**

Atrial fibrillation is still incompletely understood and one proposed signaling pathway involved in atrial fibrillation is the Rac1 mediated signaling cascade in cardiac myocytes, where an overexpression leads to hypertrophic responses (Sussman et al., 2000) and played a key role in the offset of atrial fibrillation (Adam et al., 2007). But little is known about the underlying signaling pathways in the single myocytes. It has been proposed that Rac1 activates the Rac1 GTPase and thus activates the NADPH (nicotinamide adenine dinucleotide phosphate) oxidase which will lead to the production of ROS (reactive oxygen species).

The analysis of  $\text{Ca}^{2+}$  sparks was intended to reveal alterations in the  $\text{Ca}^{2+}$  signaling of this mouse model for atrial fibrillation. Since the genetic background of this mouse model was the FVB/N mouse strain, the control measurements were performed on these mice in the following referred to as WT mice.

The most pronounced alterations were found in the amplitude of the sparks. In each compartment of the heart, the amplitudes of sparks measured in Rac1 overexpressing mice were significantly higher in comparison to the data derived from WT mice. These data suggest an overload of the SR leading to increased release of  $\text{Ca}^{2+}$  from the stores which has been described as an arrhythmogenic mechanism in Cardiac myocytes (Bers, 2008). Unpublished data from our group showed that the baseline  $\text{Ca}^{2+}$  concentration in the cytosol of atrial myocytes (left and right atria) was increased in Rac1 overexpressing mice in comparison to WT mice. This indicated that the significantly increased spark amplitudes observed in atrial cell from both sides might be attributed to the higher  $\text{Ca}^{2+}$  baseline levels in the cytosol. This might have increased the open probability of the RyR's. It can also be excluded that the increased spark amplitudes observed were caused by an increased SR- $\text{Ca}^{2+}$  content because in the above mentioned studies from our group, caffeine was applied to cells to empty the stores, which revealed an unaltered SR- $\text{Ca}^{2+}$  content in the Rac1 overexpressing animals in comparison to the WT mice. The decay time of the  $\text{Ca}^{2+}$  sparks was unaltered in atrial cells which indicated enhanced removal mechanisms in these cells. The spatial spread was significantly reduced in the overexpressing atrial cells which might also be attributed to enhanced removal mechanisms, i.e. the larger sparks were removed faster in relation to the smaller sparks observed in WT animals.

In ventricular cells the spark amplitude was also increased due to the overexpression of Rac1 but the experiments from our group revealed a very oppositional situation with respect to the  $\text{Ca}^{2+}$  maintenance. In Rac1 overexpressing animals the ventricles had a decreased baseline  $\text{Ca}^{2+}$  level, but an increased SR- $\text{Ca}^{2+}$  content. The increased SR load was reflected in the increased  $\text{Ca}^{2+}$  spark amplitude observed. This led to the conclusion that in ventricular cells the overexpression of Rac1 caused a different reaction than in atrial cells. Regarding the spark parameters the ventricular cells remained unaltered with the exception of their amplitudes. Since the amplitudes were increased but not the decay time, this might indicate a faster removal from the cytosol in these cells.

The overexpression of Rac1 induced a phenotype that had a highly pronounced hypertrophy of the right atrium and induced some alterations of the  $\text{Ca}^{2+}$  handling in myocytes isolated from these hearts. The underlying mechanisms remain elusive, but it might be possible that the overexpression of Rac1 caused further alterations of molecule involved in ECC. This mouse model was used as a model for studies on atrial fibrillation (AF), which is known to come along with an increased phosphorylation of phospholamban,

which in turn causes enhanced  $\text{Ca}^{2+}$  reuptake into the SR via the SERCA pump. Furthermore increased PKA levels will cause increased phosphorylation of the RyR's resulting in an increased open probability. Rac1 itself is believed to be involved in ROS production. Since RyR's display redox sensitivity this might lead to a further increase of the open probability of these channels. This could explain the increased spark amplitudes in atrial myocytes as well as the increased baseline  $\text{Ca}^{2+}$  levels observed in experiments from our group. The increased open probability of the RyR'S causes a  $\text{Ca}^{2+}$  leak from the stores, which in turn causes increased cytosolic  $\text{Ca}^{2+}$  levels.

The alterations observed in ventricular myocytes seemed to be different from those in atrial cells. Probably the overexpression caused the above effect due to the increased ROS production (i.e. increased open probability of the RyR's) leading to increased spark amplitudes, but other effects coming along with AF seemed to be negligible with respect to the  $\text{Ca}^{2+}$  sparks.

These data demonstrated that this mouse model for AF caused alterations in the myocytes that can be observed in the fundamental  $\text{Ca}^{2+}$  signals. Further experiments can help to enlighten the processes during the onset of AF.

It has to be pointed out that the n-number of control experiments was relatively low, which led to larger SEM's on these data. In order to strengthen these findings, more experiments have to be performed in control mice.

### ***C. Conclusion***

In my thesis I observed different cell organelles in cultured adult cardiac myocytes to assess whether and how these structures undergo a remodeling process due to the long term culture of 1 week duration. All observed subcellular structures were subject to more or less pronounced distinct alterations with the exception of the structure of the actin filaments, which remained unaltered.

These alterations were very reproducible and could even be reduced after supplementation of the medium with CytochalasinD implying a further improvement of our culture method. These findings also demonstrated that the remodeling process in cultured cardiac myocytes is related to the dynamics of the actin filaments and that this is a potential starting point for future attempts to rule out the remodeling of the cardiac structure in long term culture, but they also depicted a baseline for long term studies in cultured adult cardiac myocytes.

In further studies, the focus should be set on the cytoskeleton of the cultured myocytes. Expression of fluorescent fusion proteins did not alter the morphology and thus this method represents a useful tool for morphological and functional studies employing genetically encoded biosensors.

We introduced a MatLab algorithm to analyze  $\text{Ca}^{2+}$  sparks in large number and thus set the basis for screening experiments to characterize the fundamental  $\text{Ca}^{2+}$  signals. The algorithm works stable without the need of large interaction of the user. This ensures results that are independent of the person analyzing them to a maximally possible degree. The characterization of  $\text{Ca}^{2+}$  sparks, derived from the three major compartments (i.e. left and right atria as well as the ventricles) of the heart, revealed distinct differences of the sparks observed. The most important differences were first the amplitudes of the sparks that have been the largest in left atrial cells and the smallest in ventricular cells. Second, the decay time of the  $\text{Ca}^{2+}$  sparks was the same in both atria but longer in the ventricular myocytes. This indicated that the mechanisms for the cytosolic  $\text{Ca}^{2+}$  increase and decrease during ECC vary between the cell types. This might partly be attributed to the different morphology (e.g. t-tubules in ventricles but not in atria). This pointed out the necessity to analyze the physiology of the different types of cardiomyocytes separately to gain deeper insight into the mechanisms of ECC.

The findings from the study of the impact of TRPC1/C4<sup>-/-</sup> on the fundamental Ca<sup>2+</sup> signals strengthened earlier observations that TRPC1 and TRPC4 do have an impact on Ca<sup>2+</sup> handling mechanisms in cardiac myocytes in hypertrophic mice (induced by isoproterenol). These TRPC channels also had an impact on the Ca<sup>2+</sup> handling in animals without cardiac disease.

The overexpression of Rac1 in mouse hearts did cause alterations that could be detected in the Ca<sup>2+</sup> spark parameters. It could be assumed that the observed finding most obvious in the increased amplitudes of the sparks, were due to altered phosphorylation states of the RyR's and other Ca<sup>2+</sup> handling proteins.

The analysis of both mouse models for cardiac disease revealed alterations of the fundamental Ca<sup>2+</sup> signals underlying cardiac ECC. Taken together these findings could be the starting point for further analysis of the impact of various factors involved in the development of cardiac diseases on the fundamental Ca<sup>2+</sup> signals with high accuracy.



## VII. Literature

1. Adam, O., Frost, G., Custodis, F., Sussman, M.A., Schafers, H.J., Bohm, M., and Laufs, U., *Role of Rac1 GTPase activation in atrial fibrillation*. J Am Coll Cardiol, 2007. **50**(4): p. 359-67.
2. Allen, B.G. and Katz, S., *Calreticulin and calsequestrin are differentially distributed in canine heart*. J Mol Cell Cardiol, 2000. **32**(12): p. 2379-84.
3. Anderson, M., Moore, D., and Larson, D., *Comparison of isoproterenol and dobutamine in the induction of cardiac hypertrophy and fibrosis*. Perfusion, 2008. **23**(4): p. 231-5.
4. Baader, A.P., Buchler, L., Bircher-Lehmann, L., and Kleber, A.G., *Real time, confocal imaging of Ca(2+) waves in arterially perfused rat hearts*. Cardiovasc Res, 2002. **53**(1): p. 105-15.
5. Banyasz, T., Chen-Izu, Y., Balke, C.W., and Izu, L.T., *A new approach to the detection and statistical classification of Ca<sup>2+</sup> sparks*. Biophys J, 2007. **92**(12): p. 4458-65.
6. Banyasz, T., Lozinskiy, I., Payne, C.E., Edelmann, S., Norton, B., Chen, B., Chen-Izu, Y., Izu, L.T., and Balke, C.W., *Transformation of adult rat cardiac myocytes in primary culture*. Exp Physiol, 2008. **93**(3): p. 370-82.
7. Berridge, M.J., *Calcium microdomains: organization and function*. Cell Calcium, 2006. **40**(5-6): p. 405-12.
8. Berridge, M.J., Lipp, P., and Bootman, M.D., *The versatility and universality of calcium signalling*. Nat Rev Mol Cell Biol, 2000. **1**(1): p. 11-21.
9. Bers, D.M., *Excitation-Contraction Coupling and Cardiac Contractile Force*. second ed. 2001, Dordrecht: Kluwer Academic Publishers. 427.
10. Bers, D.M., *Cardiac excitation-contraction coupling*. Nature, 2002. **415**(6868): p. 198-205.
11. Bers, D.M., *Calcium cycling and signaling in cardiac myocytes*. Annu Rev Physiol, 2008. **70**: p. 23-49.
12. Birkedal, R., Shiels, H.A., and Vendelin, M., *Three-dimensional mitochondrial arrangement in ventricular myocytes: from chaos to order*. Am J Physiol Cell Physiol, 2006. **291**(6): p. C1148-58.

13. Bray, M.A., Geisse, N.A., and Parker, K.K., *Multidimensional detection and analysis of Ca<sup>2+</sup> sparks in cardiac myocytes*. *Biophys J*, 2007. **92**(12): p. 4433-43.
14. Brette, F., Despa, S., Bers, D.M., and Orchard, C.H., *Spatiotemporal characteristics of SR Ca(2+) uptake and release in detubulated rat ventricular myocytes*. *J Mol Cell Cardiol*, 2005. **39**(5): p. 804-12.
15. Brette, F., Komukai, K., and Orchard, C.H., *Validation of formamide as a detubulation agent in isolated rat cardiac cells*. *Am J Physiol Heart Circ Physiol*, 2002. **283**(4): p. H1720-8.
16. Brette, F., Salle, L., and Orchard, C.H., *Differential modulation of L-type Ca<sup>2+</sup> current by SR Ca<sup>2+</sup> release at the T-tubules and surface membrane of rat ventricular myocytes*. *Circ Res*, 2004. **95**(1): p. e1-7.
17. Brette, F., Salle, L., and Orchard, C.H., *Quantification of calcium entry at the T-tubules and surface membrane in rat ventricular myocytes*. *Biophys J*, 2006. **90**(1): p. 381-9.
18. Brochet, D.X., Yang, D., Di Maio, A., Lederer, W.J., Franzini-Armstrong, C., and Cheng, H., *Ca<sup>2+</sup> blinks: rapid nanoscopic store calcium signaling*. *Proc Natl Acad Sci U S A*, 2005. **102**(8): p. 3099-104.
19. Chambers, P., Neal, D.E., and Gillespie, J.I., *Ryanodine receptors in human bladder smooth muscle*. *Exp Physiol*, 1999. **84**(1): p. 41-6.
20. Chandler, W.K., Hollingworth, S., and Baylor, S.M., *Simulation of calcium sparks in cut skeletal muscle fibers of the frog*. *J Gen Physiol*, 2003. **121**(4): p. 311-24.
21. Cheng, H. and Lederer, W.J., *Calcium sparks*. *Physiol Rev*, 2008. **88**(4): p. 1491-545.
22. Cheng, H., Lederer, W.J., and Cannell, M.B., *Calcium sparks: elementary events underlying excitation-contraction coupling in heart muscle*. *Science*, 1993. **262**(5134): p. 740-4.
23. Cooke, P.H., Kargacin, G., Craig, R., Fogarty, K., and Fay, F.S., *Molecular structure and organization of filaments in single, skinned smooth muscle cells*. *Prog Clin Biol Res*, 1987. **245**: p. 1-25.
24. Cooper, J.A., *Effects of cytochalasin and phalloidin on actin*. *J Cell Biol*, 1987. **105**(4): p. 1473-8.
25. Craig, R.W. and Padrón, R., *Molecular Structure of the Sarcomere*, in *Myology*. 2004, The McGraw-Hill Companies, Inc. p. 129-165.

26. Di Maio, A., Karko, K., Snopko, R.M., Mejia-Alvarez, R., and Franzini-Armstrong, C., *T-tubule formation in cardiomyocytes: two possible mechanisms?* J Muscle Res Cell Motil, 2007. **28**(4-5): p. 231-41.
27. Duchen, M.R., Leyssens, A., and Crompton, M., *Transient mitochondrial depolarizations reflect focal sarcoplasmic reticular calcium release in single rat cardiomyocytes.* J Cell Biol, 1998. **142**(4): p. 975-88.
28. Ellingsen, O., Davidoff, A.J., Prasad, S.K., Berger, H.J., Springhorn, J.P., Marsh, J.D., Kelly, R.A., and Smith, T.W., *Adult rat ventricular myocytes cultured in defined medium: phenotype and electromechanical function.* Am J Physiol, 1993. **265**(2 Pt 2): p. H747-54.
29. Eppenberger, M., Hauser, I., and Eppenberger, H.M., *Myofibril formation in long-term-cultures of adult rat heart cells.* Biomed Biochim Acta, 1987. **46**(8-9): p. S640-5.
30. Eppenberger, M.E., Hauser, I., Baechli, T., Schaub, M.C., Brunner, U.T., Dechesne, C.A., and Eppenberger, H.M., *Immunocytochemical analysis of the regeneration of myofibrils in long-term cultures of adult cardiomyocytes of the rat.* Dev Biol, 1988. **130**(1): p. 1-15.
31. Flockerzi, A., *Algorithmus zur automatischen Detektion und Analyse lebender Herzmuskelzellen sowie deren subzellulären, räumlich-zeitlich komplexen Ca<sup>2+</sup> - Signalen in konfokalen, zweidimensionalen Bildserien.,* in *Institute for Molecular Cell Biology.* 2007, Saarland University, Germany: 66424 Hombur/Saar. p. 123.
32. Fowler, M.R., Dobson, R.S., Orchard, C.H., and Harrison, S.M., *Functional consequences of detubulation of isolated rat ventricular myocytes.* Cardiovasc Res, 2004. **62**(3): p. 529-37.
33. Gallagher, M.M. and Camm, A.J., *Long-term management of atrial fibrillation.* Clin Cardiol, 1997. **20**(4): p. 381-90.
34. Gatti, G., Trifari, S., Mesaeli, N., Parker, J.M., Michalak, M., and Meldolesi, J., *Head-to-tail oligomerization of calsequestrin: a novel mechanism for heterogeneous distribution of endoplasmic reticulum luminal proteins.* J Cell Biol, 2001. **154**(3): p. 525-34.
35. Gomez, A.M., Cheng, H., Lederer, W.J., and Bers, D.M., *Ca<sup>2+</sup> diffusion and sarcoplasmic reticulum transport both contribute to [Ca<sup>2+</sup>]<sub>i</sub> decline during Ca<sup>2+</sup> sparks in rat ventricular myocytes.* J Physiol, 1996. **496** ( Pt 2): p. 575-81.
36. Gyorke, I. and Gyorke, S., *Adaptive control of intracellular Ca<sup>2+</sup> release in C2C12 mouse myotubes.* Pflugers Arch, 1996. **431**(6): p. 838-43.

37. Hom, J. and Sheu, S.S., *Morphological dynamics of mitochondria--a special emphasis on cardiac muscle cells*. J Mol Cell Cardiol, 2009. **46**(6): p. 811-20.
38. Horackova, M. and Byczko, Z., *Differences in the structural characteristics of adult guinea pig and rat cardiomyocytes during their adaptation and maintenance in long-term cultures: confocal microscopy study*. Exp Cell Res, 1997. **237**(1): p. 158-75.
39. Ide, T., Tsutsui, H., Kinugawa, S., Suematsu, N., Hayashidani, S., Ichikawa, K., Utsumi, H., Machida, Y., Egashira, K., and Takeshita, A., *Direct evidence for increased hydroxyl radicals originating from superoxide in the failing myocardium*. Circ Res, 2000. **86**(2): p. 152-7.
40. Ide, T., Tsutsui, H., Kinugawa, S., Utsumi, H., Kang, D., Hattori, N., Uchida, K., Arimura, K., Egashira, K., and Takeshita, A., *Mitochondrial electron transport complex I is a potential source of oxygen free radicals in the failing myocardium*. Circ Res, 1999. **85**(4): p. 357-63.
41. Izu, L.T., Mauban, J.R., Balke, C.W., and Wier, W.G., *Large currents generate cardiac Ca<sup>2+</sup> sparks*. Biophys J, 2001. **80**(1): p. 88-102.
42. Keller, P., Toomre, D., Diaz, E., White, J., and Simons, K., *Multicolour imaging of post-Golgi sorting and trafficking in live cells*. Nat Cell Biol, 2001. **3**(2): p. 140-9.
43. Leach, R.N., Desai, J.C., and Orchard, C.H., *Effect of cytoskeleton disruptors on L-type Ca channel distribution in rat ventricular myocytes*. Cell Calcium, 2005. **38**(5): p. 515-26.
44. Lipp, P., Huser, J., Pott, L., and Niggli, E., *Spatially non-uniform Ca<sup>2+</sup> signals induced by the reduction of transverse tubules in citrate-loaded guinea-pig ventricular myocytes in culture*. J Physiol, 1996. **497** ( Pt 3): p. 589-97.
45. Lipp, P. and Niggli, E., *Submicroscopic calcium signals as fundamental events of excitation--contraction coupling in guinea-pig cardiac myocytes*. J Physiol, 1996. **492** ( Pt 1): p. 31-8.
46. Lipp, P. and Niggli, E., *Fundamental calcium release events revealed by two-photon excitation photolysis of caged calcium in Guinea-pig cardiac myocytes*. J Physiol, 1998. **508** ( Pt 3): p. 801-9.
47. Lukyanenko, V. and Gyorke, S., *Ca<sup>2+</sup> sparks and Ca<sup>2+</sup> waves in saponin-permeabilized rat ventricular myocytes*. J Physiol, 1999. **521** Pt 3: p. 575-85.
48. Luss, I., Boknik, P., Jones, L.R., Kirchhefer, U., Knapp, J., Linck, B., Luss, H., Meissner, A., Muller, F.U., Schmitz, W., Vahlensieck, U., and Neumann, J., *Expression of cardiac calcium regulatory proteins in atrium v ventricle in different species*. J Mol Cell Cardiol, 1999. **31**(6): p. 1299-314.

49. Mackenzie, L., Bootman, M.D., Berridge, M.J., and Lipp, P., *Predetermined recruitment of calcium release sites underlies excitation-contraction coupling in rat atrial myocytes*. *J Physiol*, 2001. **530**(Pt 3): p. 417-29.
50. Mitcheson, J.S., Hancox, J.C., and Levi, A.J., *Action potentials, ion channel currents and transverse tubule density in adult rabbit ventricular myocytes maintained for 6 days in cell culture*. *Pflugers Arch*, 1996. **431**(6): p. 814-27.
51. Montell, C., Birnbaumer, L., Flockerzi, V., Bindels, R.J., Bruford, E.A., Caterina, M.J., Clapham, D.E., Harteneck, C., Heller, S., Julius, D., Kojima, I., Mori, Y., Penner, R., Prawitt, D., Scharenberg, A.M., Schultz, G., Shimizu, N., and Zhu, M.X., *A unified nomenclature for the superfamily of TRP cation channels*. *Mol Cell*, 2002. **9**(2): p. 229-31.
52. Moore, D.H. and Ruska, H., *Electron microscope study of mammalian cardiac muscle cells*. *J Biophys Biochem Cytol*, 1957. **3**(2): p. 261-8.
53. Moore, L.E., Schmid, A., and Isenberg, G., *Linear electrical properties of isolated cardiac cells*. *J Membr Biol*, 1984. **81**(1): p. 29-40.
54. Nag, A.C. and Cheng, M., *Adult mammalian cardiac muscle cells in culture*. *Tissue Cell*, 1981. **13**(3): p. 515-23.
55. Nag, A.C. and Lee, M.L., *Breakdown and rebuilding of myofibrils in cultured adult cardiac muscle cells*. *Tsitologia*, 1997. **39**(10): p. 907-12.
56. Nag, A.C., Lee, M.L., and Sarkar, F.H., *Remodelling of adult cardiac muscle cells in culture: dynamic process of disorganization and reorganization of myofibrils*. *J Muscle Res Cell Motil*, 1996. **17**(3): p. 313-34.
57. Niggli, E. and Egger, M., *Calcium quarks*. *Front Biosci*, 2002. **7**: p. d1288-97.
58. Niggli, E. and Shirokova, N., *A guide to sparkology: the taxonomy of elementary cellular Ca<sup>2+</sup> signaling events*. *Cell Calcium*, 2007. **42**(4-5): p. 379-87.
59. Nishida, M. and Kurose, H., *Roles of TRP channels in the development of cardiac hypertrophy*. *Naunyn Schmiedebergs Arch Pharmacol*, 2008. **378**(4): p. 395-406.
60. Ohba, T., Watanabe, H., Murakami, M., Takahashi, Y., Ino, K., Kuromitsu, S., Mori, Y., Ono, K., Iijima, T., and Ito, H., *Upregulation of TRPC1 in the development of cardiac hypertrophy*. *J Mol Cell Cardiol*, 2007. **42**(3): p. 498-507.
61. Orchard, C. and Brette, F., *t-Tubules and sarcoplasmic reticulum function in cardiac ventricular myocytes*. *Cardiovasc Res*, 2008. **77**(2): p. 237-44.

62. Poindexter, B.J., Smith, J.R., Buja, L.M., and Bick, R.J., *Calcium signaling mechanisms in dedifferentiated cardiac myocytes: comparison with neonatal and adult cardiomyocytes*. *Cell Calcium*, 2001. **30**(6): p. 373-82.
63. Powell, T. and Twist, V.W., *A rapid technique for the isolation and purification of adult cardiac muscle cells having respiratory control and a tolerance to calcium*. *Biochem Biophys Res Commun*, 1976. **72**(1): p. 327-33.
64. Pratusевич, V.R. and Balke, C.W., *Factors shaping the confocal image of the calcium spark in cardiac muscle cells*. *Biophys J*, 1996. **71**(6): p. 2942-57.
65. Quintana, A., Schwarz, E.C., Schwindling, C., Lipp, P., Kaestner, L., and Hoth, M., *Sustained activity of calcium release-activated calcium channels requires translocation of mitochondria to the plasma membrane*. *J Biol Chem*, 2006. **281**(52): p. 40302-9.
66. Rambourg, A., Segretain, D., and Clermont, Y., *Tridimensional architecture of the Golgi apparatus in the atrial muscle cell of the rat*. *Am J Anat*, 1984. **170**(2): p. 163-79.
67. Riedl, J., Crevenna, A.H., Kessenbrock, K., Yu, J.H., Neukirchen, D., Bista, M., Bradke, F., Jenne, D., Holak, T.A., Werb, Z., Sixt, M., and Wedlich-Soldner, R., *Lifeact: a versatile marker to visualize F-actin*. *Nat Methods*, 2008. **5**(7): p. 605-7.
68. Rios, E., Shirokova, N., Kirsch, W.G., Pizarro, G., Stern, M.D., Cheng, H., and Gonzalez, A., *A preferred amplitude of calcium sparks in skeletal muscle*. *Biophys J*, 2001. **80**(1): p. 169-83.
69. Rohr, S. and Salzberg, B.M., *Multiple site optical recording of transmembrane voltage (MSORTV) in patterned growth heart cell cultures: assessing electrical behavior, with microsecond resolution, on a cellular and subcellular scale*. *Biophys J*, 1994. **67**(3): p. 1301-15.
70. Rossi, A.E. and Dirksen, R.T., *Sarcoplasmic reticulum: the dynamic calcium governor of muscle*. *Muscle Nerve*, 2006. **33**(6): p. 715-31.
71. Rossi, D., Barone, V., Giacomello, E., Cusimano, V., and Sorrentino, V., *The sarcoplasmic reticulum: an organized patchwork of specialized domains*. *Traffic*, 2008. **9**(7): p. 1044-9.
72. Scales, S.J., Pepperkok, R., and Kreis, T.E., *Visualization of ER-to-Golgi transport in living cells reveals a sequential mode of action for COPII and COPI*. *Cell*, 1997. **90**(6): p. 1137-48.
73. Schwarzfeld, T.A. and Jacobson, S.L., *Isolation and development in cell culture of myocardial cells of the adult rat*. *J Mol Cell Cardiol*, 1981. **13**(6): p. 563-75.

74. Scriven, D.R., Dan, P., and Moore, E.D., *Distribution of proteins implicated in excitation-contraction coupling in rat ventricular myocytes*. Biophys J, 2000. **79**(5): p. 2682-91.
75. Segretain, D., Rambourg, A., and Clermont, Y., *Three dimensional arrangement of mitochondria and endoplasmic reticulum in the heart muscle fiber of the rat*. Anat Rec, 1981. **200**(2): p. 139-51.
76. Seth, M., Sumbilla, C., Mullen, S.P., Lewis, D., Klein, M.G., Hussain, A., Soboloff, J., Gill, D.L., and Inesi, G., *Sarco(endo)plasmic reticulum Ca<sup>2+</sup> ATPase (SERCA) gene silencing and remodeling of the Ca<sup>2+</sup> signaling mechanism in cardiac myocytes*. Proc Natl Acad Sci U S A, 2004. **101**(47): p. 16683-8.
77. Sharp, W.W., Terracio, L., Borg, T.K., and Samarel, A.M., *Contractile activity modulates actin synthesis and turnover in cultured neonatal rat heart cells*. Circ Res, 1993. **73**(1): p. 172-83.
78. Sheehan, K.A., Zima, A.V., and Blatter, L.A., *Regional differences in spontaneous Ca<sup>2+</sup> spark activity and regulation in cat atrial myocytes*. J Physiol, 2006. **572**(Pt 3): p. 799-809.
79. Smith, G.D., Keizer, J.E., Stern, M.D., Lederer, W.J., and Cheng, H., *A simple numerical model of calcium spark formation and detection in cardiac myocytes*. Biophys J, 1998. **75**(1): p. 15-32.
80. Sobie, E.A., Dilly, K.W., dos Santos Cruz, J., Lederer, W.J., and Jafri, M.S., *Termination of cardiac Ca(2+) sparks: an investigative mathematical model of calcium-induced calcium release*. Biophys J, 2002. **83**(1): p. 59-78.
81. Sussman, M.A., Welch, S., Walker, A., Klevitsky, R., Hewett, T.E., Price, R.L., Schaefer, E., and Yager, K., *Altered focal adhesion regulation correlates with cardiomyopathy in mice expressing constitutively active rac1*. J Clin Invest, 2000. **105**(7): p. 875-86.
82. Suzaki, E. and Kataoka, K., *Three-dimensional visualization of the Golgi apparatus: observation of Brunner's gland cells by a confocal laser scanning microscope*. J Struct Biol, 1999. **128**(2): p. 131-8.
83. Tokiwa, T., Miyagiwa, M., Kawai, A., Matsuura, K., Taketa, K., Okigaki, T., and Sato, J., *The effect of conditioned medium on fetal human liver cells in primary culture*. Res Exp Med (Berl), 1986. **186**(6): p. 463-8.
84. Viero, C., Kraushaar, U., Ruppenthal, S., Kaestner, L., and Lipp, P., *A primary culture system for sustained expression of a calcium sensor in preserved adult rat ventricular myocytes*. Cell Calcium, 2008. **43**(1): p. 59-71.

85. Volz, A., Piper, H.M., Siegmund, B., and Schwartz, P., *Longevity of adult ventricular rat heart muscle cells in serum-free primary culture*. J Mol Cell Cardiol, 1991. **23**(2): p. 161-73.
86. Wang, S.Q., Song, L.S., Xu, L., Meissner, G., Lakatta, E.G., Rios, E., Stern, M.D., and Cheng, H., *Thermodynamically irreversible gating of ryanodine receptors in situ revealed by stereotyped duration of release in Ca(2+) sparks*. Biophys J, 2002. **83**(1): p. 242-51.
87. Watanabe, H., Murakami, M., Ohba, T., Ono, K., and Ito, H., *The pathological role of transient receptor potential channels in heart disease*. Circ J, 2009. **73**(3): p. 419-27.
88. Woo, S.H., Cleemann, L., and Morad, M., *Spatiotemporal characteristics of junctional and nonjunctional focal Ca<sup>2+</sup> release in rat atrial myocytes*. Circ Res, 2003. **92**(1): p. e1-11.
89. Woo, S.H., Cleemann, L., and Morad, M., *Diversity of atrial local Ca<sup>2+</sup> signalling: evidence from 2-D confocal imaging in Ca<sup>2+</sup>-buffered rat atrial myocytes*. J Physiol, 2005. **567**(Pt 3): p. 905-21.
90. Yang, Z., Pascarel, C., Steele, D.S., Komukai, K., Brette, F., and Orchard, C.H., *Na<sup>+</sup>-Ca<sup>2+</sup> exchange activity is localized in the T-tubules of rat ventricular myocytes*. Circ Res, 2002. **91**(4): p. 315-22.
91. Zima, A.V., Picht, E., Bers, D.M., and Blatter, L.A., *Termination of cardiac Ca<sup>2+</sup> sparks: role of intra-SR [Ca<sup>2+</sup>], release flux, and intra-SR Ca<sup>2+</sup> diffusion*. Circ Res, 2008. **103**(8): p. e105-15.



## VIII. Publications

M.R. Moeller, K. Hammer, O. Engel, *Poppy seed consumption and toxicological analysis of blood and urine samples*, Forensic Sci. Int. 143(2004) 183-185.

S.M. Wille, E. Raes, P. Lillsunde, T. Gunnar, M. Laloup, N. Samyn, A.S. Christophersen, M.R. Moeller, K.P. Hammer, A.G. Verstraete, *Relationship Between Oral Fluid and Blood Concentrations of Drugs of Abuse in Drivers Suspected of Driving Under the Influence of Drugs*, Ther Drug Monit. (2009) [Epub ahead of print]

→ K. Hammer, S. Ruppenthal, L. Kaestner, P. Lipp, *Confocal Visualization of Subcellular Morphology in Adult Ventricular Myocytes by Adenoviral Transfected Fluorescent Fusion Proteins*, in preparation.

→ A. Flockerzi, K. Hammer, A. Zeug, P. Lipp, L. Kaestner, *Robust automated detection and analysis of localised signalling events in high speed 3D-imaging*, in preparation.

→ L. Kaestner, A. Scholz, K. Hammer, A. Vecerdea, S. Ruppenthal, P. Lipp. *Isolation and Genetic Manipulation of Adult Cardiac Myocytes for Confocal Imaging*. JoVE. Accepted for publication.

Publications related to my thesis are indicated with an arrowhead.

## IX. Abbreviations

[Ca <sup>2+</sup> ] <sub>i</sub>	intracellular (cytosolic) Ca <sup>2+</sup> concentration
abs	actin binding protein
AF	atrial fibrillation
AM	acetoxymethylester
AOTF	Acousto Optic Tunable Filter
ATP	Adenosine Triphosphate
AV Node	atrioventricular Node
CCD	charge-coupled device
CICR	Ca <sup>2+</sup> induced Ca <sup>2+</sup> release
DIV	days <i>in vitro</i>
DMSO	Dimethylsulfoxide
DNA	Deoxyribonucleic acid
ECC	excitation contraction coupling
ECG	electrocardiogram
ECM	extracellular matrix
eGFP	enhanced green fluorescent protein
EGTA	ethylene glycol tetraacetic acid
ER	endoplasmic reticulum
FFT	Fast Fourier Transform
FLAP	fluorescence loss after photobleach
FP	fluorescent protein
fps	frames per second
FRAP	fluorescence recovery after photobleach
FWHM	Full Width at Half Maximum
GPI	Glycosylphosphatidylinositol
GTP	guanosine triphosphate
Iso	Isoproterenol
ITS	insulin, transferrin, selenite
KO	knock out
MOI	multiplicity of infection
NADPH	nicotinamide adenine dinucleotide phosphate

NCX	Na <sup>+</sup> -Ca <sup>2+</sup> -exchanger
PCR	polymerase chain reaction
PSF	point spread function
roi	region of interest
ROS	reactive oxygen species
RT	room temperature
RyR	Ryanodine Receptor
SEM	standard error of the mean
SERCA	sarco-/endoplasmic reticulum ATPase
SOC	store operated channel
SR	sarcoplasmic reticulum
TRP	transient receptor potential
t-tubules	transverse tubules
WT	wildtype
YFP	yellow fluorescent protein

## **X. Acknowledgments**

I would like to express my thankfulness to Prof. Dr. Peter Lipp for giving me the opportunity to work in his group and for his constant support, hours of discussion and especially for his sweeping cheerfulness and optimism.

I especially would like to thank Dr. Lars Kaestner for his constant support, critical discussions and technical help. His patience and frankly comments definitely pushed me on many times.

I would like to thank Aline Flockerzi for the great time working on the Spark-Algorithm and for writing this software so fundamental for my work.

I would also like to thank Prof. Dr. Markus Hoth for accepting to be a member of my thesis committee, for efficient discussions and steadily support.

I am very thankful to Anne Vecerdea for all the animal preparations and the support in cell isolations. I would also like to thank Dr. Sandra Ruppenthal and Dr. Anke Scholz for the preparation of the Adenoviruses and for critically reading this thesis. Special thanks go to Dr. Anke Scholz who supported during the last three years as a colleague and a friend.

My special thanks go to all members of the Institute for Molecular Cell Biology for their constant support, helpful advice and collegiality accounting for the pleasant and comfortable atmosphere.

Finally, I would like to thank my mother and my father for their loving support and my brother for his immovable believe in me.

This work was supported by the International Graduate Research School „Calcium Signaling and Cellular Nanodomains“ (GRK 1326) of the DFG.

## XI. Curriculum Vitae

### CIVIL STATUS

First Name Karin  
Middle Name Petra  
Family Name Hammer  
Date & Place of Birth May 29<sup>th</sup> 1977 in Zweibruecken, Germany  
Sex female  
Marital Status not married  
Occupation PhD-student

Address

**Resident:** Entenmuehlstr. 20b, D-66424 Homburg, Germany  
phone: +49 6841 174803  
mobile: +49 179 9104456  
mail: [karin.p.hammer@gmx.de](mailto:karin.p.hammer@gmx.de)

**Office:** Institute for Molecular Cell Biology, Saarland  
University,  
Medical Faculty, Building 61, D-66421 Homburg,  
Germany  
phone: +49 6841 16 26094  
fax: +49 6841 16 26104  
mail: [k.hammer@uks.eu](mailto:k.hammer@uks.eu)  
web: [www.lipplab.de](http://www.lipplab.de);  
[www.uniklinikum-saarland.de/en/forschung/gk-calcium](http://www.uniklinikum-saarland.de/en/forschung/gk-calcium)

### LANGUAGES

German (native speaker), English (very good), French (basic)

### EDUCATION

January 2006 Diploma in Biology, Technical University  
Kaiserslautern, Germany, Diploma thesis: "Purinergic  
receptors in the cerebellum of the rat"

September 1999 Graduation from academy for Medical Technical  
Assistants as Medical Technical Laboratory Assistant

July 1996 Diploma from German High School  
(qualifying for university admission)  
*Gymnasium Johanneum*, Homburg, Germany

## **PRE-DOCTORAL EXPERIENCE**

May 2006 – July 2006      Qualification period of the Graduate School 1326 „Calcium Signaling and Cellular Nanodomains“, Saarland University, Homburg, Germany

## **DOCTORAL EXPERIENCE**

July 2006 – July 2009      Graduate Student at the Graduate School 1326 „Calcium Signaling and Cellular Nanodomains“, Saarland University, PhD-thesis at the Institute for Molecular Cell Biology, Medical Faculty, Saarland University, Homburg, Germany; Title: “High Resolution 3D-Imaging of the Physiology and Morphology of Isolated Adult Cardiac Myocytes from Rat and Mice”  
Supervisors: Prof. Dr. Peter Lipp; Dr. Lars Kaestner

## **PROFESSIONAL EXPERIENCE**

June 2000 – Dec. 2000      Student Assistant;  
Umweltlabor Westpfalz GmbH, Kaiserslautern, Germany;  
preparation of soil samples for GC/MS analysis

June 2001 – Sept. 2002      Student Assistant;  
Institute of Legal Medicine, Saarland University,  
66421 Homburg, Germany;  
screening of blood samples for drug abuse utilizing ELISA

May 2003 – Dec. 2005      Assistant;  
Prof. Dr. Manfred Moeller, Forensic Toxicologist, GTFCh,  
Institute of Legal Medicine, Saarland University,  
66421 Homburg, Germany;  
ELISA-analysis of blood, urine, hair and oral fluid

- GC/MS-analysis of blood and oral fluid
- Research project *FE82.255/2003/AP* of the *Bundesanstalt fuer Strassenwesen* (Federal Highway Research Institute);
- EU-project ROSITA2
- EU-project PHARE-Twinning

## ORAL COMMUNICATIONS

33. Meeting of the *Oberrheinischen Rechtsmediziner*, Heidelberg, Germany, 2003: „Mohnkonsum, §24a StVG und FeV“

34. Meeting of the *Oberrheinischen Rechtsmediziner*, Homburg, Germany, 2004: „ROSITA2 – Status Report“

BLT-Meeting, Luxembourg, 2003: „Poppy Seed Consumption, §24a StVG and FeV“

2. ROSITA2-Meeting, Tampa, Florida, USA, 2004: “Status Report”

3. ROSITA2-Meeting, Santiago de Compostela, Spain, 2004: “Status Report”

Roche Symposium at the MEDICA 2004, *The role of the laboratory in drug abuse and drug withdrawal*: “Toxicological analysis after Hemp- and poppy seed consumption”

Neurobiological Seminar at the technical University Kaiserslautern, Germany, 2005: presentation of the Diploma thesis: “Purinergic receptors in the cerebellum of the rat.”

Colloquium of the Graduate School 1326, Saarland University, Homburg, Germany, 2006: “High-resolution 3D-imaging of the physiology and morphology of isolated cardiac myocytes”

Colloquium of the Graduate School 1326, Saarland University, Homburg, Germany, 2007: “High-resolution 3D-imaging of the morphology of isolated cardiac myocytes”

Colloquium of the Graduate School 1326, Saarland University, Homburg, Germany, 2008: “High-resolution 3D-imaging of the physiology and morphology of isolated cardiac myocytes: Cardiac EC-Coupling and Elementary Calcium Signals”

Joint PhD-student Symposium, UIBK, Obergurgl, Austria, 2008: „Cardiac EC-Coupling and Elementary Calcium Signals”

14<sup>th</sup> European Microscopy Congress, Aachen, Germany, 2008: “Observation of Ventricular Myocyte Morphology in Long Term Culture using High Resolution Confocal Imaging”

53rd Annual Meeting of the Biophysical Society, Boston, MA, USA, 2009: “Ventricular Myocyte Morphology in Long Term Culture”

## POSTERS

TIAFT-Meeting in Melbourne, Australia, 2003: “Toxicological Analysis of Blood, Urine, and Saliva after a Hemp Lunch. *Manfred R. Moeller, Karin Hammer, Oliver Engel, Stefan Steinmeyer*”

86<sup>th</sup> Annual Meeting of the German Physiological Society, Hannover, Germany, 2007: “High resolution 3D-imaging of isolated cardiac myocytes. *Karin Hammer, Lars Kaestner, Sandra Ruppenthal, Anne Vecerdea and Peter Lipp*”

Microscopy Conference MC, Saarbruecken, Germany, 2007: “Characterization of Ventricular Myocyte Morphology in Long Term Culture – A Combinatory Approach. *Karin Hammer, Ludwig Edelmann, Martin Oberhofer, Anne Vecerdea, Lars Kaestner and Peter Lipp*”

87<sup>th</sup> Annual Meeting of the German Physiological Society, Cologne, Germany, 2008: “Characterization of Ventricular Myocyte Morphology in Long Term Culture. *Karin Hammer, Sandra Ruppenthal, Martin Oberhofer, Anne Vecerdea, Lars Kaestner and Peter Lipp*”

87<sup>th</sup> Annual Meeting of the German Physiological Society, Cologne, Germany, 2008: “Calcium spark detection and analysis in time series of two-dimensional confocal images. *Aline Flockerzi, Andre Zeug, Karin Hammer, Peter Lipp and Lars Kaestner*”

Joint PhD-student Symposium, UIBK, Obergurgl, Austria, 2008: „Characterization of Ventricular Myocyte Morphology in Long Term Culture by High Resolution Confocal Imaging. *Karin Hammer, Sandra Ruppenthal, Martin Oberhofer, Anne Vecerdea, Lars Kaestne and, Peter Lipp*”

53rd Annual Meeting of the Biophysical Society, Boston, MA, USA, 2009: “Automatic Calcium Spark Detection and Analysis in Time Series of Two-Dimensional Confocal Images. *Peter Lipp, Karin Hammer, Aline Flockerzi, Andre Zeug, Lars Kaestner*”



## FROM WHOM REFERENCES CAN BE OBTAINED:

**Prof. Dr. Peter Lipp**

Institute for Molecular Cell Biology,  
Saarland University,  
Medical Faculty, Building 61,  
D-66421 Homburg, Germany  
phone: +49 6841 16 26103  
fax: +49 6841 16 26104  
mail: [peter.lipp@uks.eu](mailto:peter.lipp@uks.eu)

**Prof. Dr. Markus Hoth**

Biophysics  
Saarland University,  
Medical Faculty, Building 76  
D-66421 Homburg, Germany  
phone: +49 6841 16 26266  
fax: +49 6841 16 26060  
mail: [markus.hoth@uks.eu](mailto:markus.hoth@uks.eu)

**Prof. Dr. Joachim W. Deitmer**

Division of General Zoology  
Department Biology  
University of Kaiserslautern  
Erwin-Schrödinger-Straße 13  
D 67663 Kaiserslautern, Germany  
phone: +49-(0)631-205 2877  
fax: +49-(0)631-205 3515  
mail: [deitmer@biologie.uni-kl.de](mailto:deitmer@biologie.uni-kl.de)